GEORG-AUGUST-UNIVERSITÄT
GÖTTINGEN

CANDIDATE MECHANOSENSITIVE TRANSDUCTION CHANNELS IN *DROSOPHILA MELANOGASTER*

Dissertation

for the award of the degree

"Doctor rerum naturalium"

Division of Mathematics and Natural Sciences

of the Georg-August-Universität Göttingen

Submitted by

Thomas Effertz

From Cologne, Germany

Göttingen, 2011

Members of Thesis Committee

Prof. Dr. Martin Göpfert (Supervisor/Reviewer)

Georg-August-University of Göttingen, Cellular Neurobiology

Prof. Dr. André Fiala (Reviewer)

Georg-August-University of Göttingen, Molecular Neurobiology of Behaviour

Prof. Dr. Andreas Stumpner

Georg-August-University of Göttingen, Neuroethology

Oral examination: June 9th 2011

I, Thomas Effertz, herewith declare that my PhD thesis entitled "Candidate mechanosensitive transduction channels in *Drosophila melanogaster*" was written independently. No other sources and aids than the quoted were used.

_____

Thomas Effertz

Göttingen, April 2011

Index of contents

1. Introduction

1.1. Hearing

Hearing is a specialized form of mechanoreception. All animals can perceive mechanical stimuli but only a few are able to perceive sound. An animal is said to hear, if it behaviourally responds to biological relevant sounds (Figure 1). Among terrestrial animals, the ability to hear is only widespread in vertebrates and insects hear [1-6]. In *Drosophila*, for example, first evidence for hearing was provided in the late 1950's, early 60's by the discovery that male flies produced a courtship song that drives female mating-decision [7-9]. The mechanotransduction process that allows *Drosophila melanogaster* to hear is in the focus of this thesis.
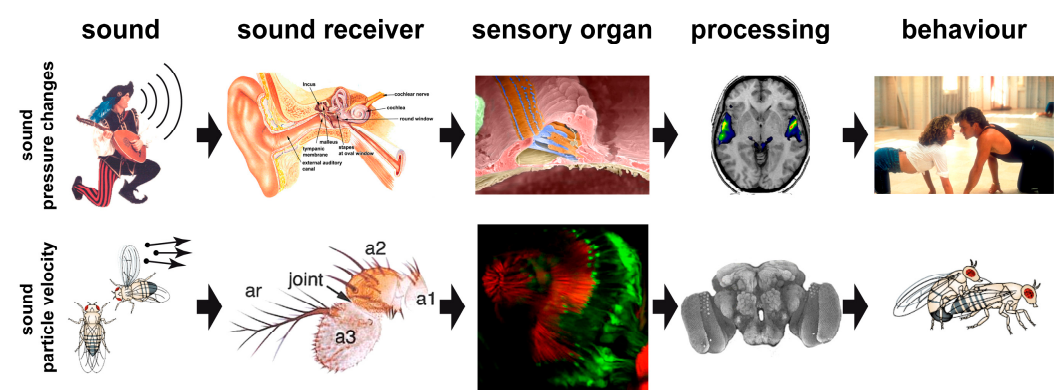
Figure 1 Illustration of the sensory process of hearing
Ears detect either the pressure- or the particle-velocity component of sound. Tympanal ears detect sound-pressure differences and insect antennal ears monitor particle-velocity changes. Sound receiving tympana and insect antennae relay on sound-induced vibrations to sensory organs that transduce the vibrations into electrical signals, which are processed by the nervous system and ultimately initiate behaviour.
[Montage from different sources, a complete list can be found in the figure table at the end of this thesis]

1.2. Hearing in *Drosophila melanogaster*

Fly auditory research started with the discovery that male flies produce songs by fanning their wings; the songs are diverse amongst *Drosophila* species [7-12] and two song types can be distinguished: Sine songs [13] and a pulse songs [14] (Figure 2). In *Drosophila melanogaster*, both song types have a dominant frequency of ca. 150-200 Hz. Courtship songs drive female mating decision, providing information about male quality and species identity [11,15]. Although copulations will occur without courtship songs, the songs increase the mating probability by a factor of about 100 [12]. Whilst only males produce the songs, both sexes behaviourally respond to the songs and, accordingly, are able to hear. In *Drosophila*, the ability to hear is mediated by particle velocity-sensitive antennal ears.
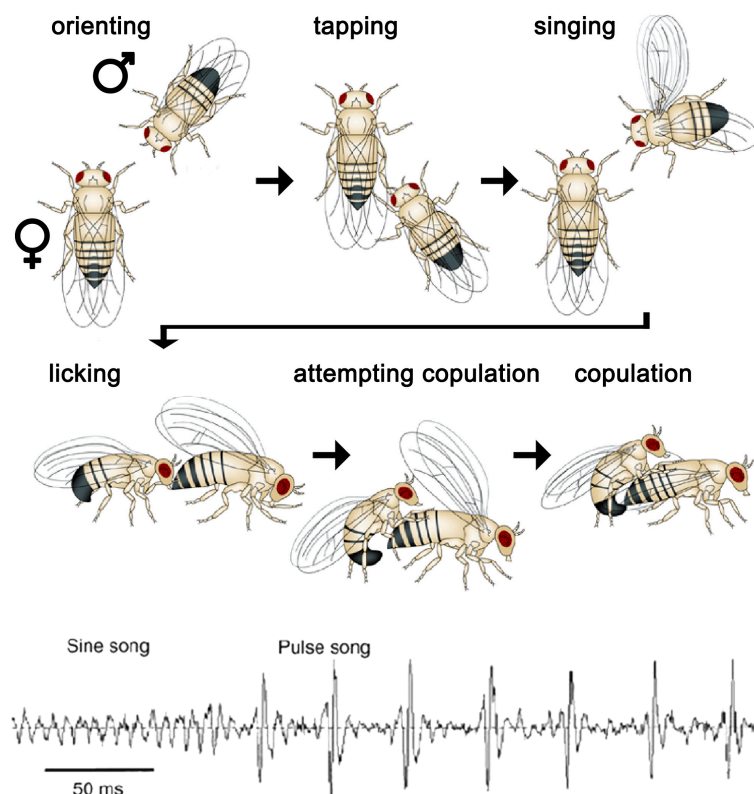
Figure 2 *Drosophila melanogaster* courtship behaviour and courtship song
Upper panel: The male initiates courtship behaviour by tapping at the female's abdomen. If the female is able to copulate it releases certain odours, which induce the male's "singing" behaviour. The male orientates itself to the female and starts singing. If the female responses positively the male starts to lick the females abdomen followed by attempted and successful copulations Lower panel: The courtship song consists of a sine-song (140-170 Hz) and a pulse. It is produces by the males fanning their wings. Modified from [16]

1.2.1 Anatomy of the fly's ear

Flies hear with their antennae. Each antenna consists of three main segments: scape (1st antennal segment; a1), pedicel (2nd antennal segment; a2), and funicle (3rd antennal segment; a3). The distal antennal segments form a featherlike appendix to the funicle called the Arista (ar) [16] (Figure 3). Only the 1st segment harbours muscles, allowing the fly to actively move its entire antenna. The 2nd segment houses the auditory organ, Johnston's organ (JO) [17-20]. The 3rd segment together with the Arista, in turn, vibrates in response to sound stimuli as a rigid body and serves as the sound receiver [21]. A joint connects the 2nd and 3rd segment (a2/a3-joint), allowing for rotational movements of the 3rd segment about its longitudinal axis in the presence of sound. The auditory sensory organ, Johnston's organ, is a chordotonal organ. It consists of 230 chordotonal sensilla=scolopidia that together comprise ca. 480 sensory neurons (ca. 10% of the scolopidia of JO have three sensory neurons [22], the rest two [23]). Each scolopidium consists of a primary sensory neuron, a ligament cell, a scolopale cell, and a cap cell. The ligament cell is directly attached to the distal cuticle and the cap cell to the proximal cuticle via an extracellular matrix. The scolopale cell

Figure 3 Head of *Drosophila* and close-up of the antenna

Upper panel: Three major antennal segments are distinguished, the 1st segment "scape" (a1, yellow), the 2nd segment "pedicel" (a2, red), and the 3rd segment "funicle" (a3, green). The distal antennal segments are fused together and form a featherlike appendix to the funicle, the Arista (ar). Only the scape (a1) is musculated. Lower panel : the pedicel (a2) harbours the auditory organ (Johnston's organ; JO), the funicle (a3) harbours mostly olfactory sensory neurons. The funicle (a3) rotates about its longitudinal axis, relative to the pedicel (a2) in response to sound. Those rotational movements are picked up by Johnston's organ at the a2/a3 joint.
Altered after Rochester.edu John Jaenike and [150]

encloses the sensory neuron and forms a fluid filled space around the neuron's
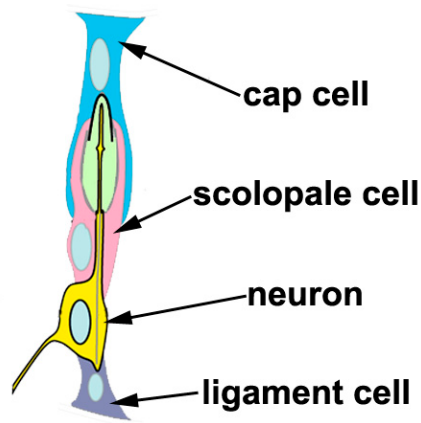
Figure 4 Type I sensory organ, subtype chordotonal organ (*ch*), scolopidia

The basic subunit of all chordotonal organs is the scolopidia, consisting of the sensory neuron(s) and its supporting cells. Chordotonal organs are found between every segment of an insect body and serve as stretch receptors. The mechanical forces are relayed to the sensory neuron by the cap-cell (distal) and the ligament cell (proximal).

dendritic cilium (Figure 4, green). The scolopidia of JO span across the a2/a3 joint between the 2nd and 3rd antennal segment. Vibrations of the 3rd segment relative to the 2nd segment are thus relayed to JO sensory neurons. Those vibrations will exert mechanical forces onto neurons [21]. The neurons are endowed with mechanically gated transduction channels that convert these forces into electrical signals [24-26]. Because these mechanoelectrical transduction channels are directly connected to the antennal sound receiver, the receiver's mechanics betray the gating of these channels. Hence, monitoring the mechanics of the sound receiver betrays auditory transduction events.

1.3. Similarities between vertebrate and insect ears

Hearing in vertebrates has been extensively studied over the last decades. Hearing in *Drosophila*, however, is comparatively little understood. Therefore, my introduction focuses on the hearing process of vertebrates and I will compare it to the hearing process in the fly.

Although a vertebrate tympanal ear and the *Drosophila* antennal ear look different, they share conserved genes for mechanosensory cell- and organ formation and function in similar ways. Both types of ears use specialized sensory organs to detect changes in mechanical force. These sensory organs developmentally depend on the transcription factor *atonal* (the gene *atonal* in *Drosophila*, *Atoh1* in the mouse). Mice lacking *Atoh1* fail to produce hair cells and flies missing *atonal* fail to form Johnston's organ (Figure 5). The functional relevant sequence of *atonal* is well conserved and thus a rescue of mutant phenotypes in either species is possible by the ectopic expression of the *atonal* gene of the other [27-31]. A possible explanation for this similarity is the idea that

the last common ancestor of vertebrates and invertebrates, the protostom/deutorostom-ancestor [32], already possessed an *atonal* dependent protosensory cell. This cell than gave rise to the hearing organs we see today in vertebrates and invertebrates. This apparent evolutionary relation raises the possibility that some molecular components of the mechanotransduction machineries used by hair cells and JO scolopidia are evolutionary conserved [1,33-37]. The ears of vertebrates and *Drosophila* consistently work close to the physical boundaries set by thermal noise. For example, the energy needed to gate a single mechanotransduction channel is 7-19 zJ in mammals [38,39] and 10-13 zJ in flies [40], which is roughly twice as high as the thermal energy at 20°C, ca. 4 zJ. The sensitivity and frequency specificity of vertebrate and the fly ear depends on an active process called "cochlear amplifier" [41-46].
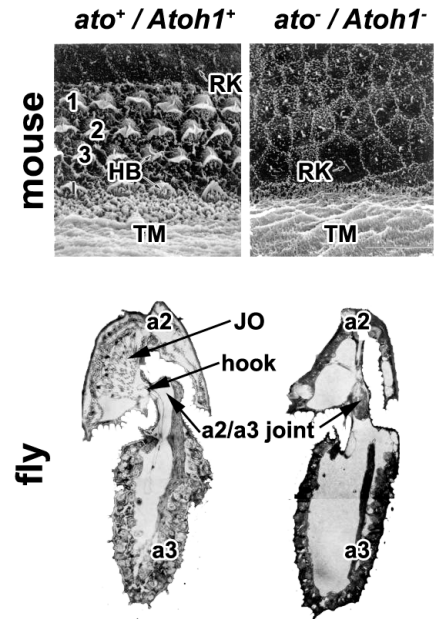
Figure 5 *atonal* dependent morphology of mice organ of Cortin and fly JO
Upper pannel: SEM images of the organ of Corti in wildtype and *Atoh1* missing mice. *Atoh1*- missing mice faile to develop haircells. Lower pannel: Light microscopic images of longitudinal sections through the antenna of wildtype and *ato* missing flies. *ato*- missing flies faile to develop the Johnston's organ. **1-3** rows of outer hair cells, **HB** hairbundle, **RK** rudimentary kinocilia, **TM** tectorial membrane, **JO** Johnston's organ, **a2** pedicel, **a3** funicle. modified from [28] & [47]

1.4. Cochlear amplifier

The cochlear amplifier relies on an active process. Gold proposed the idea of an active process in the cochlea in 1948 [47,48] but it took 40 years until the necessary experiments to test his theory were conducted. Until then the organ of Corti was believed to be passive. In 1961, von Békésy received the Nobel Prize in Physiology or Medicine [49] for discovering travelling waves that maps sound frequencies along the length of the basilar membrane. This tonotopic frequency representation along the basilar membrane was however not sharply tuned. Unfortunately, he worked on corpses and missed the active component present in a living cochlea [50] (Figure 6). The discrepancy between the broad frequency
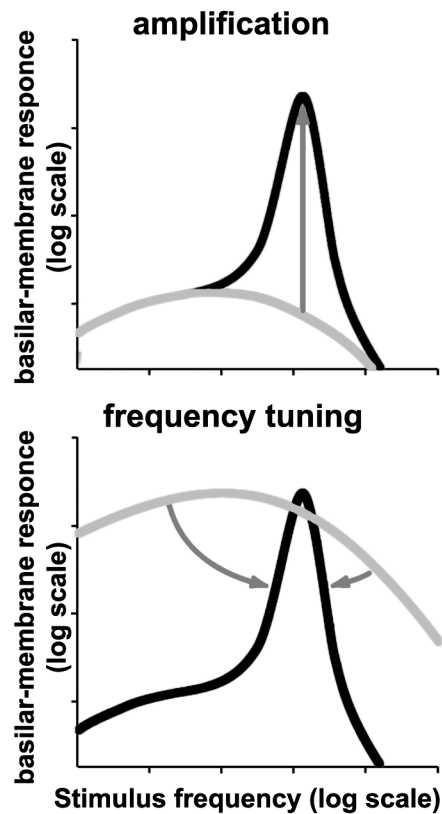
Figure 6 Passive and active contribution to amplification and frequency tuning in the cochlea
The passive properties of the basilar membrane (light grey) allow for a broad frequency tuning. The outer hair cell based active process (black) increases amplification and sharpens the frequency tuning. Altered after [57]

representation of a dead cochlea and the fine pure tone resolution human ears can distinguish was believed to be the result of dampening [51] rather than the active process proposed by Gold.

Davis coined the term "cochlear amplifier" [52]. He used it as a designation for the mechanism that feeds mechanical energy into basilar membrane motion. Four characteristics define the cochlear amplifier [45,46]:

- *Compressive nonlinearity*
- *Frequency specific amplification*
- *Active amplification/power gain*
- *Self sustained oscillations*

Compressive nonlinearity

The compressive nonlinearity derives from the nonlinear, intensity-dependent amplification of sound-induced vibrations. In mammals, this nonlinear effect increases the ear's mechanical sensitivity for faint sound stimuli by a factor of ca. 1000 [53], whereas the corresponding nonlinear sensitivity gain for the *Drosophila* ear is ca. 10 [25,54-56]. By-products of the compressive nonlinearity are an increase in the dynamic range a reduced intensity resolution.

Frequency specific amplification

The frequency specificity of the mammalian cochlea derives from passive mechanical properties of the basilar membrane and the active motility of outer hair cells [44,57-59]. Stiffness changes along the basilar membrane account for a broad, passive tuning, whereas the active process sharpens the frequency tuning and increases sensitivity [57] (Figure 6). These site-specific properties give rise to a tonotopic frequency representation from high frequencies near the oval window to low frequencies at the apex of the cochlea [60-62]. Whereas the cochlea can effectively be described as a series of band-pass filters [63-65], a single band-pass filter suffices to describe the ear of the fly [21].

Active amplification/power gain

The hallmark of active amplification is a gain in power. Rigorously testing for power gain required the demonstration of violations of fundamental theorems in equilibrium thermodynamics, the equipartition or the related fluctuation-dissipation theorem. Frog hair cells [66,67] and the fly ear [40] have been shown to violate the fluctuation-dissipation theorem (Figure 7), demonstrating that they are active and exhibit power gain. By contrast, power gain has not yet been established for mammalian cochleae and hair cells, and if their putative activity originates from outer hair cell body motility [68,69] or hair bundle motility [70,71] is still a point of debate. In the fly ear, the question remains whether the source of activity resides in the neuronal cell body or the dendrite.
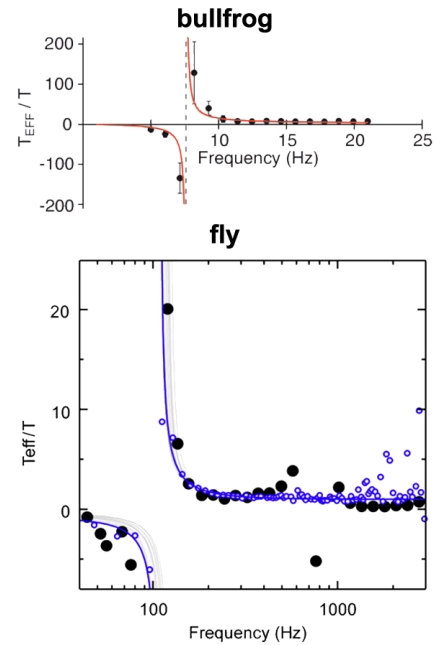
Figure 7 Violation of the fluctuation-dissipation theorem in bullfrog hair bundle and fly sound receiver

The fluctuation-dissipation theorem persists a ratio between effective- and ambient temperature of one if a system is in thermal equilibrium with its environment. Upper panel: The bullfrog hair bundle violates the theorem at ca. 8Hz. Lower panel: The fly's sound receiver violates the theorem at ca. 120 Hz, corresponding to the iBF of the fly's sound receiver. [40,66]

Self-sustained oscillations

A positive feedback can drive active systems into self-sustained oscillation, if the mechanical feedback becomes excessive. This happens e.g. with a public-address system when a loudspeaker is positioned directly in front of a microphone that drives the loudspeaker. The same holds true for the ears of mammals or the fly. For example, *nanchung* and *inactive* mutants show self-sustained oscillation of their antennal sound receiver. In mammals, self-sustained oscillations sometimes reach levels where ears emit measurable sound, SPOAEs (spontaneous otoacustic emissions) [57]. Though SPOAEs originate from instability and, if strong, may indicate a lack of feedback control, their occurrence well illustrate that the system is active. All four characteristics of the cochlear amplifier rely on an active amplification of vibrations by outer hair cells [57,70-75] or JO-neurons in the fly [40,54,76]. In both cases, one can understand the active amplification as a correctly timed push. The sensory cells increase the sound-induced oscillations with active, phase locked oscillations of their own [66,74,77-80]. To do so ears work at the verge of a Hopf bifurcation [57,59,67,72,81], where small parameter changes suffice to shift the state transitions from quiescent to oscillating. Mathematical analysis shows that all key characteristics of the cochlear amplifier are generic properties of a system operating at a Hopf bifurcation. This included, amplification, sharpened frequency tuning, and a compressive nonlinearity [57,59,67,72,81]. And spontaneous oscillation arise if the system enter the oscillating regime [57,82-85]. A theoretical framework connecting the active amplification in hair cell bundles and molecular processes is the gating-spring model [38,86-88].

1.5.   Gating-spring model

The gating-Spring model describes the mechanotransduction process in hair cells [38,86,87]. The model posits that deflections of the hair bundle directly gate mechanoelectrical-transduction channels (MET-channels). The channels are assumed to operate in parallel, and each channel is associated with an elastic element, the grating spring that funnels forces to its gate. The channel/spring-complex is connected to adaptation motors (Figure 8). Changes in mechanical force will change the extension of the gating spring and, thus, the open probability of the channels (Figure 9). The channel can assume 2-states, open or closed. At the resting position, the open probability is ca. 0.5. In the open state ions (most likely Ca^{2+}) enter the sensory cell [89]. Calcium ions presumably interact with the channel complex and close the channel gate. After channel closure the gate cannot be opened for a short period of time [39,59,88]. Followed by this fast reaction a slower, presumably motor driven, adaptation process takes place [87]. This slow adaptation process decreases the tension on the gating spring and restores the initial open probability of the channel (Figure 9). A revised and modified version of the mammalian gating spring model describes transduction and amplification in the ear of
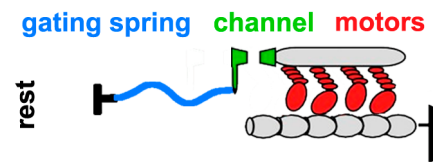
Figure 8 gating spring model
comprising a linear stiffness (gating spring; blue), a mechanical gated transduction channel (green), and motors (adaptation/amplification motors; red) altered after [40]
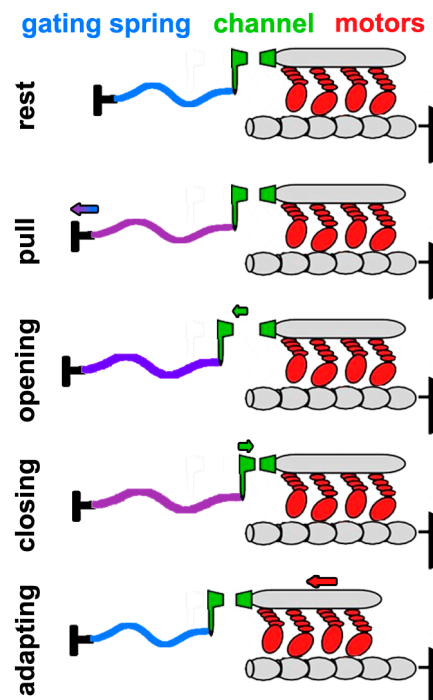
Figure 9 activation of a MET-channel, described by the gating spring model
Pull: External mechanical force stretches the gating spring (blue). opening: The force is relayed to the MET-channel increasing its open probability. closing: Ca^{2+} enters trough the channel, interacts with the machinery and closes the channel. adapting: adaptation motors alter the MET-channel position, reducing the gating spring tension, thus restoring the resting open probability. Altered after [40]

the fly [40] (Figure 10). The model mathematically describes the fly ear by a set of coupled differential equations that couple opposing gating spring modules with feedback-controlled motors to a harmonic oscillator that represents the sound receiver. This model quantitatively captures the mechanics of a fly's antennal sound receiver, including its response to force steps, its free fluctuation, its nonlinear compression, its frequency characteristics and activity, and its ability to display self-sustained oscillations [40]. Based on this modified gating spring model one can predict the impact of loss of MET-channels, supporting structures, and motor activity on the receiver's mechanics [25]. One such prediction is that the loss of MET-channels leads to a decrease of maximum/asymptotic stiffness (K_{inf}) of the antennal receiver, whereas the receiver's passive stiffness (K_{steady}) remains unaltered [25] (calculation see 2.7.4.). Hence, by monitoring and fitting the mechanical properties of the sound receiver with the modified gating spring model allows for estimation of mechanical changes in the mechanotransduction channel. Be it the opening of its gate, the work of adaptation motors or the coupling of those motors to the channel. The gating compliance of the mechanotransduction channel thereby directly relates to the changes in sound receiver compliance via a linear factor (γ).
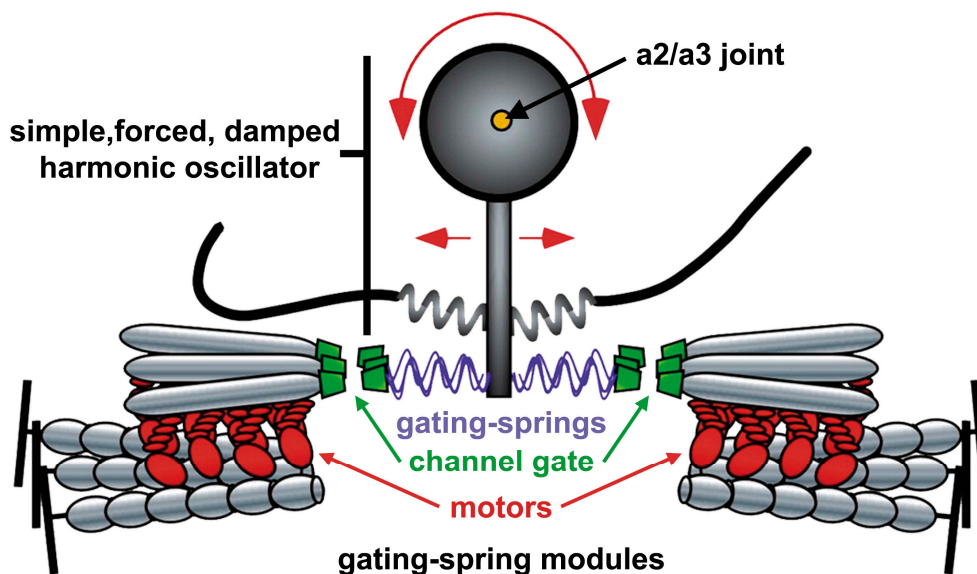
Figure 10 gating spring model adapted for the fly's ear
Symmetric arrangement of opposing gating spring models attached to the a2/a3 joint. modified from [40]

1.6. Known mechanoelectricaltransduction channels

Three types of mechanoelectrical transduction channels (MET-channels) have been identified so far, the Msc-channels (MscL, MscS, and MscM) of *E. coli* [90] the MEC-4-complex of *C. elegans*, and the TRP-4 channel of *C. elegans* [91,92]. MscL in *E. coli* is the best-studied member of the Msc-channel family and serves as osmoreceptor in *E. coli*. The channel opens like the iris of a camera, allowing for the exchange of solutes and solvent [93] (Figure 11). No Msc-channel homologues are known in vertebrates or insects, only *Archae* and plants harbour related channels that are also implicated in osmoreception [94-96] (Mscl-like channels; MSL). In *C. elegans* MEC-2, MEC-4, MEC-6, and MEC-10 form a channel complex (MEC-4 complex). The Deg/ENaC (**deg**enerin/**e**pithelial **Na**$^{2+}$ **c**hannel) subunits MEC-4 and MEC-10 form the pore-region of the complex, while MEC-2 and 6 are associated proteins that increase single channel conductance (MEC-2), channel localization and availability (MEC-6) [91,97-99] (Figure 12). The MEC-4 channel complex is Na^{2+} permeable and implicated in touch sensation. Members of the Deg/ENaC family are also found in invertebrates and vertebrates. In vertebrates ASIC (**a**cid-**s**ensing **i**on **c**hannel) results in responses [100,101]. In invertebrates, Deg/ENaC channels are required for harsh

Figure 11 Two models of MscL gating
Upper panel: Barrel-stave model: the transmembrane (TM)-1 helices move away from the axis of symmetry, opening a pore lined by TM-1 and TM-2 helices. Lower panel: Helix-tilt model: both TM helices are tilted significantly but only TM-1 helices face the pore. One subunit of the homopentamer is highlighted in dark green.[93]
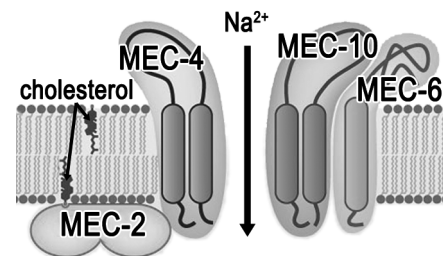
Figure 12 MEC-4 complex
MEC-2, MEC-4, MEC-6, and MEC-10 form the MEC-4 channel complex. MEC-4 and MEC-10 constitute the Na^{2+} selective pore region, whereas MEC-2 and MEC-6 associate to the complex and facilitate channel activity. Altered after [100]

disrupting the Deg/ENaC relative in slightly altered touch-evoked

touch sensation. Multidendritic neurons in *Drosophila,* (see Appendix D) require the Deg/ENaC channel *pickpocket* for nociception. The third MET-channel type, TRP-4, has been shown to be activated by mechanical stimuli and mutations in the predicted pore region of TRP-4 altered the biophysical properties of the mechanically evoked currents [92]. This strongly supports the idea of TRP-4 being a constitutive component of a mechanotransduction machinery. The *Drosophila* homologue of TRP-4 is TRPN1 (a.k.a. NompC). TRPN1 is implicated in the fly touch sensation and hearing and evidence from C. elegans supports a possible function of TRPs in mechanosensory signal transduction.

1.7. TRPs
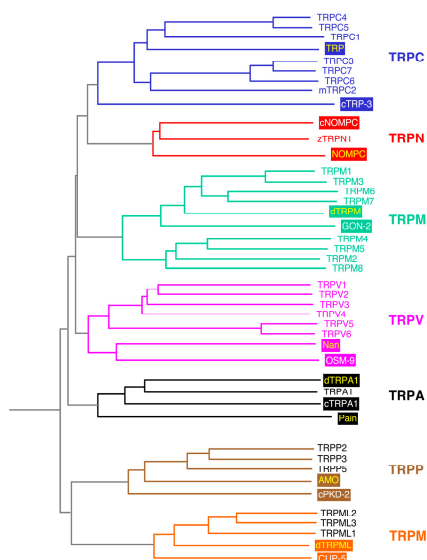
Figure 13 TRP channels different animals
Vertebrates TRPs in plain text, *Drosophila* TRPs in boxes. [104]

The transient receptor potential (TRP) superfamily comprises more than 30 cation channels present throughout animal phyla [102-107]. The TRP superfamily is subdivided into five group-1, TRPC ('Canonical'), TRPV ('Vanilloid'), TRPM ('Melastatin'), TRPA ('Ankyrin'), TRPN ('NompC'), and two distantly related group-2 subfamilies, TRPP ('Polycystin'), and TRPML ('Mucolipin') [105] (Tab. 1, Figure 13). Compared to other groups of ion channels TRPs show a high diversity in ion selectivity, modes of activation, and physiological functions [104]. However all TRP-channels share common features such as six putative transmembrane domains, a permeability to cations, and a varying degree of sequence similarity. Members of different subfamilies are implicated in a variety of sensory processes including vision, taste, smell, hearing, mechanosensation, thermosensation, and hygrosensation [102,107-112]. 27 TRP-channels have been found so far in humans, 28 in mice, 27 in zebra fish, 17 in worms, and 13 in the fly [106]. In *Drosophila* all subfamilies are present [113]. The TRPN subfamily is missing in mammals; it is present in Zebra fish [114] and the Bullfrog [115] (Tab.1). Due to

certain motifs in the pore region, it is predicted that TRPs form tetramers [106]. It has been shown that heterogenic tetramers are possible (*nanchung*, *inactive* [116]); a tetramer between TRPs of different subfamilies has been shown for TRPP2 and TRPC1 [117].

Tab. 1 List of TRP-subfamilies and their occurrence in different animals. Note that the TRPN subfamily seems to be missing in mammals.

Subfamily	Humans	Mice	Zebra fish	Worms	Flies
TRPC	6	7	8	3	3
TRPV	6	6	4	5	2
TRPM	8	8	6	4	1
TRPA	1	1	2	2	4
TRPN	0	0	1	1	1
TRPP	3	3	4	1	1
TRPML	3	3	2	1	1
Total	**27**	**28**	**27**	**17**	**13**

1.8. TRPs in *Drosophila*

13 TRP-channels are known in *Drosophila melanogaster* including representatives of all seven subfamilies [118] (Figure 14). Trp, Trpγ and Trpl, constitute the TRPC subfamily and are implicated in phototransduction [119]. The TRPV subfamily comprises Nanchung (nan) and Inactive (iav), which are implicated in hearing, thermo-, and touch sensation [18,116,120,121]. The only member of the TRPM subfamily, Trpm, has recently been connected to homeostatic regulation of certain metals [122,123]. The four members of the TRPA subfamily dTRPA1, dTRPA2 (Pyrexia), dTRPA3 (Water witch), and Painless (Pain) are implicated in mechanical nociception [124,125], thermo- [109,126-128], touch- [76,116,121,129], and gravity sensation [130]. The sole TRPN subfamily member NompC is implicated in touch sensation [114,131-137]. The group-2 subfamilies TRPP and TRPML are represented by Amo and Trpml [138-142]. Mutations in *amo* impair the transport of sperm from the fly female uterus into the storage organ, thus reducing male fertility [117]. Trpml is implicated in the homeostatic regulation of Calcium [143].
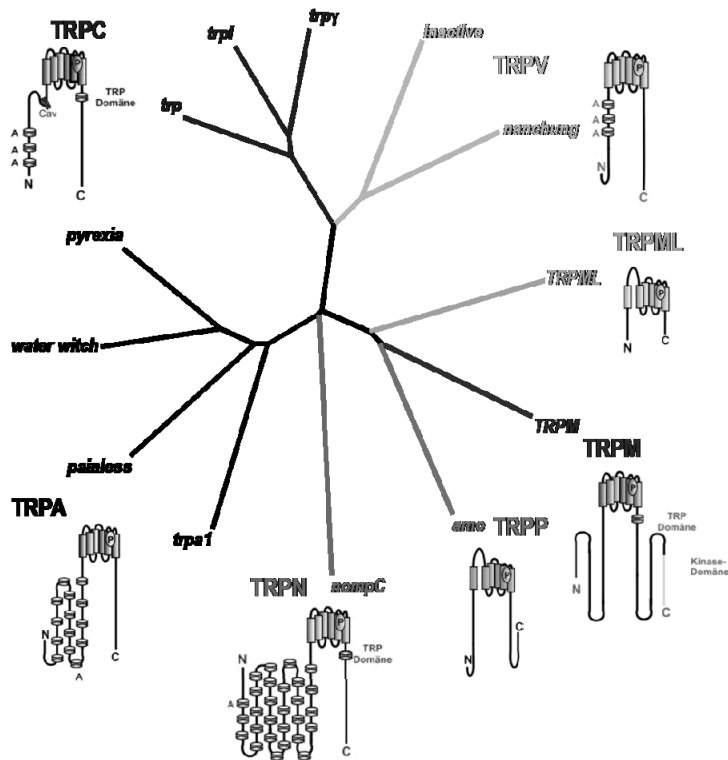
Figure 14 Drosophila TRP channels
Members of all seven TRP subfamilies are present in Drosophila. Especially members of the TRPA and TRPN family are of interest because of their ankyrin repeats which might form the predicted gating spring of a presumed MET-channel. Modified from [118]

Tab. 2 TRPs in *Drosophila melanogaster*

Subfamily	Gene	Chromosome location	Length (amino acids)	*ankyrin* repeats	Implied in
TRPC	*trp*	3R 99C6-7	1275	4	phototransduction
	trpl	2R 46B2	1124	4	phototransduction
	trpγ	2L 36A9-10	1128	4	phototransduction
TRPV	*nan*	3L 70D3	833	5	hearing
	iav	X 7A5-C1	1123	5	hearing
TRPM	*trpm*	2R 51E11-F1	1947	0	
TRPN	*nompC*	2L 25D6-7	1619	29	light touch, hearing
TRPA	*painless*	2R 60E5-7	913	9	thermal and mechanical nociception
	trapA1	3L 66E3	1274	13	thermotaxis
	pyrexia	3L 61B2	956	9	
	waterwitch	3R 84E4	986	9	hygrosensation
TRPP	*amo*	2L (33E3)	924	0	Male fertility
TRPML	*trpml*	3L (76C3)	652	0	

1.9. NompC (TRPN1)

Drosophila nompC mutants were first described by Kernan et al. [144]. They conducted a forward genetic screen to identify mutations that impair mechanosensation. Amongst mutations that impaired larval movement and touch response, Kernan et al. also found three mutants that abolished the mechanoreceptor potential (MRP) in sensory bristle neurons (structure of bristles see Appendix D), sequentially naming them *no mechanoreceptor potential A*, *B*, and *C*. In 2000, mutations in *nompC* were mapped to a gene (Figure 15). The missence mutation *nompC⁴* altered the adaptation kinetics of measured MRPs respectively mechanoreceptor currents (MRC) in sensory bristles [131] rather than abolishing the mechanical evoked currents completely. Based in these findings Walker et al. suggested that NompC is a mechanotransduction channel.
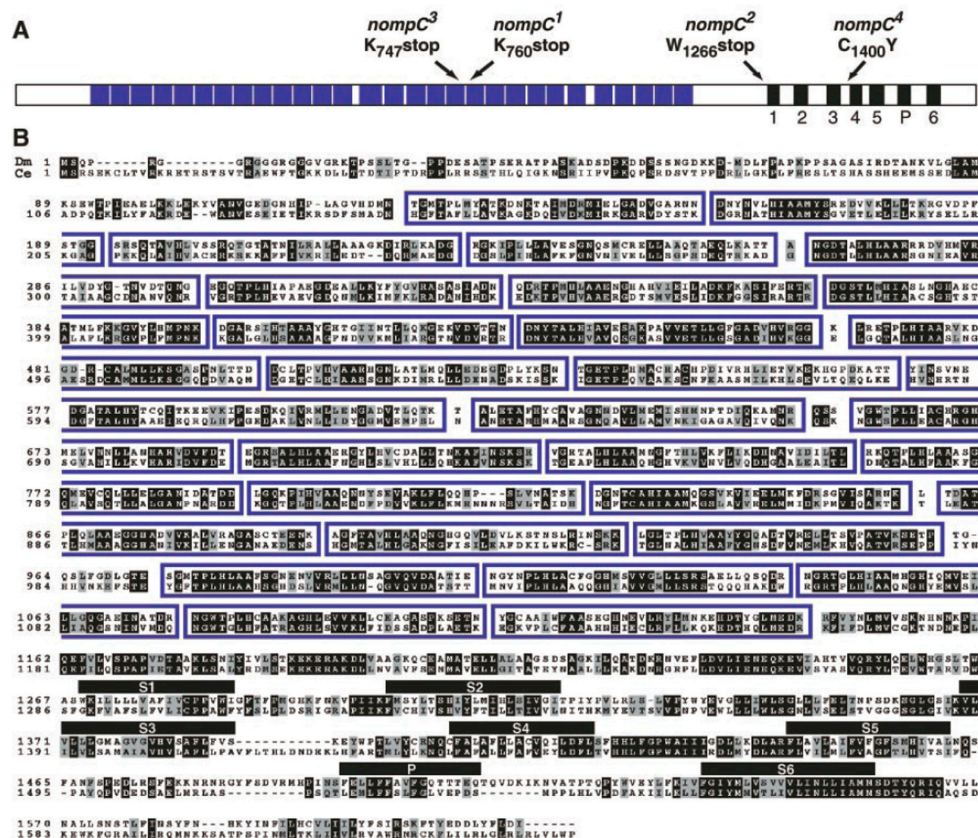
Figure 15 *nompC* sequence by Walker with predicted domains
The N-terminal region of NompC comprises 29 ankyrin repeats, two null mutations introduce a stop codon in this region (*nompC¹*, *nompC³*), a third null mutation (*nompC²*) introduces a stop codon in the first transmembrane domain. The missence mutation *nompC⁴* introduces a tyrosine instead of a cysteine. The predicted pore region would be between the transmembrane domains 5 and 6. Modified from [131]

1.9.1   NompC a mechanotransduction channel candidate
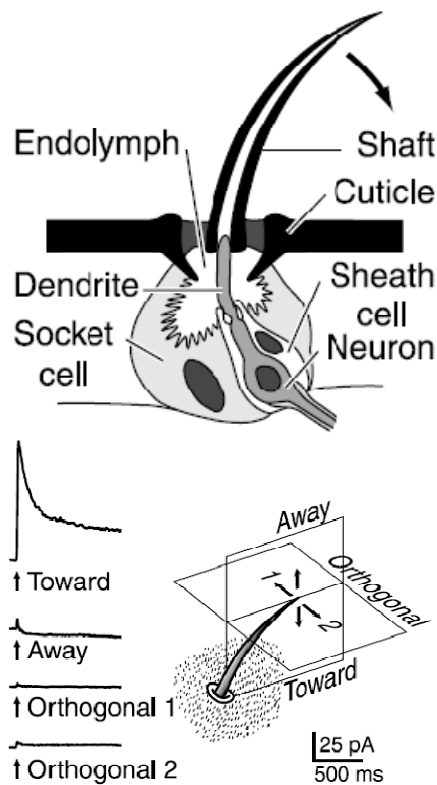
Figure 16   mechanoreceptive bristle of *Drosophila*
Walker et al. used an experiment where they took advantage of the bristles structural organisation. The hollow shaft is filled with an endolymph secreted by the socket cell. This endolymph is isolated from the hemolymph. The dendrite of the sensory neuron protrudes into this endolymph and connects to the base of the shaft. Bristle movements in different directions (lower panel) will lead to different responses of the sensory neuron, which can be recorded by placing a pipette over the cut shaft and thereby measuring a transcuticular potential over the sensory neuron. [131]

nompC was of particular interest because it affected the mechanoreceptor potential responses of sensory bristle neurons in adult flies (Figure 16). Mechanosensitive bristles are innervated by one sensory type I mechanosensitive neuron [36,145]. Measured transepithelial currents and potentials thus are likely to correspond to receptor currents and potentials, respectively. Three different *nompC* alleles, *nompC^1*, *nompC^2*, and *nompC^3*, reduced MRCs drastically (ca. 90% reduction), while the *nompC^4* allele did not change the MRC amplitude but accelerated adaptation [131]. This 'hyperadapting' effect of the *nompC^4* allele is particularly interesting because the MRC and its adaptation are intimately tied to the function and regulation of an assumed mechanotransduction channel. A change in adaptation speed thus suggests that NompC might either be an essential component of the mechanotransduction apparatus or the channel proper. Besides the electrophysiological peculiarities of sensory bristles in a *nompC* mutant background, the predicted 3D structure of NompC seems to support the idea that NompC is a mechanotransduction channel. The main characteristic of NompC that sets it apart from other TRP channels is its N-terminal domain of 29 ankyrin repeats (ANK repeats) - other TRPs that maximally harbour 13 ANK repeats (see Tab.2). It was shown that the 29 ANK repeats of NompC can form a single turn of a spring

[134,146] (Figure 17) and that it mechanically behaves like a spring [147]. The predicted stiffness of a 29 ANK repeat spring (assuming a tetramer constitution of TRPs) matches the predicted stiffness for the gating spring of the hair cell transduction channel [134,147,148]. This structural evidence of an elastic element that might be the actual gating spring further supported the idea of NompC being a mechanotransduction channel.

Figure 17 Predicted 3D structure of a molecule consisting of 29 ankyrin repeats
predicted 3D structure of 29 ankyrin repeats. The structure resembles a spring not only in the looks but also in its stiffness characteristics. [135]

1.9.2 NompC localization

A GAL4-*nompC* promotor construct indicated that *nompC* is only expressed in a subset of JO-neurons [149]. Judged from response characteristics, this subset serves sound-detection, whereas the remnant JO-neurons serve the detection gravity and wind [149,150]. However, recent antibody staining results contradict the GAL4 evidence. Three independently developed antibodies, two antibodies against N-terminal epitopes [135,136] and one against a C-terminus epitope [132], localized the NompC protein at the distal end of the dendritic cilium in virtually all JO-neurons [132,135,136] (Figure 18 & Figure 19). All antibodies show consistent localization, which supports the localization of NompC proximal of the dendritic cap of JO-neurons and distal of their ciliary dilation (further explanation: Appendix D). In chordotonal organs, the null mutations *nomp²* and *nompC³* lead to a complete loss of NompC protein whereas the *nompC⁴* mutation leads to a mislocalization of NompC into the cell body. In flies carrying the P-element insertion *nompC^{f00642,}* the protein localized correctly but the

Figure 18 NompC localization
Antibody staining localizes NompC distal of the ciliary dilation and proximal of the dendritic cap.

expression rate was diminished [135]. In sensory bristles, the *nompC* nulls show no NompC expression whereas the *nompC⁴* mutant shows a diminished expression. The localization of NompC in different sensory organs (*es* and *ch* organs, see Appendix D) supports a role in mechanotransduction. However, the localization of NompC in all chordotonal sensilla of Johnston's organ contradicts the assumption that NompC is only expressed in a subset of JO-neurons, the sound-receptors.
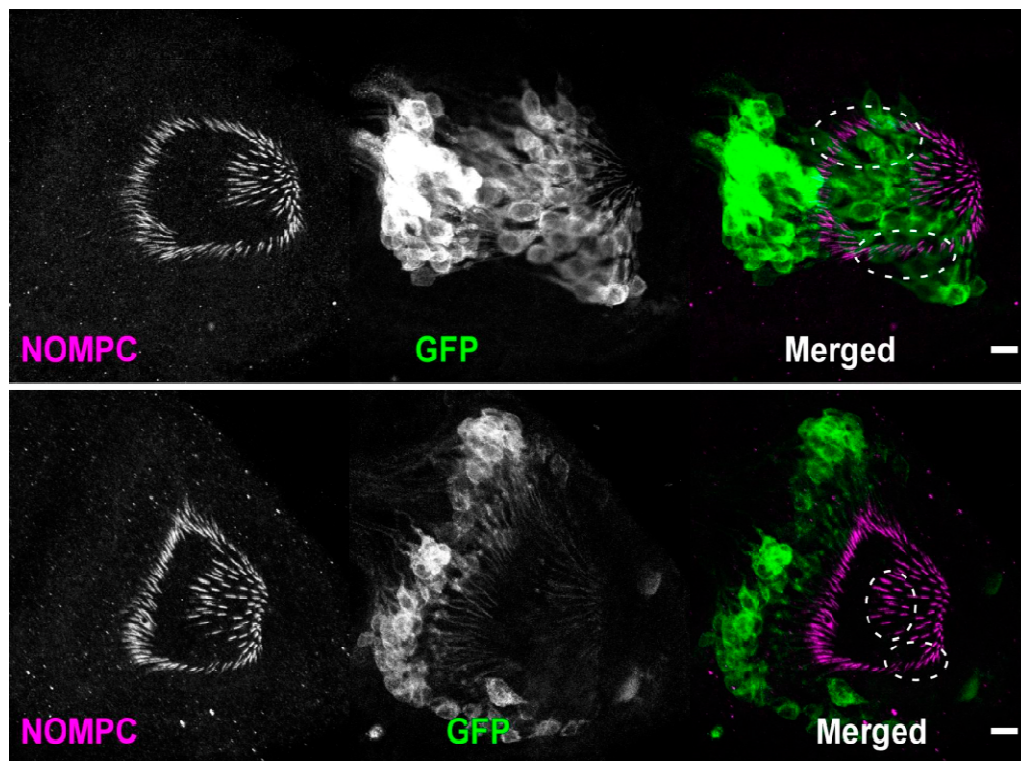
Figure 19 NompC antibody staining and CD8::GFP expression in sound-sensitive respectively gravity/wind-sensitive JO-neurons
Upper panel: NompC antibody staining shows equal distribution of NompC in the distal dendrite of JO-neurons. The merged image shows NompC staining without an associated CD8::GFP signal driven by a sound-sensitive neuron specific GAL4 driver line. Lower panel: NompC antibody staining shows equal distribution of NompC in the distal dendrite of JO-neurons. The merged image shows NompC staining without an associated CD8::GFP signal driven by a gravity/wind-sensitive neuron specific GAL4 driver line after [135]

1.9.3 Is NompC the only MET-channel in *Drosophila*?

It has been shown that the loss of *nompC* reduced but not completely abolished mechanically evoked MRP in sensory bristles and sound-evoked compound CAPs in JO-neurons [131,151]. These remnant responses challenged the idea that NompC is the mechanotransduction channel required for touch or hearing. One explanation for these observations was an additional, mechanotransduction channel that would be present in sensory neurons of bristles and chordotonal organs. This channel would be responsible for remnant responses that persist in *nompC* nulls [131,151]. Support for this hypothesis had come from the discovery that JO houses different subpopulation of mechanosensory neurons that responded to sound or gravity/wind [149].
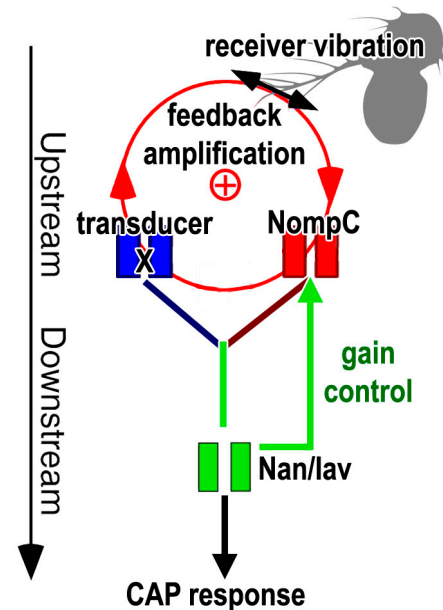
Figure 20 auditory transduction cascade
feedback amplification requires NompC (red). Nan/Iav control the amplification through NompC (green). A NompC independent mechanotransduction channel is responsible for remnant CAPs in *nompC* mutants (blue). All transduction events need Nan/Iav for signal propagation modified from [133]

1.9.4 Other TRPs: Nan & Iav

The TRPV subfamily in *Drosophila* consists of Nanchung (Nan) and Inactive (Iav). They localize to the sensory cilium of JO-neurons, distal of the basal body and proximal of the ciliary dilation (Figure 21). Although both TRPVs are required to generate CAPs in the fly's auditory nerve [116,120], a hyper-amplification and spontaneous self-sustained oscillation of their sound receiver [133] excluded them from the list of possible mechanotransduction channels. Because the
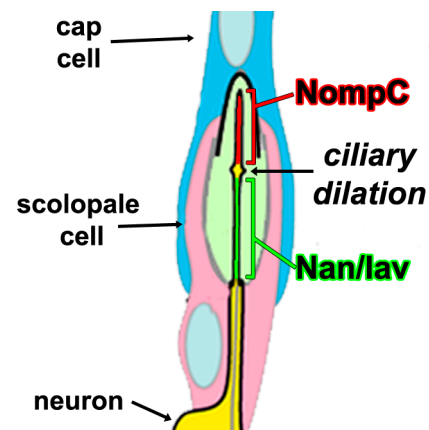
Figure 21 Localization of NompC and Nan/Iav
NompC localizes to the distal part of the dendritic cilium. Nan/Iav localizes to the proximal part of the dendritic cilium.

loss of the mechanotransduction channel should lead to a loss of amplification and not a boost [24,25,40,152]. In addition, a *nompC-nan/iav* double mutant showed no amplification and no sound-induced CAP responses, thus positioning NompC upstream of the TRPV channels in the transduction cascade [133] (Figure 20).

1.9.5   Other TRPs: TRP

TRP is the eponym of the transient receptor potential channel superfamily and was first found as one of two transduction channels (the other being TRPL) in the fly's photo-transduction cascade [105,153-155]. The mutant phenotype of *trp* was first described in the late 1960s [156] by testing for abnormal electroretinogramm (ERG) responses of mutants.

1.9.6   Other TRPs: Painless (TRPA)

Painless (Pain) is involved in the behavioural response to noxious heat stimuli and mechanical nociception [110]. Mutants are indifferent to noxious heat stimuli (≥ 38°C) and harsh touch, while wild-type flies showed avoidance behaviour. *UAS*-reporter constructs under *painless*-Gal4 control showed a broad expression of *painless* in the fly's peripheral nervous system [Kamikouchi preliminary]. Chordotonal type I sensory neurons as well as type II multidendritic neurons seemed to express Painless [130]. Besides its proposed role in nociception and temperature detection, the loss of Painless also abolished the fly's gravytaxis behaviour [130]. Thus, Painless might be required for gravity/wind-receptor function.

1.9.7   Other TRPs: TRPML

TRPML is the sole representative of the TRPML subfamily in *Drosophila,* while mammals possess three TRMLs. This might indicate that in the mammalian TRPML might have been duplicated, at least twice. The mammalian TRPML3 has been implicated in hearing [157,158]. Compared to other TRP-channels TRPML is a rather small protein of approximately 650 amino acids and it has no ankyrin repeats. Mammalian TRPMLs have a function in vesicle transport, calcium homeostasis, and stereo cilia bundle formation [142,158,159].

2. Material & Methods

2.1. Genetic tools to dissect *Drosophila* hearing

Drosophila melanogaster offers powerful genetic tools. The fly's genome is completely sequenced, balancer chromosomes guarantee the stability of established mutations, transgenic animals can be "easily" fabricated, and P-elements allow for an easy introduction of genes into the fly's genome.

2.1.1 P-elements

P-elements have first been described by Kidwell et al. in 1977, as factors causing hybrid dysgenesis, when male P- strains were crossed with female M-strains [160], hence the name "P"-element. Although the functional understanding of P-elements took some more time [161,162] they are now the most common used genetic manipulation method in *Drosophila*. The wild-type (wt) P-element has entered the *melanogaster* family ca. 100 years ago by horizontal gene transfer from other *Drosophila* family members [163]. The wt P-element still harbours its own Transposase enabling it to jump on its own through the *Drosophila* genome in the germ-line. The wt P-element consists of four open reading frames (ORF) flanked by a 5' and 3' inverse terminal repeats of 31 base pairs (Figure 22). The enzyme Transposase cuts the P-element out of the genome by connecting the inverse repeats. A circular DNA strand is formed, which can be inserted elsewhere in the DNA, and the double strand of genomic DNA is rejoined. These excisions are not always precise, thus it happens that fragments of DNA up- or downstream of the P-element

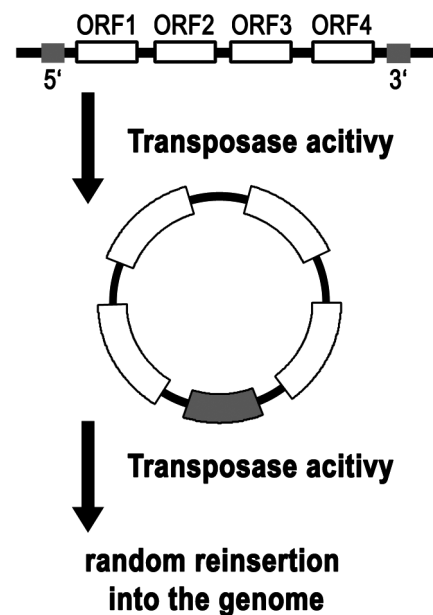**Figure 22 P-element structure and function**

a basic P-element consists of four open reading frames (ORF) flanked by a 5' and a 3' inversed sequence of 31 bp. The enzyme Transposase recognizes this inversed sequences, cuts the P-element out of the genome and joins the 5' and 3' end. Afterwards the P-element is motile and can be inserted by the Transposase at a random position into the genome.

are excised as well. This recombination process normally occurs in the germ-line, due to different Transposase splice variants present in the somatic- and germ-line cells. The somatic-isoform of the Transposase works as an inhibitor of recombination [164-166]. Deletion of as splice variant regulating intron led to a Transposase, which was active in any tissue [167]. The necessary restriction of P-element motility was achieved by removing the Transposase sequence from the P-element. The genomic insertion site of the P-element was thus stable. To remobilize the P-element one had to cross those fly-strains against Transposase-strains, which contained an active Transposase. Having the control over the P-element motility was the most important step to use it as a genetic tool. The most apparent use of this technique was to produce mutants where the P-element insertion disrupted a genes function. This was done by injecting cyclic P-elements into the region of an embryo that would form the germ cells. Embryos with an active Transposase would randomly insert those P-elements into their germ cells. The offspring of these flies would thus yield mutants, each having a random insertion of a P-element into its genome [168]. A second use of the P-elements was to use them as shuttles to introduce genes of interest into a fly's genome. The technique was the same as disrupting a genes function but with the difference that not the disruption of genes was the target but the insertion and expression of a gene of interest [169,170]. Over the past decades, those P-element techniques were used to:

- Screen for tissue specific enhancers (enhancer trapping) [171-174]
- Disrupt gene function (gen trapping) [175,176]
- Deletion of bigger portions of DNA (creating deficiencies) [177-179]
- Targeted deletion/silencing of genes by hijacking the homologous recombination system [180,181]

Besides the classical P-element, a second transposon, Minos-element originally from *Drosophila hydei*, has been introduced and successfully mobilised in *Drosophila melanogaster*. Further information on P-element function is given by the Reviews of Ryder & Russel [163], Engels [182], and Hummels & Klämbt [183].

2.1.2 GAL4/UAS System

The GAL4/UAS System is based on the transgenic expression of two yeast-derived genes and allows for tissue- and/or time specific ectopic gene expression in *Drosophila melanogaster* [174,184], reviewed [185]. GAL4 is a transcriptional activation factor [184,186-190] and the UAS **U**pstream **A**ctivation **S**equence (UAS) its natural target motif (Figure 24). Once a GAL4 homodimer binds to a UAS motif, translation of genes downstream of the UAS is facilitated [191] (Figure 23). This process is used for example in enhancer trapping experiments. In these cases, a GAL4 sequence is randomly introduced into the fly's genome with a P-element. If by chance the GAL4 inserted near an enhancer, that enhancer will control the GAL4 expression. If a UAS is present in the fly's genome GAL4 homodimers will bind to that UAS in all cells where the enhancer is active. If an eGFP is positioned downstream of the UAS motif, the GAL4/UAS system can thereby be used to screen for tissue/time specific enhancers. Once such GAL4 lines are established they can be used to express any kind of gene tissue or time specific [149].
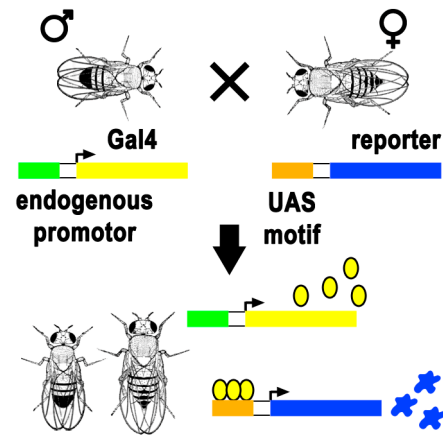
Figure 23 Gal4/UAS system schematic

An endogenous promoter region regulates the specific expression of Gal4. The Gal4 proteins promote the expression of the reporter-protein by binding the UAS motif. Increase in UAS motifs can yield higher expression rates.
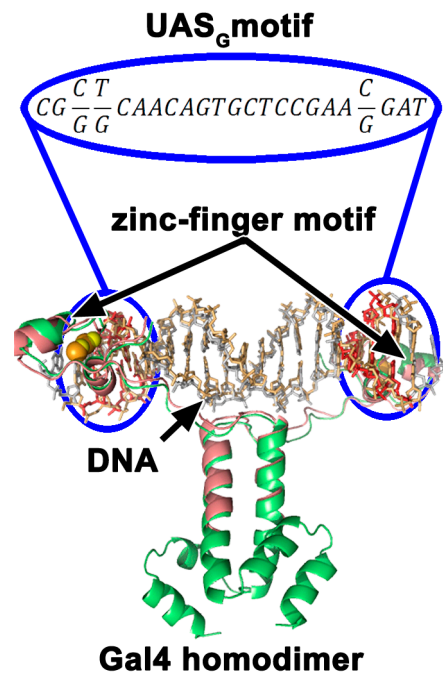
Figure 24 Gal4 homodimer bound to UAS motif

The transcription factor Gal4 originates from yeast. Its targets sequence is the UAS-motif. The motif consists of two repetition á 23 bp separated by 55 bps. Modified from [184,186]

2.1.3   In vivo calcium imaging
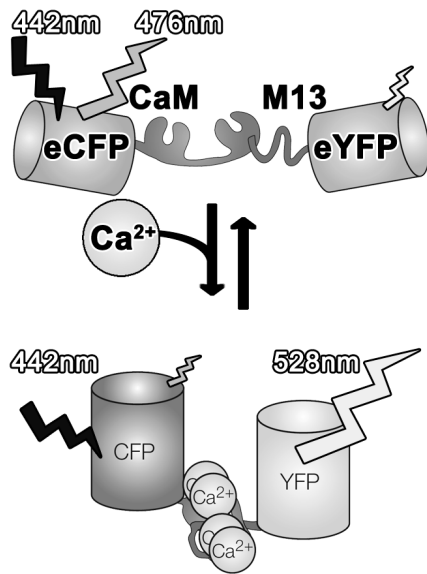
Figure 25 changes of *cameleon 2.1* while binding Ca^{2+}
enhanced cyan fluoresent protein (**eCFP**), calmodulin (**CaM**), calmodulin binding domain (**M13**), and enhancend yellow fluoresent protein (**eYFP**). At an excitation wavelenght of 442nm, without calcium bound to the calmodulin, the majority of emitted light has a wavelenght of 476nm. Once calcium bind to calmodulin the protein changes its structure and binds to the M13 domain, bringing the eCFP and eYFP near to one another (<10nm). Thus an Förster resonance energy transfer occurs (FRET) and the majority of emitted light shifts to a wavelenght of 528nm. modified from [199]

Cameleon 2.1 is a calmodulin based calcium indicator. The fusion protein consists of a calmodulin, a calmodulin binding domain (M13), an eCFP (**e**nhanced **C**yan **F**luorescent **Pr**otein), and an eYFP (**e**nhanced **Y**ellow **F**luorescent **Pr**otein) [192,193]. The eCFP is fused to the N-terminus of the calmodulin; its C-terminus is fused to the M13 domain, which is than fused to the eYFP (eCFP ► calmodulin ► M13 ► eYFP; Figure 25). Under normal conditions the eCFP has a peak-light-absorption at 442nm and emits light at 476nm; the eYFP has a peak-light-absorption at 480nm and emits light at 528nm. Using an excitation wavelength of 442nm should thus lead to a light emission at 476nm. However, if calmodulin binds Ca^{2+}, the protein will change its structure, bind to the M13 domain, bringing the two fluorescent proteins close to one another, and thus allowing for a Förster resonance energy transfer (FRET; distance <10nm) between the eCFP and eYFP. Measuring the ratiometric change between the light emissions at 476nm (eCFP) and 528nm (eYFP) provides thus a possibility to monitor the increase and decrease of intracellular calcium-levels respectively of the buffered calcium [149,194-200]. The biggest advantage of this FRET based calcium indicator protein is that it is a protein. Hence, the expression of *cameleon2.1* under different GAL4 driver lines allows for an *in-vivo* dissection of Johnston's organ [201].

2.1.4   Tissue specific, conditional cell ablation

The holotoxin ricin is classified as a type 2 ribosome inactivating protein (RIP), it consists of the active A-chain [202] and a B-chain [203-205] (Figure 26, middle panel) that facilitates the uptake of the A chain into the cytosol [206]. It occurs naturally for example in the castor bean (*ricinus communis* [207]; Figure 26, upper panel) together with the ricin toxin B chain. The catalytic active A chain targets the 28S RNA in the ribosomal 60S subunit of eukaryotes and cleaves a glycosidic bond within the rRNA. Thus, the elongation factor-2 fails to bind to the ribosomes and translation is blocked. In eukaryote ribosomes the target motif is 5'-AGUACGAGAGGA-3', coined the 'sarcin-ricin loop' [206,208-213]. A single ricin toxin A chain molecule is capable of cleaving ca. 1500 ribosomes per

Figure 26 ricin toxin
Upper panel: the holotoxin ricin consists of a catalytic A chain and a B chain that facilitates the uptake into the cytosol. The catalytic A chain targets the 28S RNA of the ribosomal 60S subunit and cleaves a glycosidic bond, thus rendering the ribosomes unable to bind the elongation factor-2, thereby effectively blocking translation. Lower panel: UFWTRA P-element containing a UAS-motif, a mini-white gene framed by two half-FRT sites, and a ricin toxin A chain encoding sequence [213].

minute. In this thesis, the GAL4/UAS system was used to express the ricin toxin A chain in different JO-neurons subpopulations and thus ablate them tissue specific. To this end a mutant fly strain carrying the UFWTRA-vector [214] was crossed against tissue specific GAL4 strains (JO1, JO15, JO31 [215]). The UFWTRA-vector contains an UAS motif, followed by a *mini-white* gene framed by two half-FRT sites, a polyA sequence as a separator and the ricin toxin A chain encoding sequence (Figure 26, lower panel). The FRT sites allowed for a conditional expression of ricin under heat shock control of FLP activity (see 2.1.5 eyFLP [201,216]).
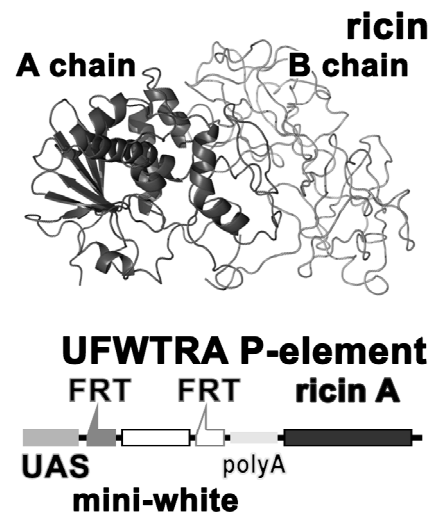
2.1.5 eyFLP

Flippase recognition target

GAAGTTCCTATTCtctagaaaGTATAGGAACTTC
CTTCAAGGATAAGatctctttCATATCCTTGAAG

Promo FRT **STOP** FRT   Reporter

↓ **Flippase activity**
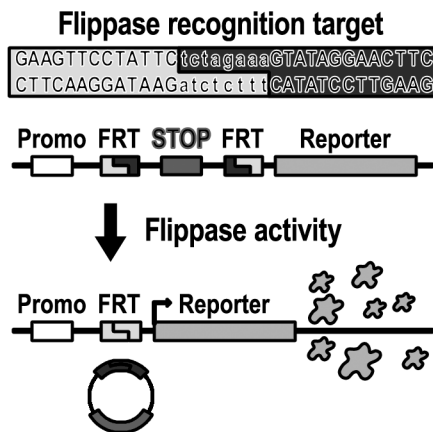
Promo FRT ↱ Reporter

Figure 27 FLP/FRT
The Flippase (FLP) recognizes a 34 bp
long DNA sequence (FRT) and cleaves it
asymmetrical. The cleaved ends joine to
form a circular DNA strand containing
one FRT site, leaving one FRT in the
genome. E.g. the excision of a stop
codon (red) would allow the reporter
protein to be expressed under promoter
(Promo) control.

The FLP/FRT [217] system is used to gain mosaic gene expression in targeted tissue [218]. The enzyme Flippase (FLP) originates from the 2μm plasmid of yeast (*S. cerevisiae*) and recognizes a 34 base pair long motif (5'-GAAGTTCCTATTCtctagaaaGTATAGGAACTTC-3'; FRT: **f**lippase **r**ecognition **t**arget). If two FRT sites are near one another and correctly aligned (inversed sequences opposing one another), the FLP binds to the first 13 base pairs and cleaves the DNA double strand asymmetrical before respectively after the eight central base pairs (5'….tctagaaa….3'). The cleaved DNA strand is than joined forming a circular DNA strand containing one FRT site and leaves one FRT site in the genomic DNA [219] (Figure 27). This process can work backwards leading to an insertion of a circular DNA strand into the genomic DNA at a FRT site. FLP expression is heat shock controlled, thus allowing for a mosaic expression during short heat shock durations. In practice it comes all down to statistics, a heat shock of a given time and a given intensity has a certain probability to induce FLP expression and thereby FRT site cleavage [214]. If the heat shock is short and has a low intensity the FLP expression probability is low, thus only a small number of cells will express FLP hence only in a few cells a cleavage of the FRT sites occurs. Cleaving the two FRT-sites will excise a stop codon allowing the translation of a downstream gene (in case of this thesis: ricin toxin A chain). I used a slightly altered FLP/FRT system [216], which contained besides the FLP also a functional fragment of the *eyeless* enhancer sequence, thus the FLP would only be expressed in the eye and the antennae of heat shocked flies, thus guarantying FLP activity only in cells of interest, the neurons of Johnston's organ.

2.2. Fly Lines

Tab. 3 List of mutants used during the thesis

genotype	allele	mutation
nompC	*nompC²*	W_{1266}stop
	nompC³	K_{747}stop
	nompC⁴	$C_{1400}Y$
	nompC^{f00642}	P-element insertion PBac{WH}*nompC^{f00642}* 2L:5,352,777
nompC rescue	*UAS-nompC-L*	Long splice variant rescue (1732 amino acids)
trp	*trp¹*	effective null, loss of function allele, spontaneous mutation
trpml	*trpml¹*	Imprecise excision -456 to +641 relative to *trpml* translation start site
painless	*pain¹*	P-element insertion P{EP(2)2451} 2R:20,815,805
	pain²	P-element insertion P{EP(2)2621} 2R:20,815,781
	pain³	P-element insertion P{EP(2)2251} 2R:20,815,790
inactive	*iav¹*	Q_{455}stop
nanchung	*nan^{36a}*	imprecise excision -1450 to +575 relative *nan* translation start site
	nan¹	imprecise excision -3330 to +1746 relative to *nan* translation start site

Tab. 4 List of used GAL4- and UAS-strains

Gene	Type	Description
JO1	*Gal4-line*	A.k.a. NP0761. Gal4 expression in Johnston's organ subpopulations: A,B,C,D,E Johnston's organ subzones: AA AP AV1 AV2 AD BI BO CL CM DA DP EVM EVP EDM EDP EDC
JO2	*Gal4-line*	A.k.a. NP1046. Gal4 expression in Johnston's organ subpopulation: B Johnston's organ subzones: BI BO
JO15	*Gal4-line*	Gal4 expression in Johnston's organ subpopulation: A,B Johnston's organ subzones: AA AP AV1 AV2 AD BO
JO31	*Gal4-line*	A.k.a. NP6250. Gal4 expression in Johnston's organ subpopulation: C,E Johnston's organ subzones: CL CM EVM EDM EDP EDC
Cameleon2.1	*UAS-fusion construct* 2nd *chromosome*	Calcium indicator fusion protein on the 2nd chromosome *calmodulin* fused at its N-terminus with eYFP and at its C-terminus with eCFP
	UAS-fusion construct 3rd *chromosome*	Calcium indicator fusion protein on the 3rd chromosome *calmodulin* fused at its N-terminus with eYFP and at its C-terminus with eCFP
UFWTRA	*UAS-fusion construct* 3rd *chromosome*	The vector UFWT containing a mini-white gene flanked by two FRT sites and a downstream ricin chain A encoding gene.
eyFLP	*UAS-fusion construct* 2nd *or* 3rd *chromosome*	Flippase fused to a functional fragment of the *eyeless* promoter. Heat shock inducible expression of Flippase in the eyes and antennae

2.3. Fly mounting

2.3.1 Mounting for mechanical measurement

Stimulus unrelated movements had to be minimal. Environmental vibrations were cancelled by the use of an air table. Unwanted animal movements were prevented by a thorough fixation of the animal using wax and dental glue. The only possible movement after fixation was the rotation of the 3rd segment about its longitudinal axis relative to the 2nd segment (Figure 28, detailed description Appendix D). Technique adapted and refined [24,54,133] (List of equipment see Appendix E.1).

2.3.2 Mounting for *in-vivo* calcium imaging

The fixation for the calcium measurements had the same requirements in terms of movement restriction but in addition, it had to allow for *in-vivo* calcium imaging.
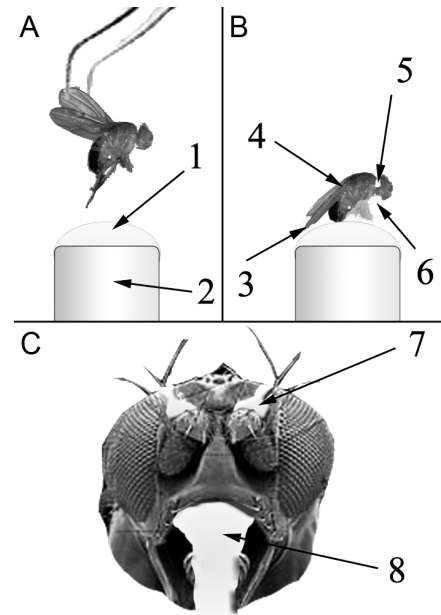

Figure 28 Fixation of the fly
Flies were narcotized with CO2. Then they are taken by the wings and put into a wax mixture (1, beewax/paraffin) on top of a Teflon rod (2). Then the head (5), the wings (3), the halters (4), and the thorax (6) were stabilized with the wax. The pedicels (7) and the mouthparts (8) were fixed to the head with dental glue.

The fixation first described by us [56,197] was refined to achieve a higher reproducibility, reliability, and to provide for new experimental demands. The fly's legs were removed; a small drop of dental glue was put between head and thorax on the dorsal site; more dental glue was put on the dorsal thorax; the thorax dorsal site was put on a cover slip; the viscous glue allowed for changes in position of the head and thorax until a satisfying position was achieved; the glue was hardened; a very small drop of dental glue was placed between the lateral site of the right pedicel and the head; the pedicel was moved into a position in which the funicle was perpendicular to the cover slip; the glue was hardened; glycerol was placed in the gap between pedicel and cover slip. To allow for the simultaneously recording of nerve responses an indifferent tungsten electrode was

inserted into the thorax and a recording electrode into the head, next to the antennal nerve. An electrostatic probe was used to actuate the antenna; it was placed in front of the right antenna's arista. The indifferent electrode served as charging electrode for the electrostatic stimulation.

2.4. Mechanical Measurements

2.4.1 Free fluctuations of the sound receiver

All objects, animate or inanimate, fluctuate with an individual frequency spectrum. The fly's sound receiver is no exception. The LDV was used to measure the free fluctuations of the fly's sound receiver by putting the laser point on the tip of the arista. The only factors that can contribute to the free fluctuation are intrinsic effects of the sound receiver and the thermal energy introduced by the bombardment with air particles. The LDV allows precise measurements of the sound receiver's velocity (nm/s resolution). A **F**ast **F**ourier **T**ransform (FFT; $\tilde{X}(\omega)_n = \int_{t_n}^{t_{n+1}} \dot{X}(t) e^{i\omega t} dt$) of the velocity time trace is conducted online by the LDV software. This transformation provides the frequency dependent velocity characteristic of the sound receiver. The LDV software also calculated the one sided power spectral density (nm²/Hz). The integral of the power spectral density between 100 and 1500 Hz was defined as the systems power (nm²) that related to the system's energy content. Thus, comparison of the power values of different mutants is a way to estimate the impact of mutations on the system's energy content.

2.4.2 Sound-induced intensity characteristic of the sound receiver

Pure tones at the iBF with different amplitudes (ranging over 96 dB) were produced with a loudspeaker/HiFi-system. Stimulus particle velocities were assessed with an Emkay NR 3158 pressure-gradient microphone as described [137]. Antennal displacements were monitored at the tip of the arista with a Polytec PSV-400 laser Doppler Vibrometer equipped with an OFV-700 close-up unit. CAPs were recorded with an electrolytic tapered tungsten electrode inserted between the 1st antennal segment and the head, with the indifferent electrode

placed in the thorax. Signals were digitized at a rate of 12.1 kHz and subjected to Fast Fourier transforms (FFT, 1 Hz frequency resolution). Signal FFT-amplitudes were measured as phase-locked amplitudes at the frequency of stimulation. Only CAP amplitudes were measured at twice the stimulus frequency because of frequency-doubling in CAPs produced by JO (1.1.4). The individual CAP response of each sound receiver was normalized $((V-V_{min})/(V_{max}-V_{min}))$, and fitted with a Hill-equation with four free parameters, y_{min}, y_{max}, m, and n $(f(x) = y_{min} + \frac{(y_{max}-y_{min})}{(1+|x/m|^n)})$. Thresholds were defined as the sound particle velocity/antennal displacement amplitude at which 5% of the maximum Hill fit amplitude was reached. The region between 5% and 95% of the maximum Hill fit amplitude was defined as dynamic range. Data analysis and statistical data evaluation were performed using PSV-VIB (Polytec), Spike 2 (Cambridge Electronic Design), Excel 2007 (Microsoft) and Sigma Plot 10 (Systat Software).

2.4.3   Gating compliance measurements

I used electrostatic actuation to apply force steps onto the antennal sound receiver. Jörg Albert described this method first for flies [24] and I improved and adapted it. Together with Dr. Albert I improved the technique by introducing two instead of one electrostatic probe, to equally push and pull the antennal receiver. In addition, we kept the animal on a static potential of -100 V over ground to compensate for polarization effects. Thus, we improved the linearity of applied forces. I used bipolar tungsten stereotrodes (WE3ST31.0A5 and WE3ST31.0A10, Micro Probe, Inc.) as actuator probes. The probes were aligned in the optical axis of the LDV anterior and posterior of the arista (Figure 29). The probes could be charged up to ± 400 V. This increased the possible forces acting on the antennal sound receiver and allowed to
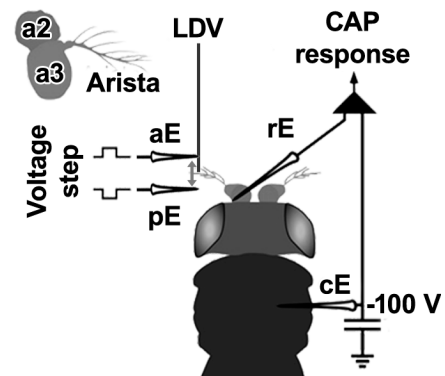

Figure 29 gating compliance setup
One bipolar electrode was positioned anterior (aE) and a second posterior (pE) of the arista. The fly was held at a static potential of -100V over ground via a charging/indifferent electrode (cE). The LDV recorded the antennal displacement and a recording electrode (rE) allowed for a simultaneous recording of the CAP response. Modified from [24]
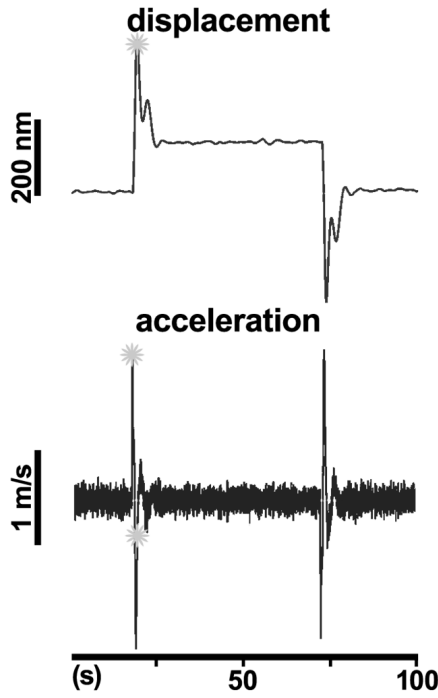
Figure 30 typical displacement response to a force step
To calculate the dynamic stiffness K_{peak} and the linear stiffness K_{steady} the external forces and the peak-respectively steady-displacement had to be measured. The force relates to the acceleration of the sound receiver by its apparent mass. With a mass of 5 ng the acceleration provided the external force. By subtracting the acceleration at the displacement peak from the onset acceleration, we corrected for inertia.

position the probes further away from the antenna, to compensate for the quadratic relation between stimulus voltage and force (previous measurements used only ± 40 V). The antennal displacement was monitored with the LDV and the CAP response was simultaneously recorded (Figure 30). We distinguished two different stiffnesses: K_{steady} and K_{peak}. K_{steady} is contributed by the combined stiffness of the a2/a3 joint and of structures that suspend JO but are not contributing to the mechanical stimulus coupling [25] from the sound receiver to the mechanotransduction channel, as such K_{steady} is linear. K_{peak} is contributed by the gating spring and the dynamic stiffness changes based on the opening and closing of transduction channels. Thus K_{peak} is nonlinear and depends on the acting force, the number of channels, their open probability, the gating swing, and the energy needed to gate a single channel.

2.4.3.1 Force estimation & stiffness calculation

Stiffness is the ratio between external force and displacement $K = \frac{F}{x}$. The displacement was measured with the LDV. The external force, however, could not be directly measured. Hence, we deduced the external force from the receiver's initial acceleration ($\ddot{x}_{onset}$) upon stimulus onset and its apparent mass (m). At a given mass of 5 ng [54] this equation provides an estimate for the external force acting on the antennal sound receiver. For K_{steady} we assume that the displacement at the end of the step only depends on this external, onset force. Thus, K_{steady} can be written as $K_{steady} = \frac{m\ddot{x}_{onset}}{x_{endofstep}}$ and should be linear over the

complete range of forces. Previous work had shown that K_{steady} was ca. 50 µN/m [24]. Whereas K_{steady} was linear and only depended on the onset acceleration, the dynamic stiffness, K_{peak}, depended on the external force but also on the mass of the sound receiver. Hence, I had to correct the external force derived from the onset acceleration for the inertia of the sound receiver. This was done by subtracting the acceleration at the displacement peak [24]) from the onset acceleration $F = m(\ddot{x}_{onset} - \ddot{x}_{peak})$. K_{peak} was thus calculated based on the peak displacement, the acceleration at the onset of the step, and corrected for inertia by subtracting the sound receivers acceleration at the peak. Accordingly it read

$$K_{peak} = \frac{m(\ddot{x}_{onset} - \ddot{x}_{peak})}{x_{peak}}.$$

2.4.3.2 Scaling of individual sound receivers based on their apparent mass

To compare the gating compliance of individual sound receivers they had to be normalized. Previously this had been done by dividing K_{peak} by K_{steady}. This however resulted in the loss of absolute amplitudes. I chose instead to use the apparent mass to scale and normalize the stiffness responses of individual sound receivers of one genotype. I corrected the apparent mass for each individual sound receiver such that the average K_{steady} of the genotype was reached. To facilitate comparison, I shifted K_{steady} and K_{peak} until an average K_{steady} of 50 µN/m was achieved and plotted the gating compliance relative to the peak antennal displacement. Thus, I retained absolute stiffness amplitudes and was able to compare between different flies of the same genotype and between genotypes. To check for the legitimacy of this method I conducted several experiments on anesthetized animals and deduced their apparent mass by fitting a simple harmonic oscillator to the free fluctuations of their sound receivers. The resulting apparent masses were in the range needed to scale the flies of one genotype. The maximal difference in apparent mass needed to scale an individual sound receiver was 15%.

2.4.3.3 Gating compliance

I used a simplified version of the gating spring model without adaptation motors $K(x) = K_{inf} - \left(\frac{Nz^2}{k_BT}\right) * P_O(1 - P_O)$. K_{inf} is the asymptotic stiffness adopted by the system at infinite displacements. It comprises the linear, passive stiffness K_{steady} and the gating spring stiffness (K_{GS}). N is the number of channels, z the single channel gating force, and P_O the channel open probability: $P_O = 1/(1 + e^{-((x-x_0)/k_BT)*z})$. The relation between K_{GS} and z is given by $z = \frac{K_{GS}}{N\gamma} d$, where γ is the scaling factor between neurons and sound receiver and d the gating swing. z can also be written as $z = \gamma\kappa d$, where κ is the single channel gating spring and relates to K_{GS} by $\kappa = \frac{K_{GS}}{N\gamma^2}$. The parameters K_{inf}, N, and z were fitted. This equation describes the stiffness changes (gating compliance) of one channel type. Based on the assumption that NompC is a mechanotransduction channel and remnant CAP responses in *nompC* mutants remained I assumed that a second mechanotransduction channel type must be present in JO-neurons. Accordingly, I introduced the term $\left(\frac{N_i z_i^2}{k_BT}\right) * P_{Ob}(1 - P_{Ob})$, which represented the gating spring equation for a second channel type. The equation than reads $K(x) = K_{inf} - \left(\frac{N_s z_s^2}{k_BT}\right) * P_{o\_s}(1 - P_{o\_s}) - \left(\frac{N_i z_i^2}{k_BT}\right) * P_{o\_i}(1 - P_{o\_i})$ (Figure 31)This leads to a set of five free parameters: K_{inf}, N_s, z_s, N_i, and z_i. The initial parameter values for N_s, z_s were taken from [24]. Sigmaplot 10 was used for fitting. The fit of the sound receiver mechanics provides the open probability of the mechanosensitive channels. The given parameters z_s and z_i were used to calculate a P_{o-all} for all mechanotransduction channels.

$$P_{o-all} = \left(1/1 + e^{-\frac{(x_{peak}*z_a)}{kBT}} + 1/1 + e^{-\frac{(x_{peak}*z_b)}{kBT}}\right) * \frac{1}{2}.$$

single channel situation

$$K(x) = K_{inf} - \left(\frac{N_a z_a^2}{k_B T}\right) * P_{Oa}(1 - P_{Oa})$$

two channel situation

$$K(x) = K_{inf} - \left(\frac{N_a z_a^2}{k_B T}\right) * P_{Oa}(1 - P_{Oa})$$
$$- \left(\frac{N_b z_b^2}{k_B T}\right) * P_{Ob}(1 - P_{Ob})$$
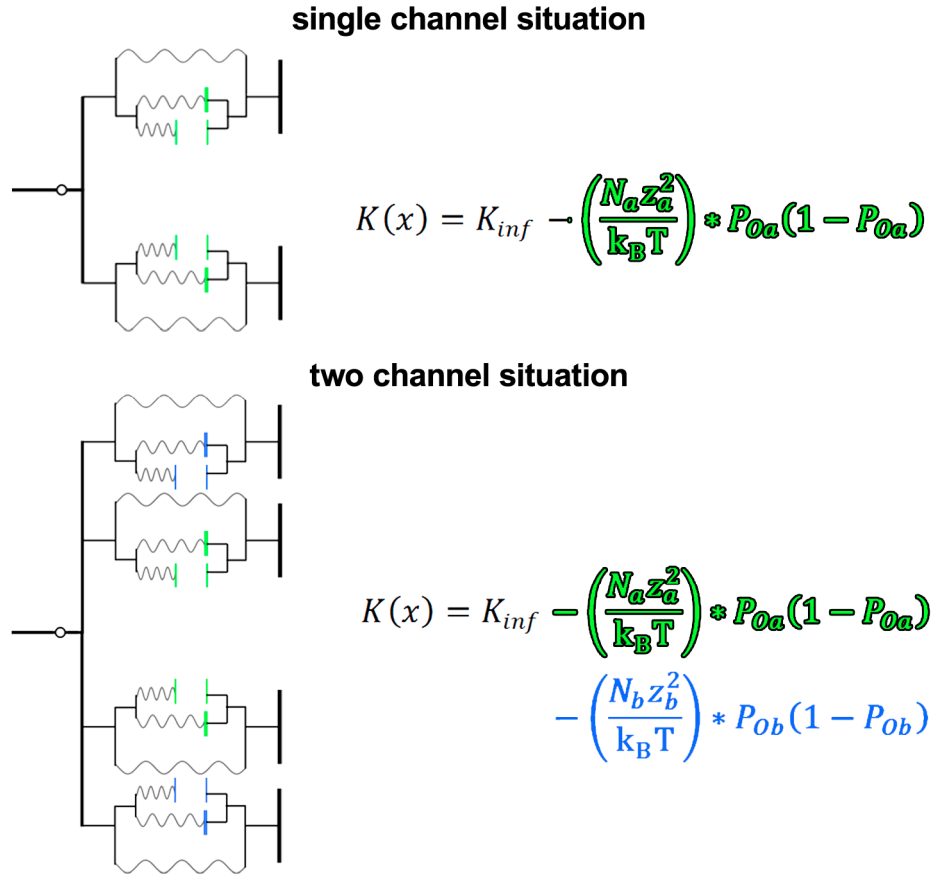
Figure 31 equations describing the single channel population situation and the two channel situation
The single channel equation comprises the parallel stiffness and the dynamic stiffness changes of a single type of mechanotransduction channel. These channels are arranged symmetrically around the a2/a3 joint. In the two channel equation system a second term describing a second type of mechanotransduction channel is added. Altered after Nadrowski unpublished.

2.4.4 *In-vivo* calcium imaging
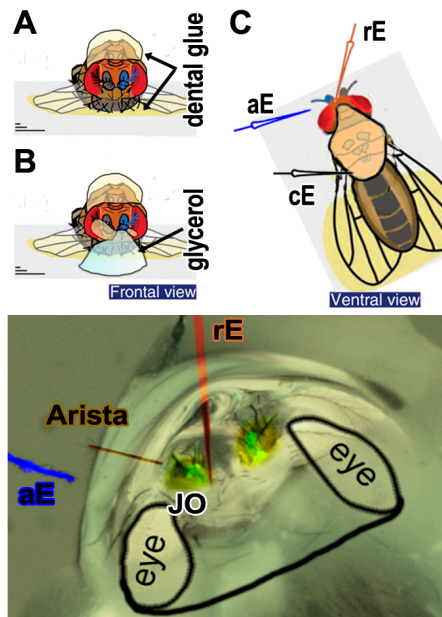
Figure 32 Schematic of calcium preparation

Upper panel A: The animal was glued with its dorsal site onto a cover slip, the legs removed, and the leg stub closed with glue. B: The left antenna and the pedicel of the right antenna were glued to the head capsule. Glycerol was placed between the right pedicel and the cover slip. C: A recording electrode (rE) was inserted next to the antennal nerve, an electrostatic actuator electrode (aE) was positioned near the arista, and a charging/indifferent electrode was inserted into the thorax. Altered after [197] Lower panel: The electrostatic actuation electrode (aE), the recording electrode (rE), and the Arista are visible.

An electrostatic actuator electrode was used to apply sinusoidal stimulation to the antennal sound receiver over a stimulus range of ca. 80 dB. Stimulus intensity, antennal displacement at the tip of the arista, CAP responses, and changes in intracellular calcium (as described [197]) were measured simultaneously. The CAP responses were recorded at twice the stimulus frequency (see also 2.6.3). To cancel stimulus artefacts in the CAP recordings, successive stimuli were phase shifted 180° and even numbered. An average from 10 stimulus repetitions at different stimulus intensity was calculated. A Cameleon two-filter set (455 nm DCLP, 515 nm DCLP, 535/30 nm emission filter, 485/40 nm emission filter, Chroma Technology) and a Dual View beam-splitter (Photometrics DV2) were used for detecting the eCFP and eYFP images simultaneous with a CCD camera (Photometrics Cascade II 512). Regions of interest (ROI) were defined and allowed for an online recording of eCFP and eYFP fluorescents intensities (Figure 32). These fluorescence intensities were corrected during data analysis to compensate for bleaching effects by adjusting each individual response. The ratios between the eCFP and eYFP fluorescent intensities were calculated and fitted with either a single-exponential- (*JO31* and *JO15* driven *cameleon2.1* expression) or double-exponential (*JO1* driven *cameleon2.1* expression) equation. The maximum, asymptotic values of the fits were plotted against the antennal displacement.

3. Results

I tested the effect of the TRP channels NompC, Nanchung, Inactive, TRP, Painless, and TRPML on JO function. I started with NompC, which was previously implicated in touch sensation and hearing in *Drosophila* (1.9).

3.1. NompC: compound action potential measurements

3.1.1 Residual sound-evoked nerve potentials in *nompC* mutants and flies with ablated sound-receptor cells

Previous observations [131,151] have shown that *nompC* mutants display remnant touch-evoked potential responses of mechanosensitive bristles and remnant sound-evoked CAPs in their JO-nerve, respectively. To assess the residual responses in the JO-nerve, I exposed the flies to pure tones at the individual best frequency (iBF) of their antennal sound receiver and recorded the ensuing antennal displacements and CAPs. Stimulus particle velocities were varied between ca. 0.001 and 10 mm/s to assess the intensity characteristics of their CAP response. Robust CAP responses were observed in $nompC^2$, $nompC^3$ mutants, and in flies carrying the weaker allele $nompC^4$. The maximal amplitudes of CAP responses were ca. 6 times smaller in *nompC* mutants than those of wild-types and controls (Figure 33). JO1 (all JO neurons) driven expression of *UAS-nompC-L* [132] rescued the *nompC* mutant phenotype and maximum CAP-response amplitudes reached the wild-type/control level (Figure 33). Reduced CAP amplitudes as observed in *nompC* mutants also ensued when JO sound-receptors were ablated by cell type-specific expression of ricin toxin A chain (Figure 33, 2.1.4). Cell ablation was confirmed by simultaneously expressing a GFP-reporter. Unlike the ablation of sound-receptors, ablating only the gravity/wind-receptors did not change the CAP amplitudes, which resembled those of wild-types and controls (Figure 33). The remnant response in flies with ablated sound-receptors illustrates that sound-evoked potentials in the antennal nerve are not only contributed by JO sound-receptors, suggesting that sound-evoked nerve potentials partly arise from gravity/wind-receptor cells.
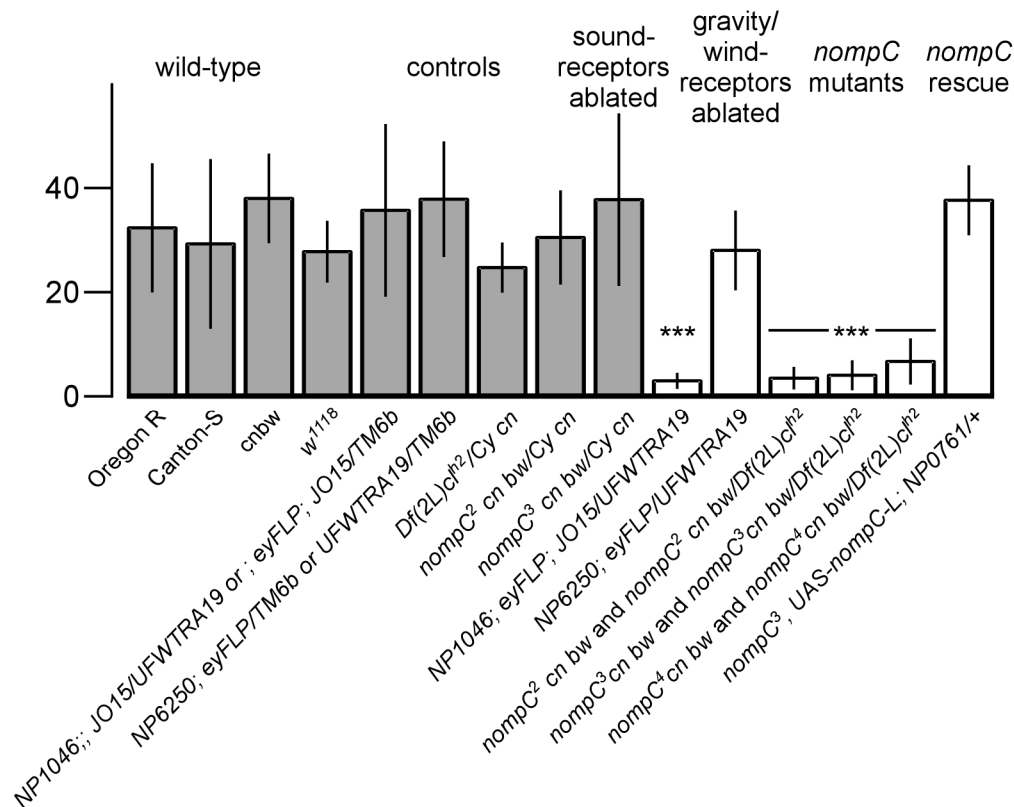
Figure 33 Maximum CAP response amplitudes (µV)
wild-type/controls, gravity/wind-receptor ablated, and *nompC* rescue flies show comparable maximum CAP response amplitude. The response of the *nompC* mutants and sound-receptor ablated flies is ca. six times smaller. (±1 STD; ***: P < 0.05, two-tailed Mann Whitney U-tests against control and wild-type strains (N = 4 –20)

3.1.2 *nompC* mutants and sound-receptor ablated flies lack sensitive hearing

Plotting CAP responses against the sound intensity provides an overall measure of auditory sensitivity, including the mechanical sensitivity of the antenna to sound stimulation and the sensitivity of JO to antennal displacements. To directly assess the displacement-sensitivity of JO-neurons, I first plotted the CAPs directly against the corresponding antennal displacement.

3.1.2.1 Displacement sensitivity of JO-neurons

In addition to reducing sound-evoked CAP potentials, mutations in *nompC* impair sensitive hearing. This reduction in JO-neuron sensitivity became apparent when I plotted the relative CAP amplitudes against sound-induced antennal displacements (Figure 34). A Hill equation was used to fit the CAP response. The threshold of CAP response onset was defined as the displacement corresponding

to 5% of the maximum amplitude assumed by the Hill-Fit. In wild-type and control flies, antennal displacements of 50 ± 8 nm were sufficient to elicit CAPs, and the CAP amplitude increased monotonously for displacements between ca. 50 and ca. 600 nm (Figure 34). In *nompC* mutants, this dynamic range of the CAP response consistently shifted to antennal displacements between 190 ± 7 nm and 1992 ± 79 nm, corresponding to a ca. 4-fold sensitivity drop (Figure 35). This shift was consistently observed in all *nompC* mutants
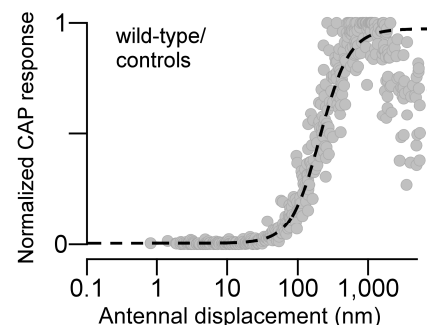
Figure 34 normalized CAP responses of wild-type & control flies plotted against antennal displacement (nm)

normalized (see 2.4.2) CAP responses of fitted with a Hill equation. 5% of the Hill fit's maximum amplitude was defined as threshold. The wild-type and control dynamic range of CAPs was from ca. 50 to ca. 600 nm. [N=15]

(see Tab. 6). JO1 driven expression of *UAS-nompC-L* rescued the *nompC* mutant phenotype and restored the dynamic range to displacements between 48 ± 4 nm and 742 ± 81 nm (Figure 35). The sensitivity shift observed in *nompC* mutants also characterized flies with ablated sound-receptors (233 ± 109 nm to 3187 ± 1913 nm; Figure 36). Ablating the gravity/wind-receptors, however, did not change displacement sensitivity or the dynamic range (46 ± 13 nm and upper threshold 759 ± 261 nm; Figure 36, Figure 37) [201].
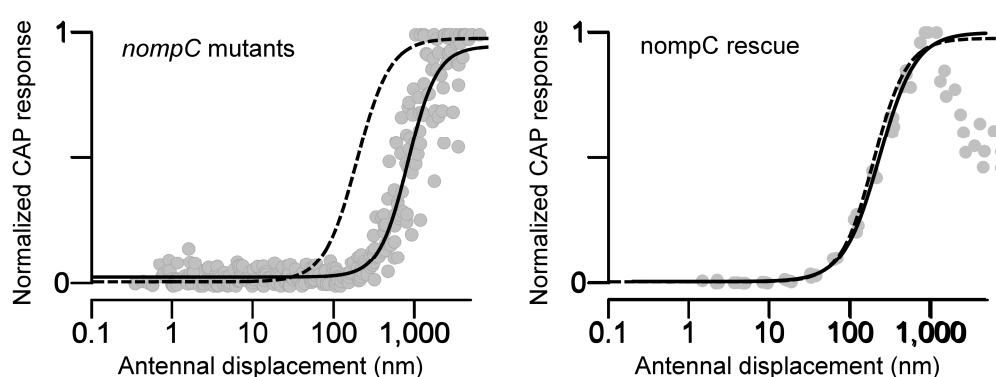
Figure 35 normalized CAP responses of *nompC* mutants & *nompC* rescues plotted against antennal displacement (nm)

normalized (see 2.4.2) CAP responses of *nompC* mutants and *nompC* rescues were fitted with a Hill equation. The dashed line indicates the Hill fit of the wild-types and controls. 5% of the Hill fit's maximum amplitude was defined as threshold. *nompC* mutants showed a shift of their dynamic range of CAP responses to ca 190-1990 nm. This effect was rescued by JO1 driven expression of *UAS-nompC-L*. The dynamic range in rescue flies returned to 48- 740 nm. [N=4-20]
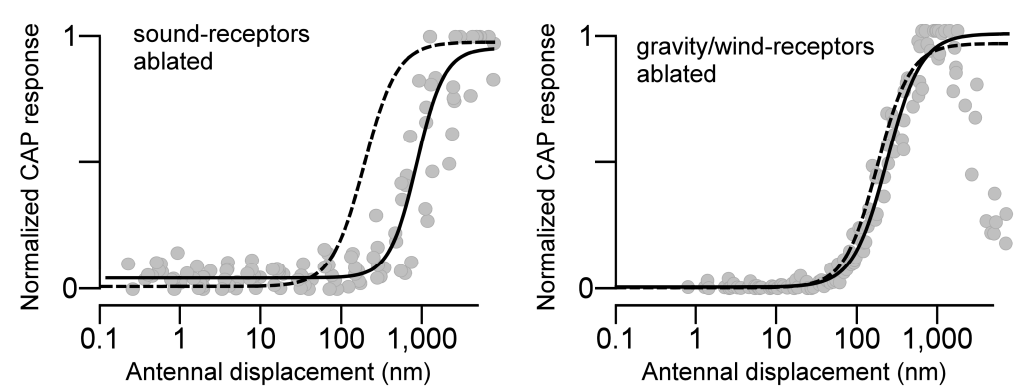
Figure 36 normalized CAP responses of sound-receptor and gravity/wind-receptor ablated flies plotted against antennal displacement (nm)

normalized (see 2.4.2) CAP responses of flies with ablated sound-receptors and gravity/wind-receptors were fitted with Hill equations. The dashed line indicates the Hill fit of the wild-types and controls. 5% of the Hill fit's maximum amplitude was defined as threshol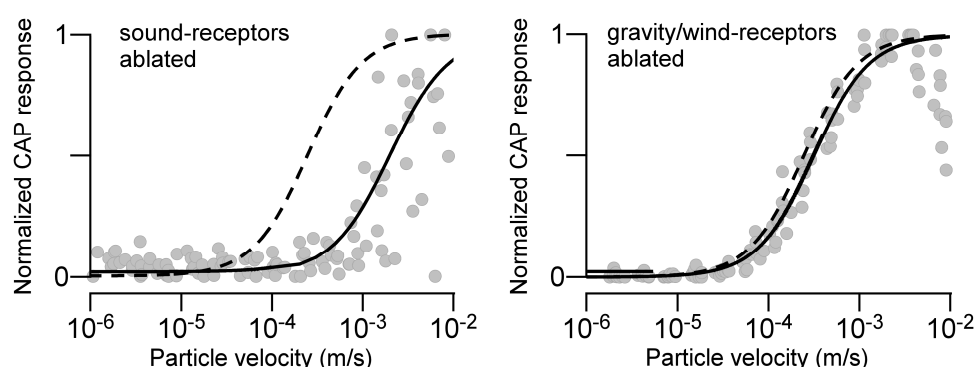d. Flies with ablated sound-receptors showed shift of the dynamic range to ca. 233 and 3190 nm, which was similar to the response shift in *nompC* mutants. Flies with ablated gravity/wind-receptor retained a dynamic range between 46-760 nm.
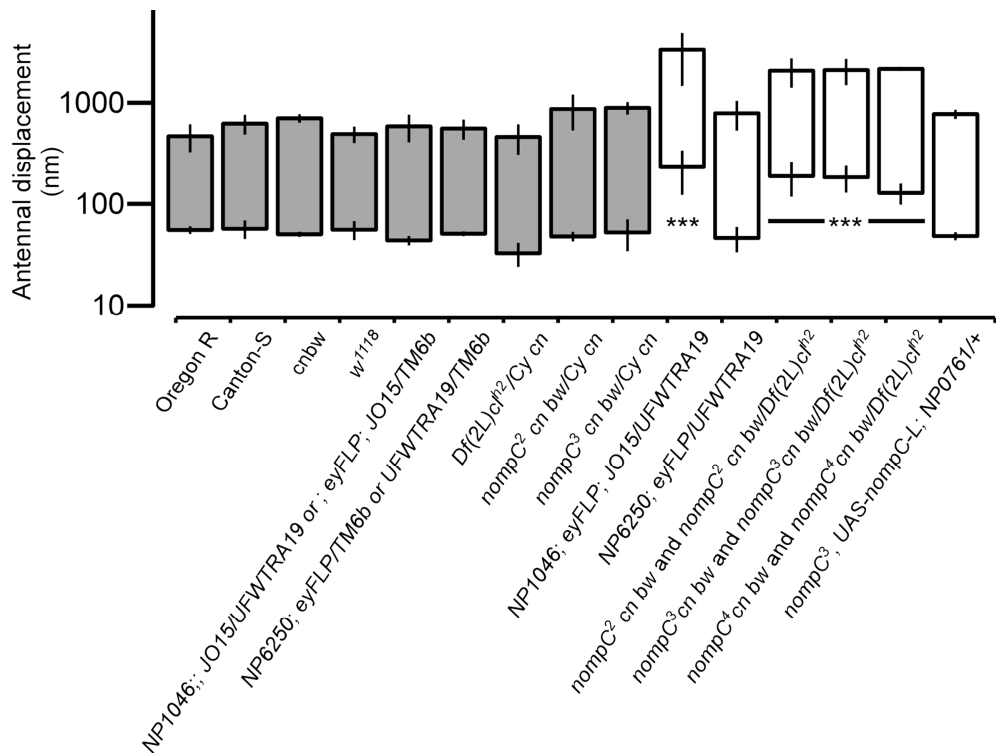
Figure 37 Dynamic range of wild-types, controls, *nompC* mutants, *nompC* rescues, sound-, and gravity/wind receptor ablated flies relative to antennal displacement
***: P < 0.05, two-tailed Mann Whitney U-tests against control and wild-type strains (N = 4 –20)

3.1.2.2   Sound particle velocity sensitivity of JO-neurons

To investigate the sound-sensitivity of JO-neurons, I plotted CAP responses against the corresponding sound particle velocity instead of the antennal displacement. The dynamic range with respect to sound particle velocity intensities was greater than the dynamic range for antennal displacements in wild-types and controls. The particle velocity dynamic ranged spanned ca. 31 dB from ca. 0.03 ± 0.01 to 1.06 ± 0.2 mm/s. In *nompC* mutants this dynamic range was shifted to higher intensities and reduced in size (0.5 ± 0.16 to 6 ± 1.2 mm/s; ca. 21 dB). JO1 driven expression of *UAS-nompC-L* rescued the *nompC* mutant phenotype and restored the dynamic range to sound particle velocities between 0.03 ± 0.01 mm/s and 1.3 ± 0.17 mm/s (ca. 30 dB). In flies with ablated sound-receptors, similar to the *nompC* mutants, a shift and reduction of the dynamic range was observed (0.46 ± 0.29 mm/s to 9.36 ± 7.57 mm/s; ca 20 dB). Ablating the gravity/wind-receptors did not change particle velocity sensitivity or the dynamic range (0.04 ± 0.01 mm/s to 1.52 ± 0.46 mm/s) [201].
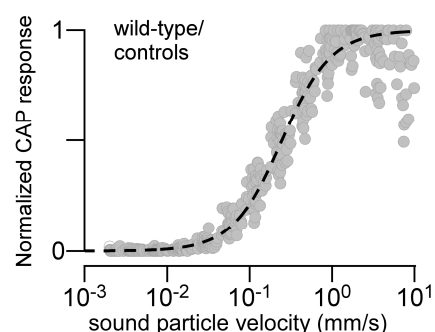
Figure 39 normalized CAP responses of wild-types & controls plotted against sound particle velocity (mm/s)
5% of the maximum Hill-Fit amplitude was defined as threshold. The dynamic range of CAP responses was 0.03 to 1.06 mm/s

Figure 38 normalized CAP responses of sound-receptor and gravity/wind-receptor ablated flies plotted against antennal displacement (nm)
flies with ablated sound-receptor and ablated gravity/wind-receptor were fitted with a Hill equations. The dashed line indicates the Hill-Fit of the wild-types and controls. 5% of the Hill fit maximum amplitude were defined as threshold. Flies with ablated sound-receptors showed a similar shift of the dynamic range like *nompC* mutants. Flies with ablated gravity/wind-receptor retained their dynamic range between 0.04-1.5 mm/s.
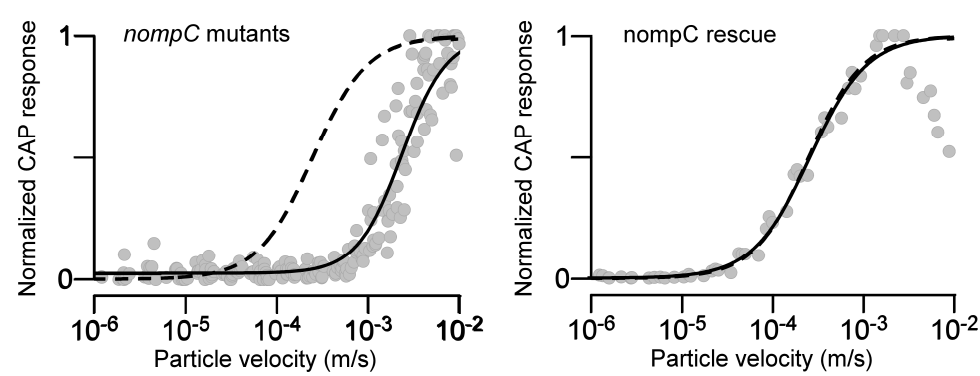
Figure 40 normalized CAP responses of *nompC* mutants & *nompC* rescues plotted against antennal displacement (nm)

CAP responses were fitted with a Hill equation. The dashed line indicates the Hill fit of the wild-types and controls. 5% of the Hill fit amplitude was defined as threshold. *nompC* mutants showed a shift in dynamic range of CAPs of ca. 0.5-6 mm/s. This effect was rescued by JO1 driven expression of *UAS-nompC-L*. The dynamic range in those flies returned to ca. 0.03-1.3 mm/s.
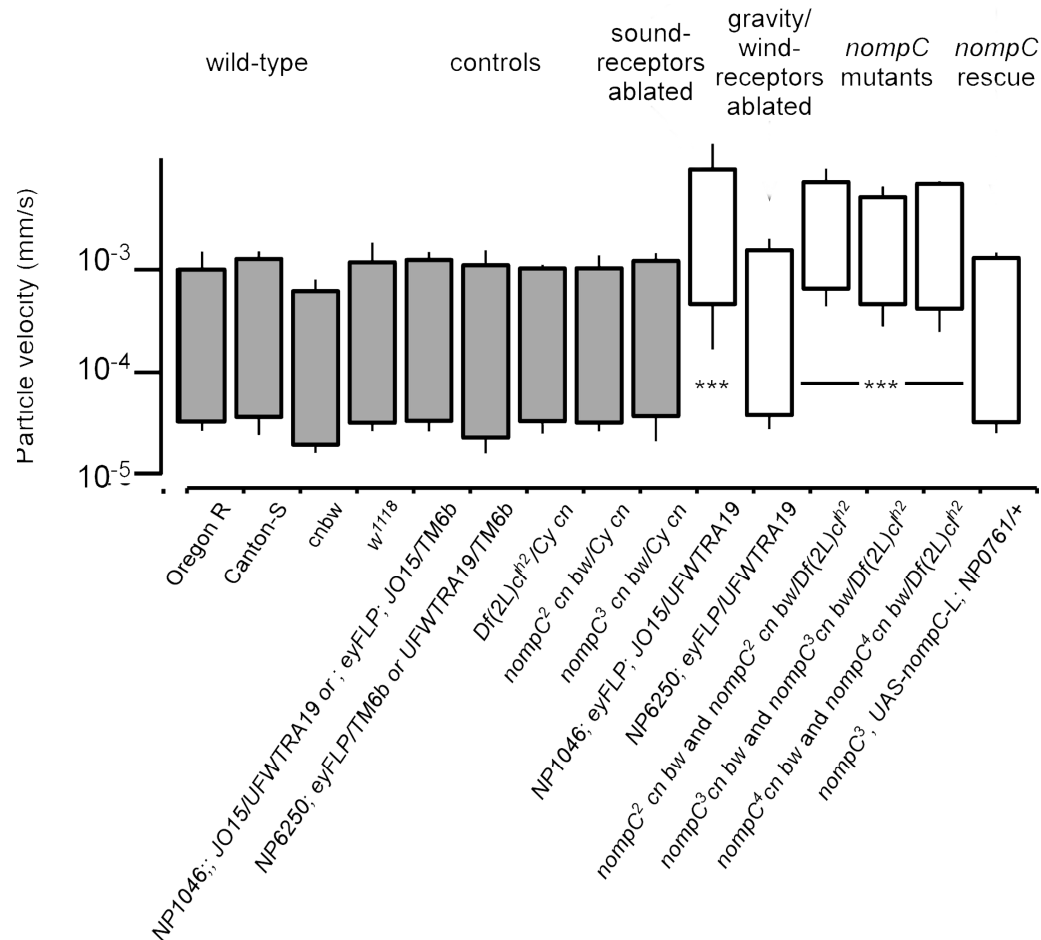
Figure 41 Dynamic range of wild-types, controls, *nompC* mutants, *nompC* rescues, sound-, and gravity/wind receptor ablated flies relative to the sound particle velocity

***: $P < 0.05$, two-tailed Mann Whitney U-tests against control and wild-type strains (N = 4 –20)

3.2. NompC: Mechanical properties of the sound receiver

To assess the mechanical properties of the sound receiver, I recorded its free fluctuations in the absence of stimulation and its mechanical response to pure tones of different intensities.

3.2.1 Free fluctuations

The sound receiver freely fluctuates in response to thermal bombardment with air particles and the mechanical activity of JO-neurons [16,137]. Thus measuring the free fluctuation provides information about the passive mechanics of the sound receiver and the active energy contribution of JO-neurons. This active contribution also lowers the iBF of the receiver from ca. 600 Hz (dead animal) to ca. 200 Hz (alive). Integrating the
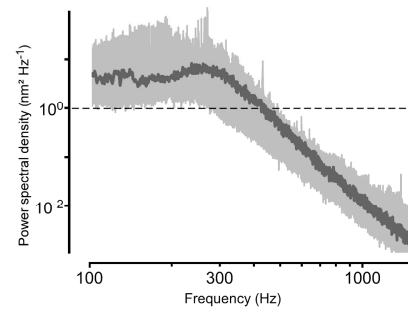
Figure 42 sound receiver power spectral densities of wild-types and controls
dark grey example measurement.

one-sided power spectrum (nm²/Hz) between 100 and 1500 Hz provides a measure for the mechanical power (nm²) of the receiver's fluctuations. Comparing the fluctuation power of the antennal receivers of controls and mutants can thus reveal changes in the active energy contribution of JO-neurons.

3.2.1.1 *nompC* mutants and flies with ablated sound-receptors show a significant loss in power

nompC mutants show a significant loss in power (111 ± 1 nm²) and an increased iBF (532 ± 9 Hz) compared with wild-types and controls (1171 ± 573 nm²; 250 ± 49 Hz). The reduction in power was comparable with a passive system as was the increase of iBF. JO1 driven expression of *nompC-L* was enough to rescue the *nompC* phenotype. The power was restored to 1034 ± 462 nm² and the iBF decreased to 280 ± 64 Hz. Similar to *nompC* mutants, ablating the sound-receptors reduced the systems power to 112 ± 53 nm² and increased the iBF to 443 ± 80 Hz. Ablating the gravity/wind-receptors had no effect on the power (960 ± 214 nm²) or the iBF (259 ± 18 Hz) [201].
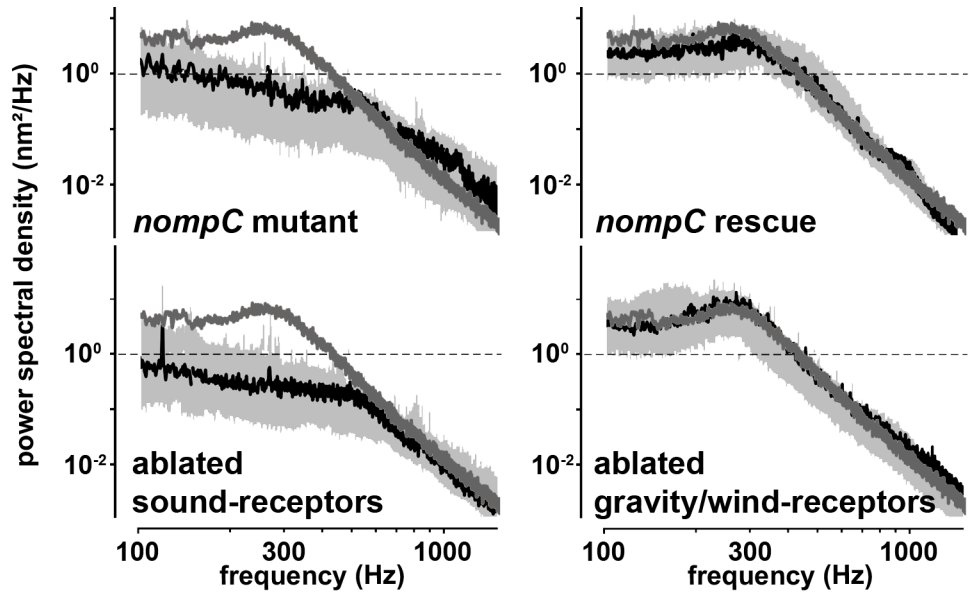
Figure 43 power spectra of different genotypes
dark grey: wild-type/control example. The loss of *nompC* reduces the power to ca. 1/10 of the wild-type/control value. The iBF of *nompC* mutants increases to ca 550 Hz. The *UAS-nompC-L* construct is able to rescue the *nompC* phenotype. Ablating the sound-receptors resembles the *nompC* phenotype, ablating the gravity/wind-receptors had no effect on power or iBF. [N=5-20]
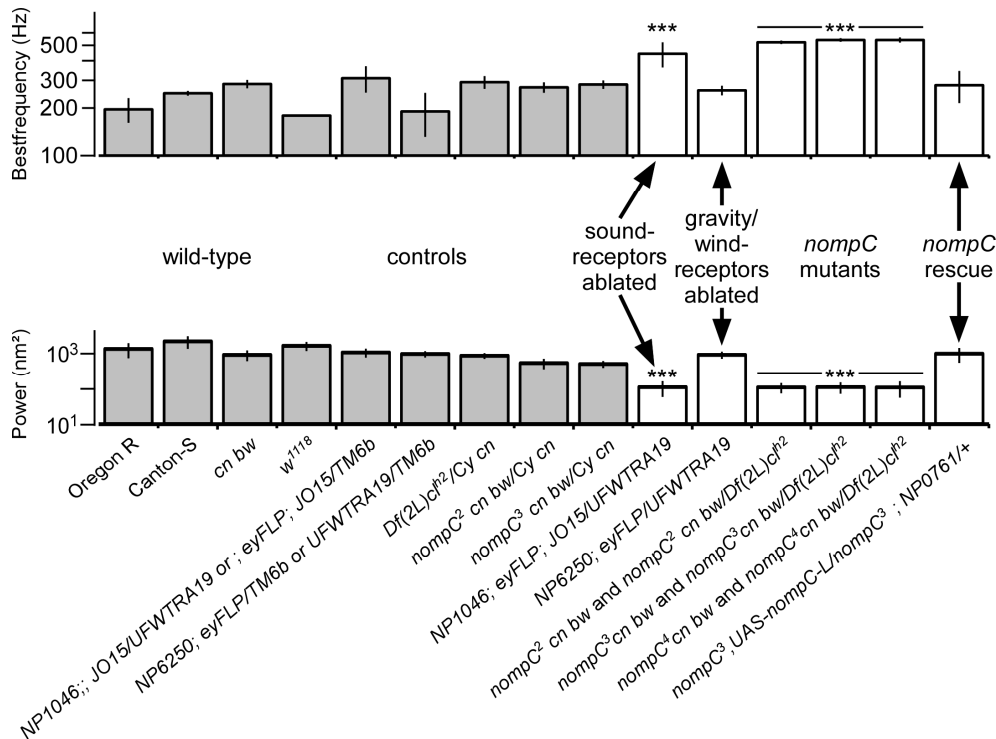

Figure 44 iBF and power of different wild-types, controls, and mutants
The iBF of wild-types and controls was quite diverse already. Still ablating the sound-receptors and the loss of NompC significantly increase the iBF to ca. 500 Hz and the power in those mutants was decreased. JO1 controlled expression of the *UAS-nompC-L* construct rescues the *nompC* phenotype.***: $P < 0.05$, two-tailed Mann Whitney U-tests against control and wild-type strains (N = 4 –20)

3.2.2 Nonlinear amplification of antennal vibrations

The antennal sound-receiver of *Drosophila* displays a compressive nonlinearity that amplifies its mechanical sensitivity to faint sounds. The source of the nonlinearity has been traced down to JO-neurons [137] and, more specifically, to the opening and closing of mechanotransduction channels [40] (see also 1.4).

3.2.2.1 Nonlinear amplification is lost in *nompC* mutants and flies with ablated sound-receptors

In wild-type and control flies the sound-induced antennal displacement increased nonlinearly with the sound particle velocity, displaying a compressive nonlinearity that enhances mechanical sensitivity ca. 8-fold when sound is faint (Figure 45, blue arrow). Consistent with previous observations [133], this nonlinear amplification was lost in *nompC* mutants, rendering their antennae mechanically less sensitive to acoustic stimuli. The nonlinear amplification was
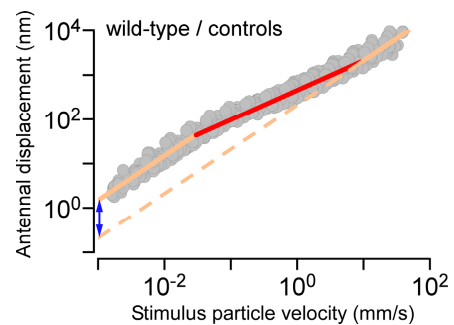
Figure 45 receiver displacement response to sound particle velocities of different intensities wild-type and control flies displayed a compressive nonlinearity. Faint sound stimuli are stronger amplified than loud.

rescued by expressing *UAS-nompC-L* under JO1-Gal4 control. Ablation of the sound-receptors abolished the nonlinear amplification, same as observed in *nompC* mutants. Flies with ablated gravity/wind-receptors, however, retained their nonlinear amplification (Figure 47). Hence, nonlinear mechanical amplification in the *Drosophila* ear requires both the NompC channel and JO sound-receptors but is independent of JO gravity/wind-receptors. The sensitivity gain provided by the nonlinear amplification can be defined by normalizing the receiver's displacement to the corresponding sound particle velocity and calculating the ratio of the respective mechanical sensitivities between the high and low-intensity regimes. In the absence of nonlinear amplification, a sensitivity gain of one will be obtained, but will assume larger values in the presence of nonlinear amplification. In wild-type, control, *nompC* rescue, and flies with ablated gravity/wind-receptor the sensitivity gain was ca. eight (Figure 46), whereas *nompC* mutants and flies with ablated sound-receptors displayed a sensitivity gain of one [201].
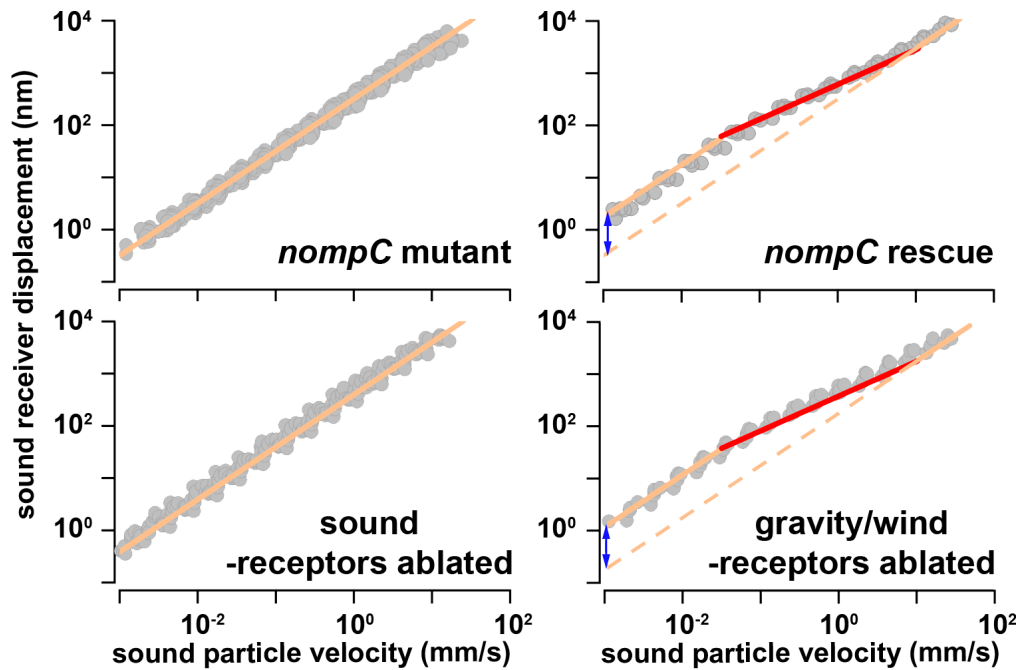
Figure 47 Sound receiver displacement response of different genotypes to sound particle velocity stimuli of different intensities

nompC mutants and flies with ablated sound-receptors lose the compressive nonlinearity. The *UAS-nompC-L* construct under JO1 control was able to rescue the *nompC* mutant phenotype. Ablating the gravity/wind-receptors had no effect on the nonlinear amplification.
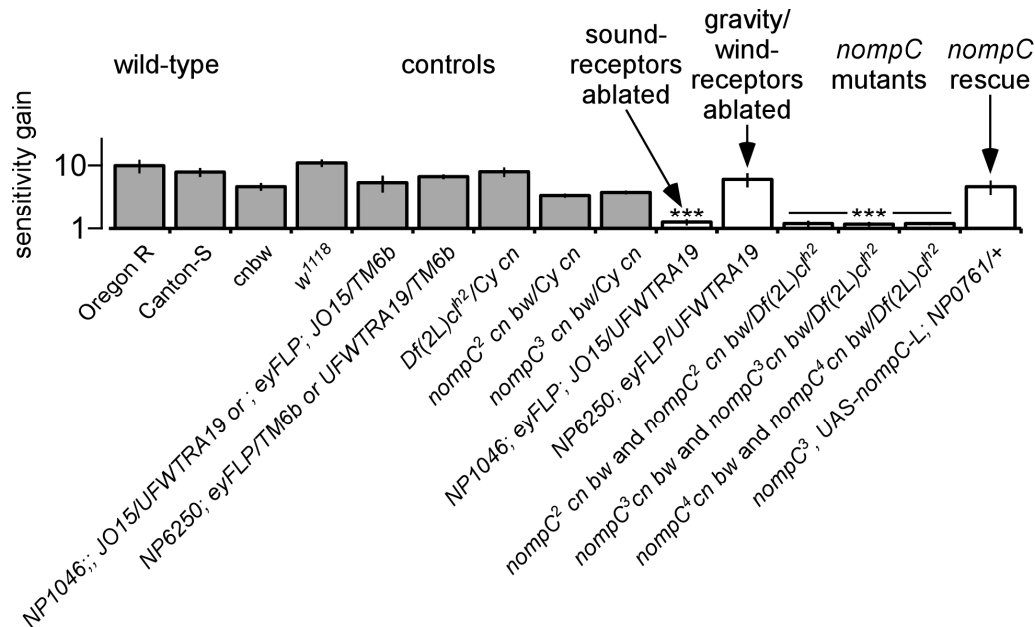

Figure 46 sensitivity gain of different genotypes

nompC mutants and flies with ablated sound-receptors display a sensitivity gain of ca. 1 and thus a loss of nonlinear amplification. wild-types, controls, *nompC* rescues, and flies with ablated gravity/wind-receptors display a sensitivity gain of ca. 8 ***: P < 0.05, two-tailed Mann Whitney U-tests against control and wild-type strains (N = 4 –20)

3.3. NompC: *In-vivo* calcium imaging

I recorded intracellular sound-evoked calcium signals in control flies and *nompC* mutants using the calcium sensor *cameleon2.1*, with simultaneous recording of antennal displacements and CAPs.

3.3.1 The calcium response of all JO-neurons does not superimpose with their CAP-response

JO1 driven expression of *cameleon2.1* allowed for the estimation of sound-induced changes in the intracellular calcium concentrations of all JO-neurons (Figure 48). At large stimulus intensities, two exponential fits described the shape of the ratiometric response, resulting in two time constants: a large one (2 ± 0.6 s) and a small one (0.3 ± 0.3 s) (Figure 49). The small time constant, however, was only apparent at antennal displacement above 400 nm. The maximum calcium response (ca. 1.2 % ΔR/R) was observed at antennal displacements of ca. 1900 nm. The simultaneously recorded CAPs did not superimpose with the calcium response. Although the calcium response showed a similar sensitivity threshold (Figure 50), its shape differed from the CAP responses and did not saturate [201].
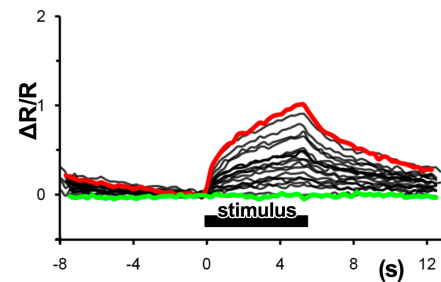
Figure 48 eYFP/eCFP ratio changes to pure tone stimuli of different intensities measured in all JO-neurons
the ratio increases steadily with stimulus intensity (green: smallest; red: largest stimulus).
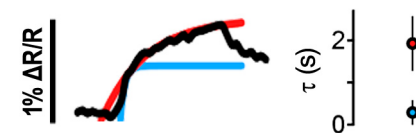
Figure 49 exponential fits and resulting time constants of the ratiometric change in all JO-neurons
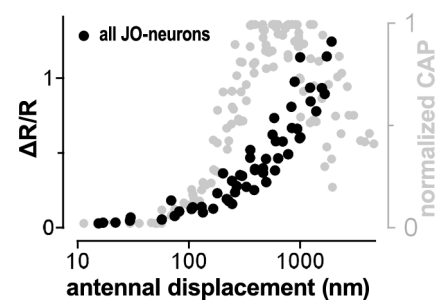

Figure 50 calcium and normalized CAP response plotted against antennal displacement
calcium response (black dots) of all JO-neurons; simultaneously recorded CAP response (grey dots).

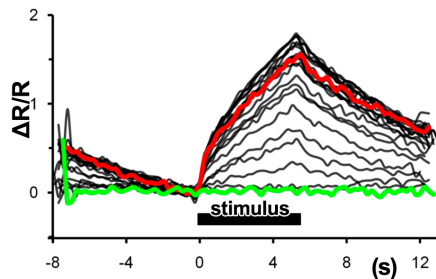## 3.3.2 The calcium response of the sound-receptors superimposes with their CAP response

Figure 51 eYFP/eCFP ratio changes to pure tone stimuli of different intensities measured in only the sound-receptors
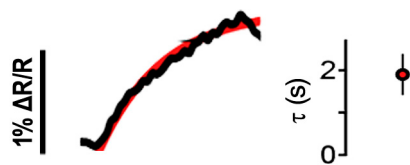(green: smallest; red: largest stimulus).

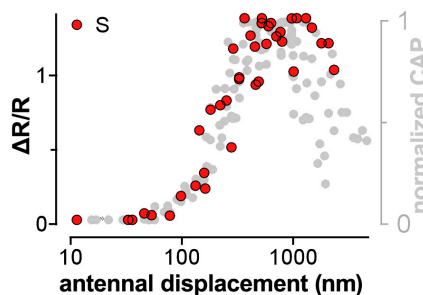**Figure 52 exponential fit and resulting time constant of the ratiometric change in only sound-receptors**

Figure 53 calcium response of sound-receptors and normalized CAP response of all JO-neurons relative to antennal displacement
The calcium response (red dots) of only sound-receptor neurons superimposes with simultaneously recorded CAPs (grey dots) of all JO-neurons

JO15 driven expression of *cameleon2.1* allowed for the estimation of sound-induced changes in intracellular calcium concentration of only sound-receptors (Figure 51). A single exponential rise-to-maximum equation was sufficient to fit the shape of the ratio change. The time constant for this fit was 1.90 ± 0.5 s (Figure 52), which was comparable with the large time constant yielded by the fit of all JO-neuron's calcium response (Figure 49). The maximal measured calcium response of ca. 1.36 % $\Delta R/R$ was observed at ca. 1000 nm antennal displacement, which coincided with the peak CAP response. Although the recorded CAP-response originated from all JO-neurons, it superimposed with the calcium response of only the sound-receptors (Figure 53) for the dynamic range of CAP responses. Indicating that the sound-receptors dominate sensitive CAPs. In addition, the CAP response of only the sound-receptors (gravity/wind-receptors were ablated, 3.1.2) superimposed with the calcium response of the sound-receptors (Figure 54). This illustrated the connection between calcium- and CAP-responses and supported the hypothesis that calcium signals lead to the generation of CAPs. Hence, the sensitive CAP responses of wild-type and control flies originate most likely from the

sound-receptors. In addition, the calcium response of the sound-receptors saturated at the same antennal displacement where the CAP response had its maximal amplitude and thus had the same dynamic range and sensitivity as sound-induced CAP responses
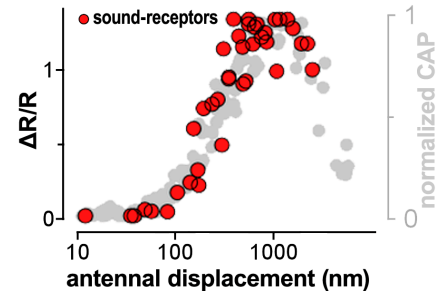

Figure 54 calcium- and CAP response of sound-receptors

3.3.3 The calcium response of gravity/wind-receptors is less sensitive than the CAP response of all JO-neurons

The stimulus intensity/antennal displacements needed to elicit calcium responses in gravity/wind-receptors were higher than the CAP threshold of all JO-neurons. Illustrating that the gravity/wind-receptors are less sensitive (Figure 55) than the sound-receptors in respect to pure tones. A single exponential rise-to-maximum fit was sufficient to describe the calcium response. The time constant yielded by this fit (0.5 ± 0.2 s) was comparable with the small time constant partly describing the calcium response of all JO-neurons (Figure 49). Consistently, displacements of more than 400 nm were needed to elicit a calcium response in gravity/wind-receptors. The maximal calcium ratio response (ca. 0.4 % $\Delta R/R$) was significantly lower than that of sound-receptors and occurred at antennal displacements of ca. 4000 nm. In addition, the calcium response of gravity/wind-receptors superimposed (Figure 58) with
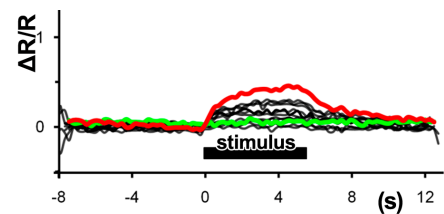

Figure 55 eYFP/eCFP ratio in response to pure tone stimuli of the gravity/wind-receptors
(green: smallest; red: largest stimulus)

Figure 56 exponential fit and resulting time constant of the ratiometric change in only gravity/wind-receptors
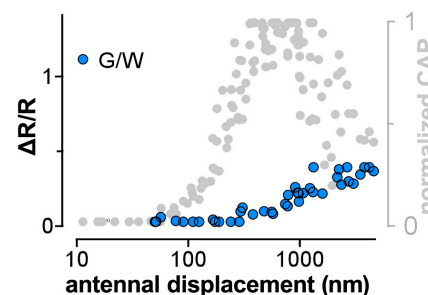

Figure 57 calcium response of gravity/wind-receptors and CAP response of all JO-neurons
Calcium response (blue) and simultaneously recorded CAPs (grey)
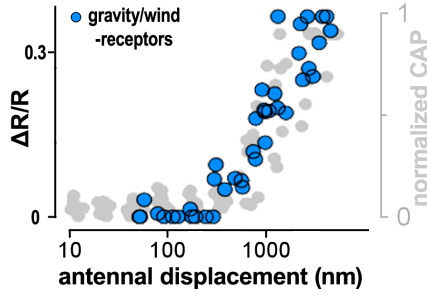
Figure 58 calcium and CAP response of gravity/wind-receptors

calcium- and CAP responses of gravity/wind-receptors superimposed.

their CAPs (sound-receptors were ablated). This latter observation indicated that the gravity/wind-receptors could be responsible for the remnant CAP response of *nompC* mutants or flies with ablated sound-receptors.

3.3.4 The calcium response of all JO-neurons can be calculated based on the response of sound- and gravity/wind-receptors

The combined calcium response of all JO-neurons is composed of the individual responses of the sound- and gravity/wind-receptors. I binned the calcium responses of all JO-neurons, only the sound-receptors, and only the gravity/wind-receptors into separate, distinct displacement ranges and was thus able to use those binned data points for further analysis. Assuming an equal number of cells for sound- and gravity/wind-receptors I calculated the combined response of all JO-receptors based on the single, binned responses of only sound-receptors and

gravity/wind-receptors $\frac{\Delta R}{R} = \dfrac{\left[\frac{(eYFP(S)_d + eYFP(^G/_W)_d)}{(eCFP(S)_d + eCFP(^G/_W)_d)} - \frac{(eYFP(S)_b + eYFP(^G/_W)_b)}{(eCFP(S)_b + eCFP(^G/_W)_b)}\right]}{\left[\frac{(eYFP(S)_b + eYFP(^G/_W)_b)}{(eCFP(S)_b + eCFP(^G/_W)_b)}\right]}$. Where S means

sound-receptors, $^G/_W$ gravity/wind-receptors, d during stimulation, and b before stimulation. The calculated values fit the recorded and binned calcium response of all JO-neurons (Figure 59). At small antennal displacements (<400 nm), the sound-receptors dominate the calcium and CAP responses. Beyond antennal displacements of 400 nm, however, the gravity/wind-receptors start to contribute to the response of all JO-neurons, be it calcium responses or CAPs.
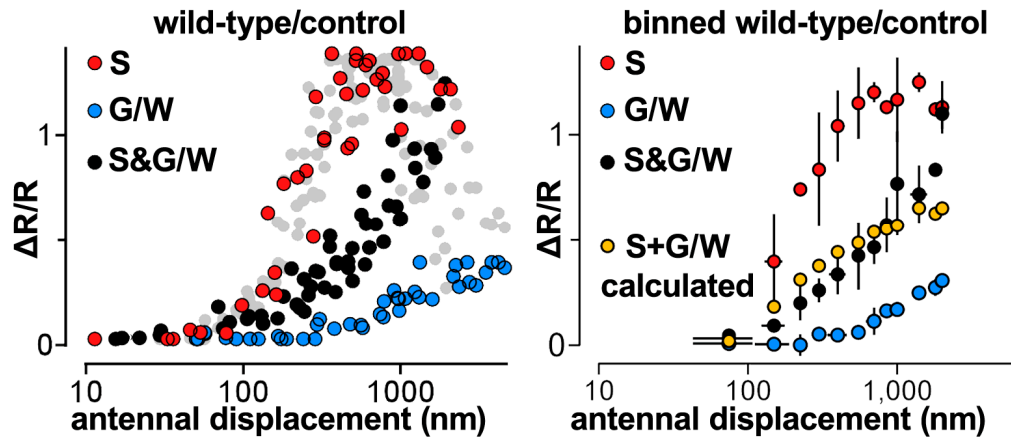
Figure 59 calcium responses of all-, sound- , and gravity/wind-receptors plotted with simultaneously recorded CAP responses of all JO-neurons
calcium response of sound-receptors (red); calcium response of gravity/wind-receptors (blue); calcium response of all-receptors (black); calculated calcium response of all-receptors based on individual response of sound-and gravity/wind-receptors (yellow).

3.3.5 NompC is required for the calcium response of sound-receptors

No calcium response was apparent in sound-receptors of *nompC* mutants (Figure 60). The simultaneously recorded CAP responses were typical for *nompC* mutants (Figure 63). The calcium response of all JO-neurons of *nompC* mutants, however, resembled the calcium response of control gravity/wind-receptors (Figure 61) and superimposed with the remnant CAP response (Figure 63) of flies with ablated sound-receptors and *nompC* mutants. The maximal calcium ratio change (0.4 % ΔR/R at ca. 4000 nm antennal displacement) and the time constant yielded from the single exponential fit (0.3 ± 0.2 s, Figure 62) of all-receptors in *nompC* mutants matched those of gravity/wind-receptors in controls (Figure 56). Consequently, the
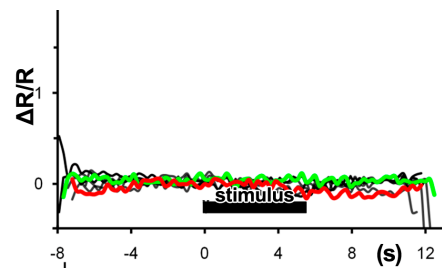

Figure 60 calcium response of sound-receptors in *nompC* mutants
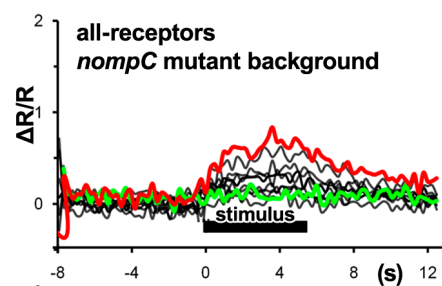(green: smallest; red: largest stimulus).

Figure 61 calcium response in all JO-neurons of *nompC* mutants
(green: smallest; red: largest stimulus)

51

all-receptors
nompC mutant

Figure 62 exponential fit and resulting time constant of the ratiometric change in all-receptors of *nompC* mutants
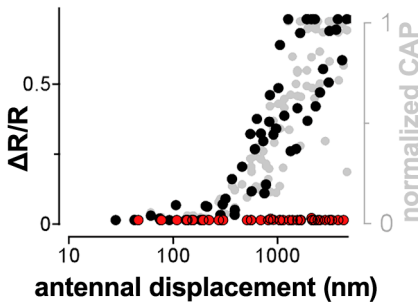

Figure 63 calcium responses of all-receptors and sound-receptors with normalized CAP response in *nompC* mutants
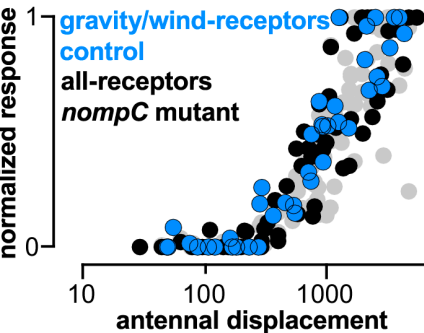calcium response of all-receptors (black); calcium response of sound-receptors (red); CAP response (grey).

Figure 64 calcium responses of gravity/wind-receptors in a controls and of all-receptors in *nompC* mutants with the remnant CAP response of *nompC* mutants
calcium response in gravity/wind-receptors (blue); calcium response in all-receptors of *nompC* mutants (black); CAP response of *nompC* mutants (grey)

calcium and CAP responses of all-receptors in *nompC* mutants and the calcium and CAP responses of gravity/wind-receptors in controls superimposed (Figure 64). Hence, we can assume that the remnant calcium and CAP responses in *nompC* mutants originate from gravity/wind-receptors. The complete loss of calcium responses in sound-receptors of *nompC* mutants further illustrates that NompC is required for sound-receptor function. Although antibody staining localized the NompC protein in gravity/wind-receptors, the calcium and CAP responses of gravity/wind-receptors in *nompC* mutants remained unaltered. If NompC is a mechanotransduction channel, however, could not be shown with the calcium measurements. To test if *nompC* mutants show a decreased asymptotic stiffness and thus satisfy the requirement for the loss of a mechanotransduction channels posited by the gating spring model, I conducted gating compliance measurements. [201]

3.4. NompC: Gating compliance measurements

Previous measurements of the gating compliance betrayed by the mechanics of the antennal receiver of wild-type flies have concentrated on that range of small stimulus forces (ca. -80 to +80 pN) that elicit CAPs [24,40] (3.1.2.1). To cover the stimulus forces that elicit remnant CAPs in *nompC* mutants, I had to increase this range to ca -1000 to +1000 pN. Examining the receiver's mechanics over this extended forcing range in wild-type flies indicated the presence of a second, insensitive type of transduction channels. This second channel increases the asymptotic stiffness K_{inf} of the fly's antennal receiver, but its linear stiffness K_{steady} remains unaltered.

3.4.1 Signatures of two mechanotransduction channel types in wild-types and controls

Because JO comprises two distinct receptor types (sound- and gravity/wind-receptors) and because *nompC* mutants show a remnant nerve response, I suspected that two different mechanotransduction channel types may be present in JO-neurons. Accordingly, I introduced a second channel type into the gating spring model to test if a gating spring model with two different channel types is able to describe the gating compliance of the sound receiver over the entire forcing range. The gating spring model with two independent channel types was

Figure 65 typical gating compliance response for the large forcing range

linear, passive stiffness K_{steady} (dashed grey line), nonlinear, active stiffness K_{peak} (yellow curve), maximal asymptotic stiffness K_{inf} (black dashed line); gating spring stiffness K_{GS}

$K(x) = K_{inf} - \left(\frac{N_s z_s^2}{k_B T}\right) * P_{o\_s}\left(1 - P_{o\_s}\right) - \left(\frac{N_i z_i^2}{k_B T}\right) * P_{o\_i}\left(1 - P_{o\_i}\right)$, where K_{inf} is the maximal, asymptotic stiffness assumed at infinite antennal displacements, N_s the number of the sensitive channels, and z_s the single channel gating force of a sensitive channel. N_i is the number of the insensitive channels and z_i the single channel gating force of an insensitive channel. The open probability of the sensitive channels depends on z_s, while the open probability of the insensitive channels
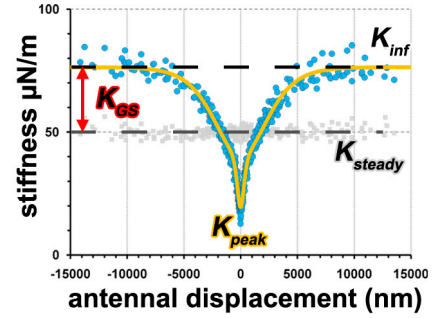
depends on z_i. The combined open probability thus reads as $P_o = \left(1/1 + e^{-\frac{(x_{peak}*z_S)}{kBT}} + 1/1 + e^{-\frac{(x_{peak}*z_i)}{kBT}}\right) * \frac{1}{2}$. To compare the gating compliance of sound receivers of different individuals, the receiver stiffnesses of individual animals of the same genotype were aligned and scaled by adjusting the apparent mass used to estimate the external forces (2.4.3.2). To facilitate visual comparisons of the gating compliances between different genotypes, K_{steady} and K_{peak} were shifted along the y-axis until an average K_{steady} of 50μN/m was reached. This adjustment was only made in the plots, and figures provided in the text represent original values. Each individual sound receiver's gating compliance was fitted with the 2-channel gating spring model equation. The initial parameter values used for fitting the sensitive channel type were: number of channels N_s=3050; single channel gating force z_s=15 fN; K_{inf} = 80 μN/m [24,25,40]. The initial parameter values for the second channel type were free. For wild-type flies (OregonR, CantonS, w[1118]), the 2-channel fit over the complete displacement range yielded the following parameter values: number of sensitive channe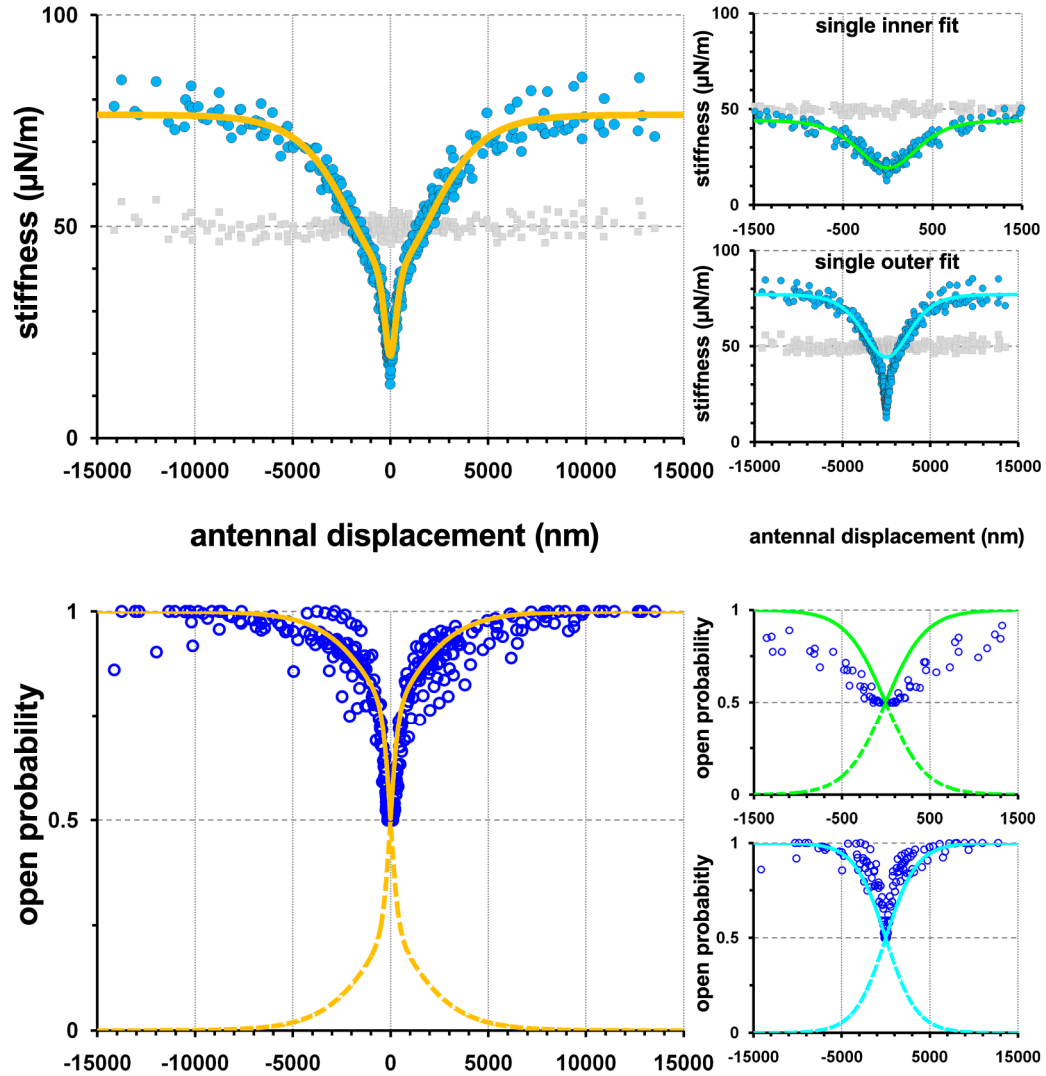ls = 756 ± 114, with a single channel gating force of 23 ± 2 fN; number of insensitive channels = 83867 ± 9649, with a single channel gating force of 2.8 ± 0.2 fN. K_{inf}, was 81 ± 1 μN/m and K_{steady} 53 ± 4 μN/m, which translates into a combined gating spring stiffness of the sensitive and insensitive channel of 28 μN/m ($K_{inf} - K_{steady} = K_{GSs+GSi}$). It was not possible to disentangle K_{GS} for the sensitive and insensitive channels. The predicted open probability (P_o) deduced from the fit superimposed with the recorded and normalized CAP response.

Figure 66 displacement responses to different forcing amplitudes
With increased forcing, the ratio between the peak and steady state displacements of the antennal receiver decreases until the steady state displacement is higher than the initial displacement peak.

Figure 67 gating compliance fits and deduced open probabilities of different wild-types (oregonR, cantonS, and w[1118])

K_{peak} (yellow) of all wild-types was fitted with a 2-channel equation system over the complete range of antennal displacement. In addition, only small displacement ([-1500,1500] nm; green) and large displacement ranges ([-15000,-1500] and [1500,15000] nm; cyan) were fitted with a 1-channel equation (upper, small panels). Based on the small and large displacement fits separate P_os were calculated (lower, small panels). The CAP responses of the sensitive and insensitive channel type could not be disentangled. To facilitated comparisons, I shifted K_{steady} and K_{peak} along the y-axis until the average K_{steady} reached 50 µN/m and plotted the data [N=15].

3.4.2 The deficiency $Df(2L)cl^{h2}$ does not affect the receiver's stiffness

The deficiency $Df(2L)cl^{h2}$ was used to uncover the *nompC* mutant phenotype. I used the deficiency because homozygous $nompC^x$ mutants were scars and crossing them against the deficiency resulted in a higher yield of *nompC* mutants. The phenotypes of homozygous and hemizygous *nompC* mutants wer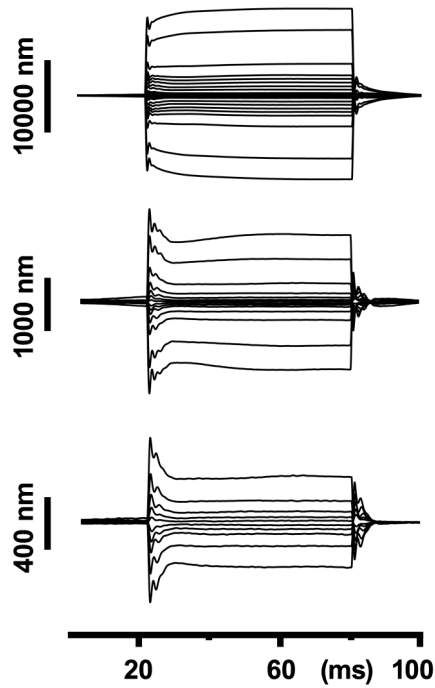e indistinguishable. K_{steady} of $Df(2L)cl^{h2}$ controls was 62 ± 6 µN/m. The fit with a 2-channel type equation yielded a K_{inf} of 94 ± 1 µN/m. Thus, the combined gating springs (K_{GS}) of the sensitive and insensitive channel was 32 µN/m. The fit further yielded a number of 774 ± 160 sensitive channels, with a single channel gating force of 25 ± 2 fN and 80604 ± 22170 insensitive channels, with single channel gating force of 2.7 ± 0.2 fN. These parameter values are comparable with those obtained for the wild-type (Tab. 5). The predicted open probability (P_o) deduced from the fit superimposed with the recorded and normalized CAP response.
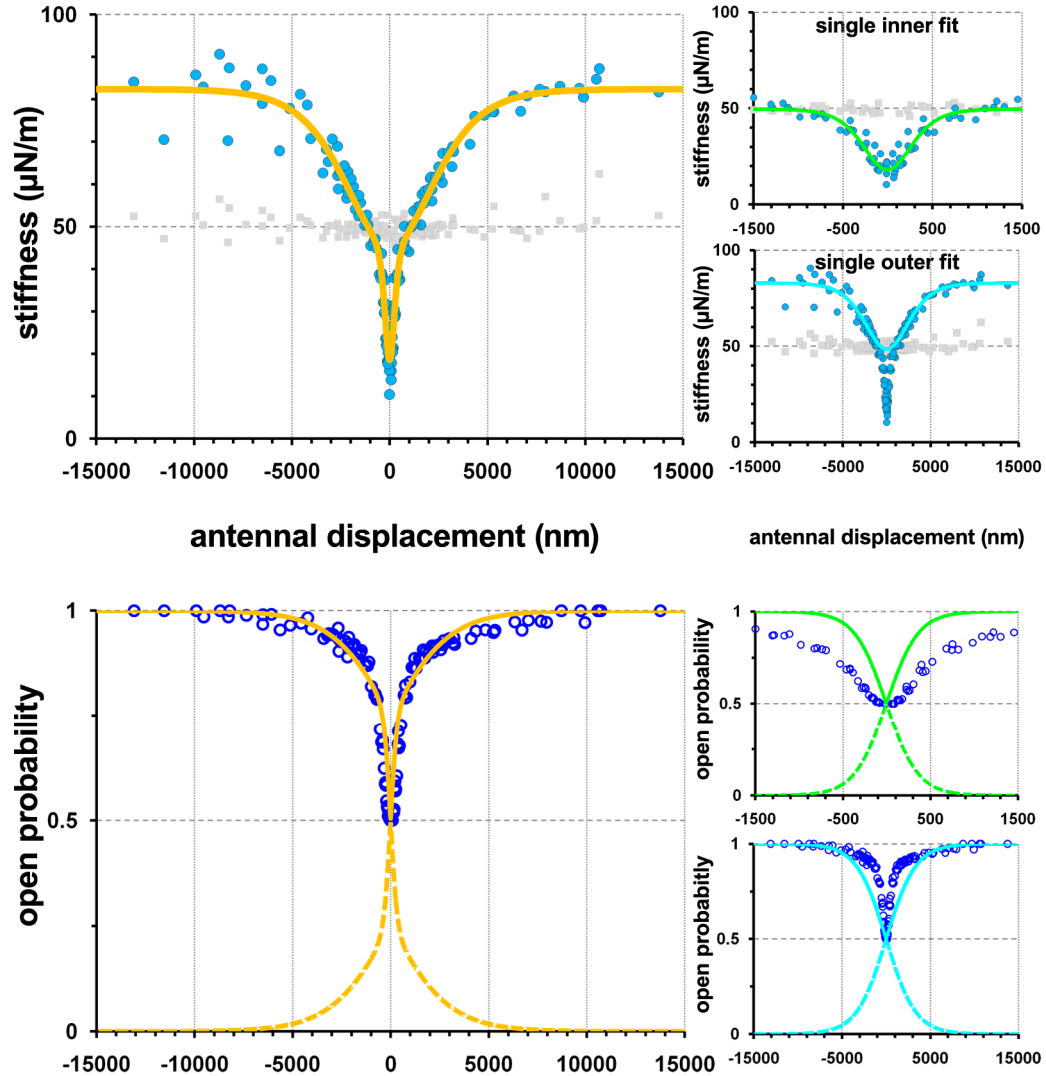

Figure 68 displacement response of different amplitudes ($Df(2L)cl^{h2}$)
No obvious differences to the displacement responses of the wild-type are apparent.

Figure 69 gating compliance fits and deduced open probabilities of *Df(2L)cl^{h2}*

K_{peak} (yellow) of *Df(2L)cl^{h2}* controls was fitted with a 2-channel equation system over the complete range of antennal displacement. Separately only small displacement ([-1500,1500] nm; green) and large displacement ranges ([-15000,-1500] and [1500,15000] nm; cyan) were fitted with a 1-channel equation (upper, small panels). Based on the small and large displacement fits separate P_os were calculated (lower, small panels). The CAP responses of the sensitive and insensitive channel type could not be disentangled. To facilitated comparisons, I shifted K_{steady} and K_{peak} along the y-axis until the average K_{steady} reached 50 µN/m and plotted the data [N=5].

3.4.3 *nompC^x/CyO* receivers show the mechanical signature of two distinct mechanotransduction channels but also a mild mutant phenotype

Balanced *nompC²/CyO, nompC³/CyO, and nompC⁴/CyO* flies served as controls for *nompC* mutants. K_{steady} of these flies was 47 ± 6 µN/m. The pooled data was fitted with a 2-ch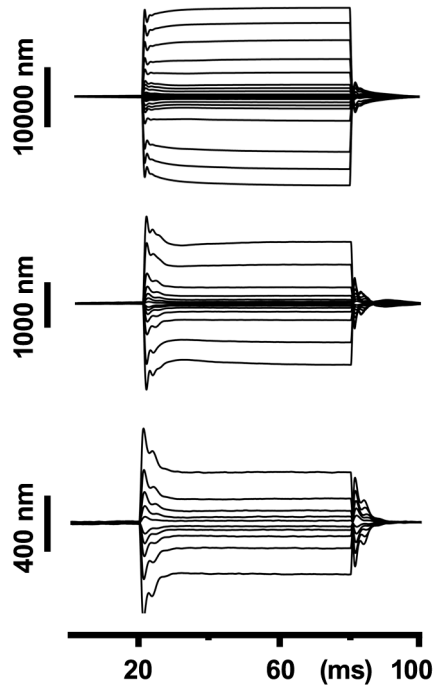annel-type gating spring equation. The fit yielded 688 ± 281 sensitive channels, with a single channel gating force of 20 ± 3 fN and 95309 ± 12897 insensitive channels, with a single channel gating force of 2.2 ± 0.2 fN. K_{inf} was 72 ± 2 µN/m and K_{steady} 47 ± 6µN/m, resulting in a combined K_{GS} of the sensitive and insensitive channel of 25 µN/m. Compared with the wild-type and *Df(2L)cl^{h2}* controls, the *nompC^x/CyO* flies showed a mild mutant phenotype that is apparent as a change of the gating compliance. K_{inf} was slightly decreased and the number of sensitive channels reduced. The predicted open probability (P_o) deduced from the fit superimposed with the recorded and normalized CAP response.
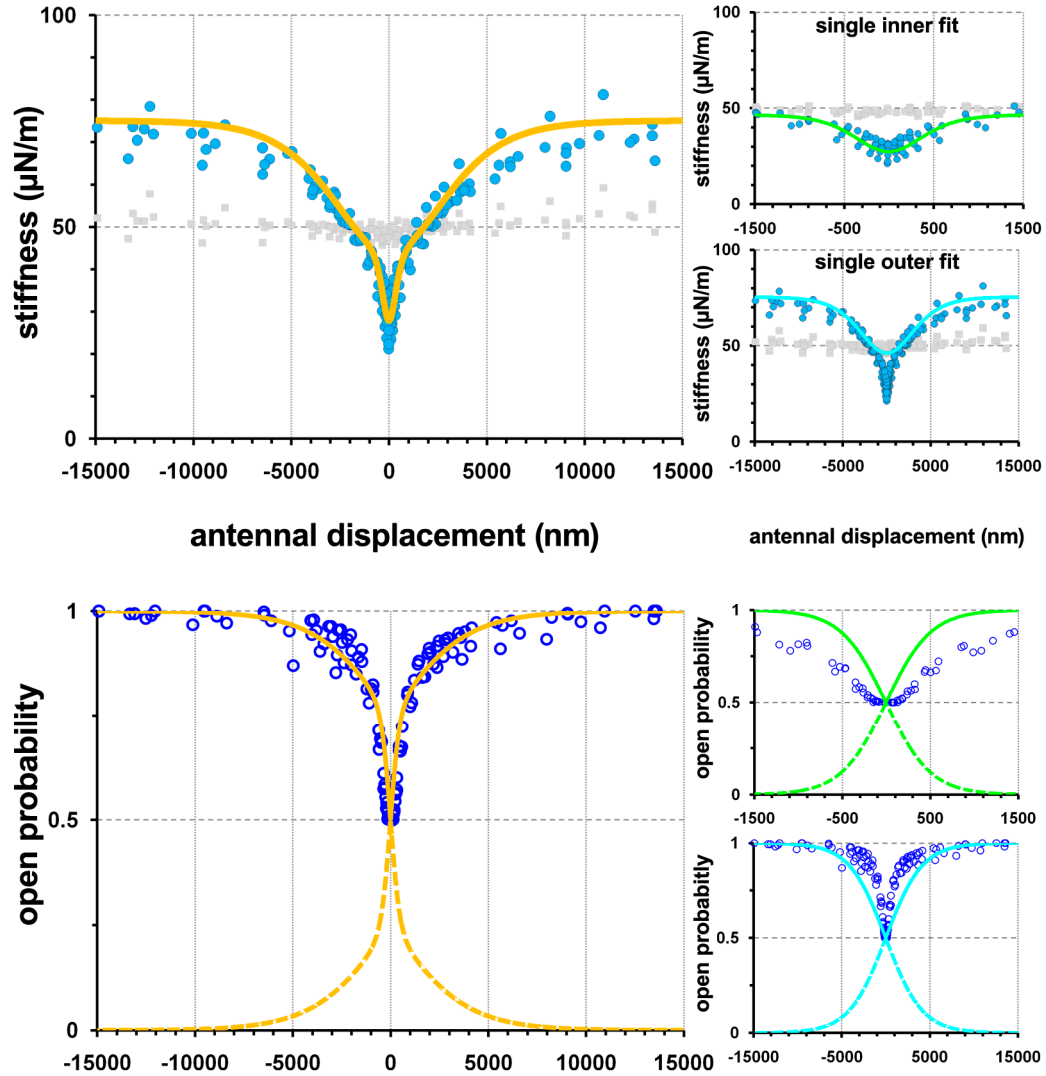

Figure 70 displacement response of different amplitudes (*nompC* control)

No obvious differences to the displacement responses of the wild-type are apparent. Although the initial peak displacement is smaller at low stimulus amplitudes.

Figure 71 gating compliance fits and deduced open probabilities for *nompC* controls (*nompC²/CyO*, *nompC³/CyO*, and *nompC⁴/CyO*)

K_{peak} (yellow) of *nompC²/CyO, nompC³/CyO, and nompC⁴/CyO* balanced flies was fitted with a 2-channel equation system over the complete range of antennal displacement. Separately only small displacement ([-1500,1500] nm; green) and large displacement ranges ([-15000,-1500] and [1500,15000] nm; cyan) were fitted with a 1-channel equation (upper, small panels). Based on the small and large displacement fits separate P_os were calculated (lower, small panels). The CAP responses of the sensitive and insensitive channel type could not be disentangled. To facilitate comparisons, I shifted K_{steady} and K_{peak} along the y-axis until the average K_{steady} reached 50 µN/m and plotted the data [N=6]

3.4.4   The signature of only one mechanotransduction channel is apparent in *nompC* mutants

The displacement response of the sound receivers of *nompC* mutants to force-steps differed from those of wild-types and controls. At small displacements (± 500 nm), the initial displacement peak that, in wild-type flies is ca. 5 times higher than the steady state displacement, was lost (compare Figure 66 and Figure 72).
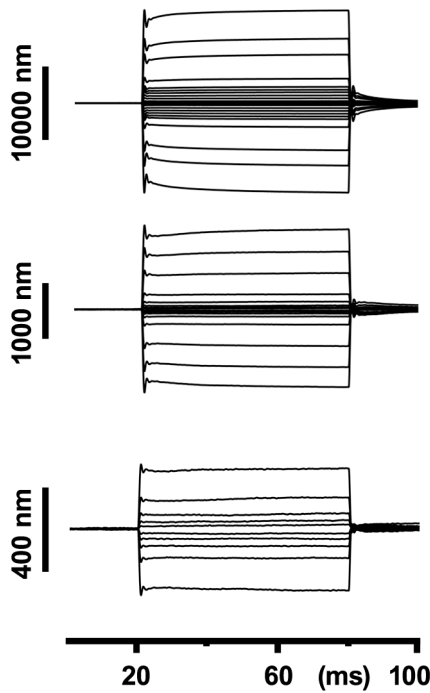

Figure 72 displacement response of different amplitudes (*nompC* mutants)

The in controls obvious initial high peak amplitude for low antennal displacements is absent in *nompC* mutants

The peak is associated with the gating of mechanotransduction channels, so its loss indicates a loss of channel gating. The shape of the step-response at large antennal displacements, however, was comparable to that of the wild-type and controls. Stiffness data obtained from *nompC²*, *nompC³*, and *nompC⁴* mutants was pooled and fitted. K_{steady} was 46 ± 7 µN/m and K_{inf} was only 63 ± 2 µN/m, resulting in a difference of only 17 µN/m . Such a reduction of K_{inf} indicates the loss of mechanotransduction channels [25]. In effect, only the signature of one mechanotransduction channel type was apparent, and a gating spring model with one channel type sufficed to describe the gating compliance of *nompC* mutants. This fit yielded 57944 ± 22480 channels with a single channel gating force of 2.3 ± 0.3 fN.

Judged from the parameter values and the observed phenotype, it is the insensitive channel type that remains in *nompC* mutants. Hence, the difference between K_{inf} and K_{steady} of 17µN/m corresponds to $K_{GS\_insensitive}$. Knowing $K_{GS\_insensitive}$ one can estimate $K_{GS\_sensitive}$, which is approximately 15 µN/m in *Df(2L)cl^{h2}/CyO* in controls. The predicted open probability (P_o) deduced from the fit superimposed with the recorded and normalized CAP response.
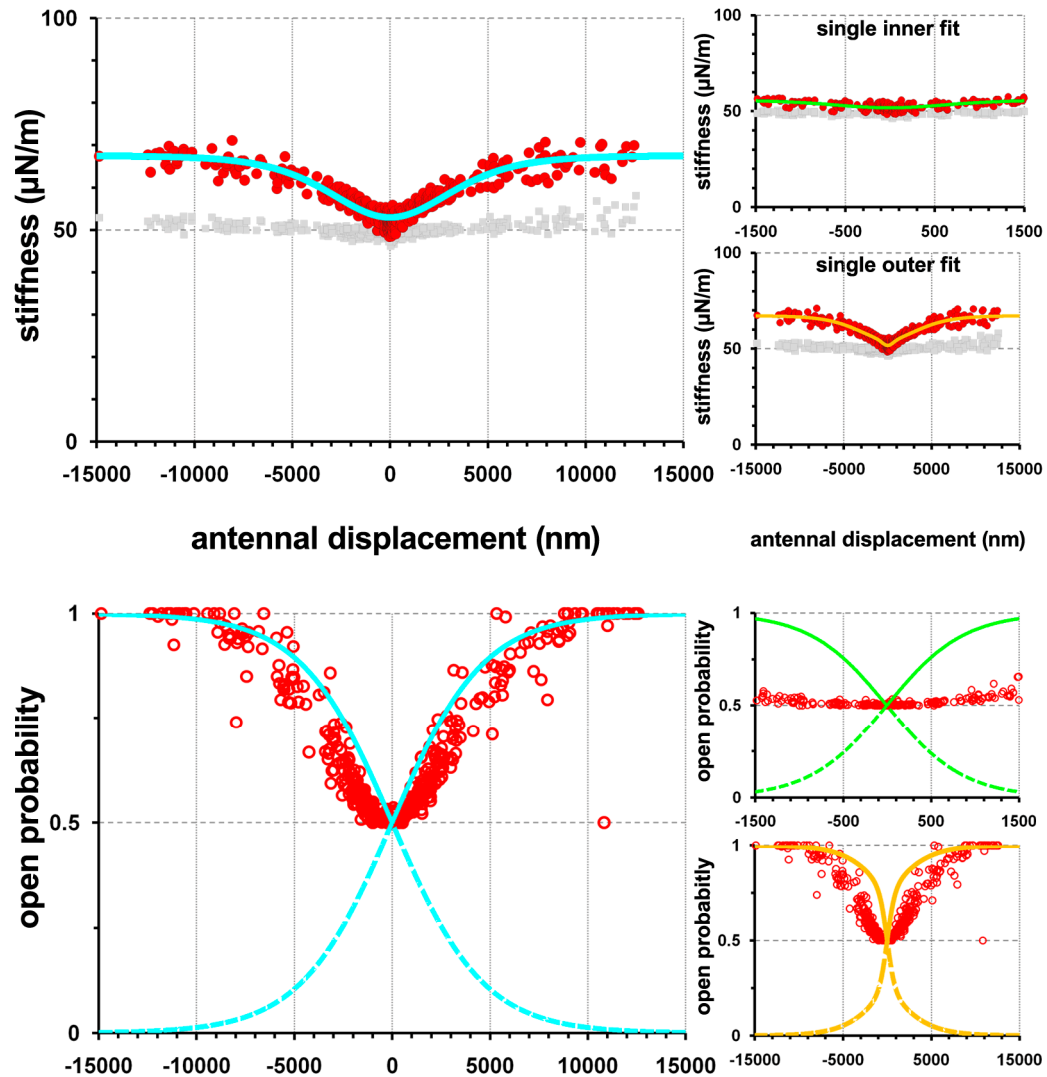
Figure 73 gating compliance fits and deduced open probabilities for *nompC* mutants

The calculated dynamic stiffness of all nompC mutants was fitted with a 1-channel equation system over the whole range of antennal displacement (cyan). Separately only small displacements ([-1500,1500] nm; green) where fitted with a 1-channel gating compliance equation. The complete displacement range was also fitted with a 2-channel equation (yellow) (upper, small panels). The open probability was deduced from the 1-channel fit parameter z and superimposed with the normalized CAP response. To facilitated comparisons, I shifted K_{steady} and K_{peak} along the y-axis until the average K_{steady} reached 50 µN/m and plotted the data [N=21].

3.4.5 JO1 driven expression of *UAS-nompC-L* in a *nompC* mutant background partially rescues channel gating

K_{steady} of *nompC-L* rescues was 54 ± 4 µN/m. The 2-channel fit yielded for the sensitive channel a number of 281 ± 180 (controls 774 ± 160), with a single channel gating force of 27 ± 7 fN and for the insensitive channel a number of 94839 ± 7659 channels, 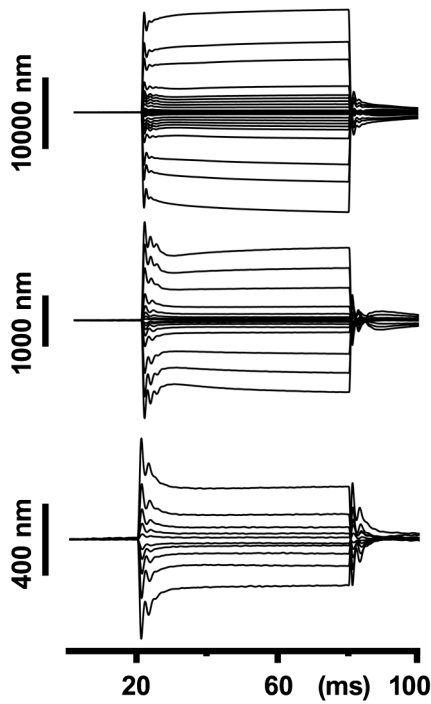with a single channel gating force of 2.2 ± 0.1 fN. K_{inf} was 76 ± 2µN/m. The combined K_{GS} for the sensitive and insensitive channel was 22 ± 1 µN/m. The predicted open probability (P_o) deduced from the fit superimposed with the recorded and normalized CAP response. Although the rescue of the *nompC* phenotype was not complete, a single copy of *nompC-L* was sufficient to rescue the mutant phenotype qualitatively. This incomplete rescue was apparent in the smaller number of sensitive channels compared to the wild-type. The ectopic expression of two copies of *nompC-L* might further increase the number of sensitive channels and restore the wild-type and control expression levels of NompC.
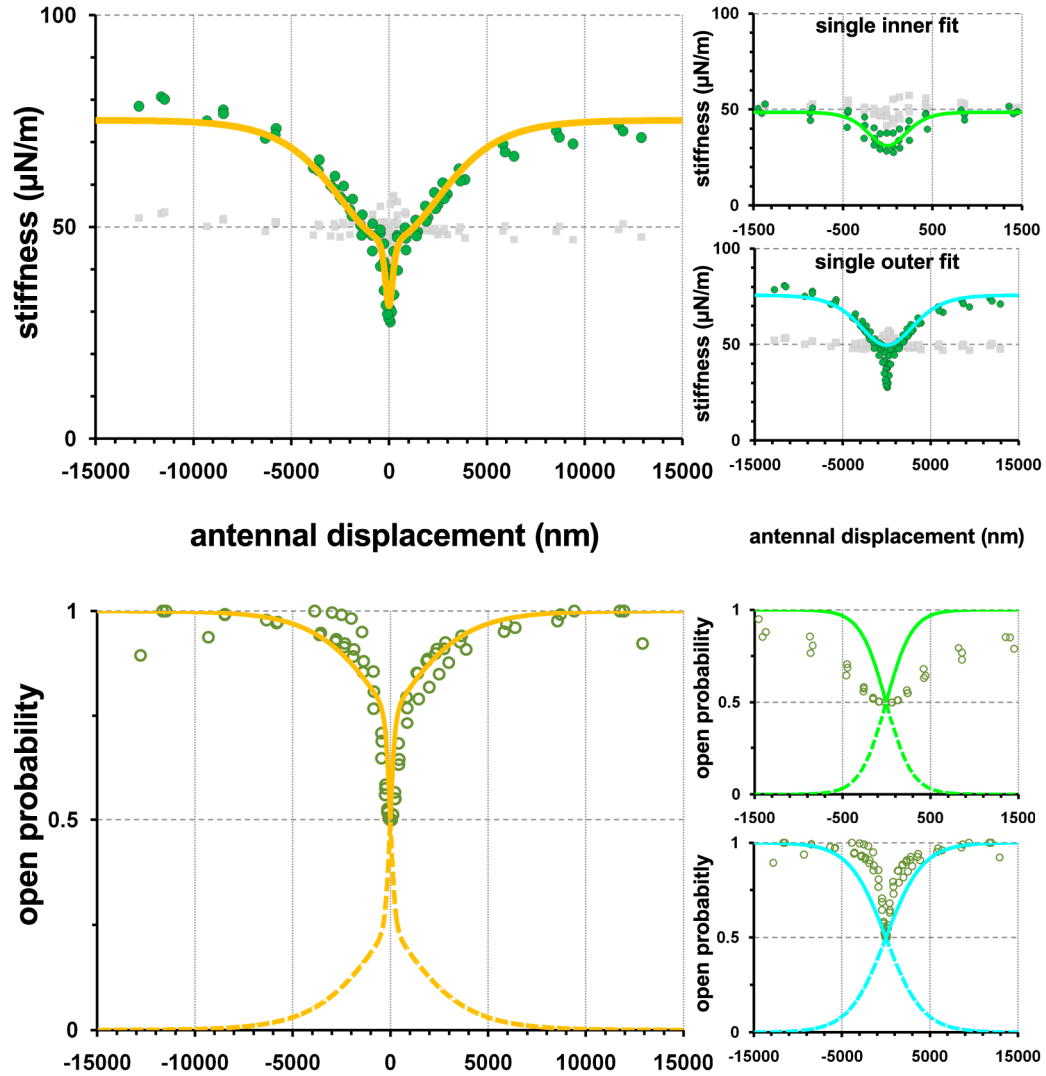

Figure 74 displacement response of different amplitudes (*nompC* rescues)

Different amplitudes of sound receiver displacement. The wild-type/control typical shape of step response is restored in *nompC* rescues.

Figure 75 gating compliance fits and open probabilities of *nompC* rescues

K_{peak} (yellow) of *nompC^2/Cyo, nompC^3/Cyo, and nompC^4/Cyo* balanced flies was fitted with a 2-channel equation system over the complete range of antennal displacement. Separately only small displacement ([-1500,1500] nm; green) and large displacement ranges ([-15000,-1500] and [1500,15000] nm; cyan) were fitted with a 1-channel equation (upper, small panels). Based on the small and large displacement fits separate P_os were calculated (lower, small panels). The CAP responses of the sensitive and insensitive channel type could not be disentangled. To facilitated comparisons, I shifted K_{steady} and K_{peak} along the y-axis until the average K_{steady} reached 50 μN/m and plotted the data [N=3].

3.4.6 Loss of sound-receptors phenocopies the gating compliance of *nompC* mutants

As previously seen, the phenotypes of *nompC* mutants and sound-receptor ablated flies were similar (3.2.1.1, 3.3.5). This similarity extended to the gating compliances betrayed by their antennal receivers. In flies with ablated sound-receptors, however, $K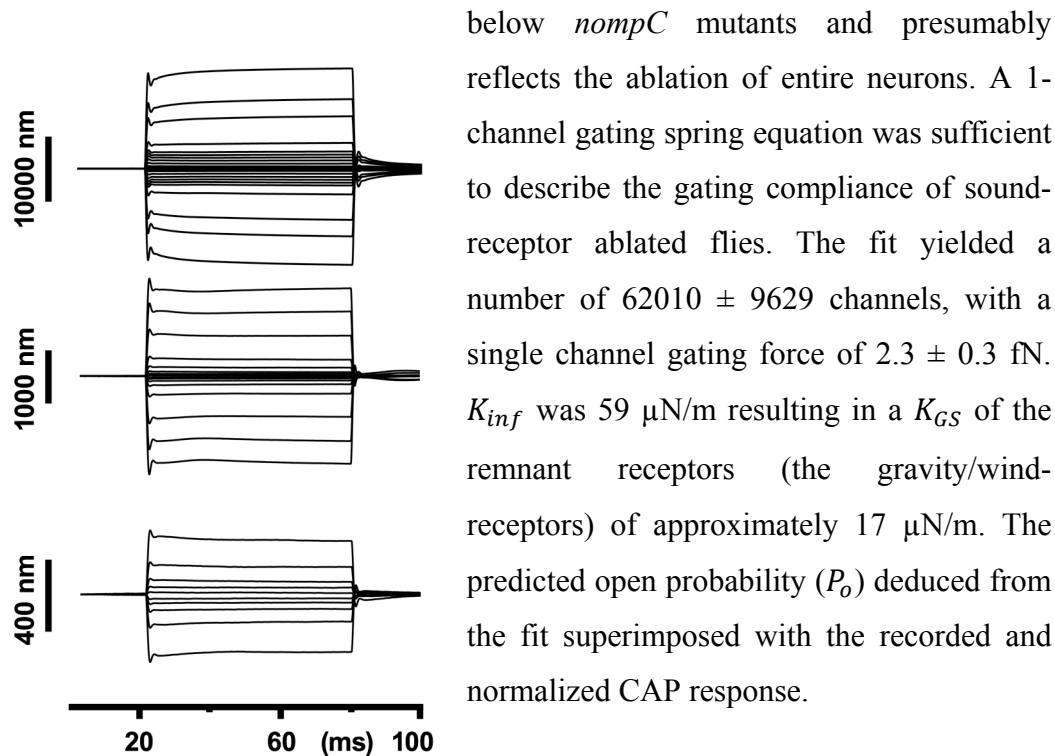_{steady}$ was decreased to 42 ± 5 μN/m, which is 4 μN/m below *nompC* mutants and presumably reflects the ablation of entire neurons. A 1-channel gating spring equation was sufficient to describe the gating compliance of sound-receptor ablated flies. The fit yielded a number of 62010 ± 9629 channels, with a single channel gating force of 2.3 ± 0.3 fN. K_{inf} was 59 μN/m resulting in a K_{GS} of the remnant receptors (the gravity/wind-receptors) of approximately 17 μN/m. The predicted open probability (P_o) deduced from the fit superimposed with the recorded and normalized CAP response.

Figure 76 displacement response of different amplitudes (sound-receptors ablated)
Different amplitudes of sound receiver displacement. The displacement response is similar to the one seen in *nompC* mutants
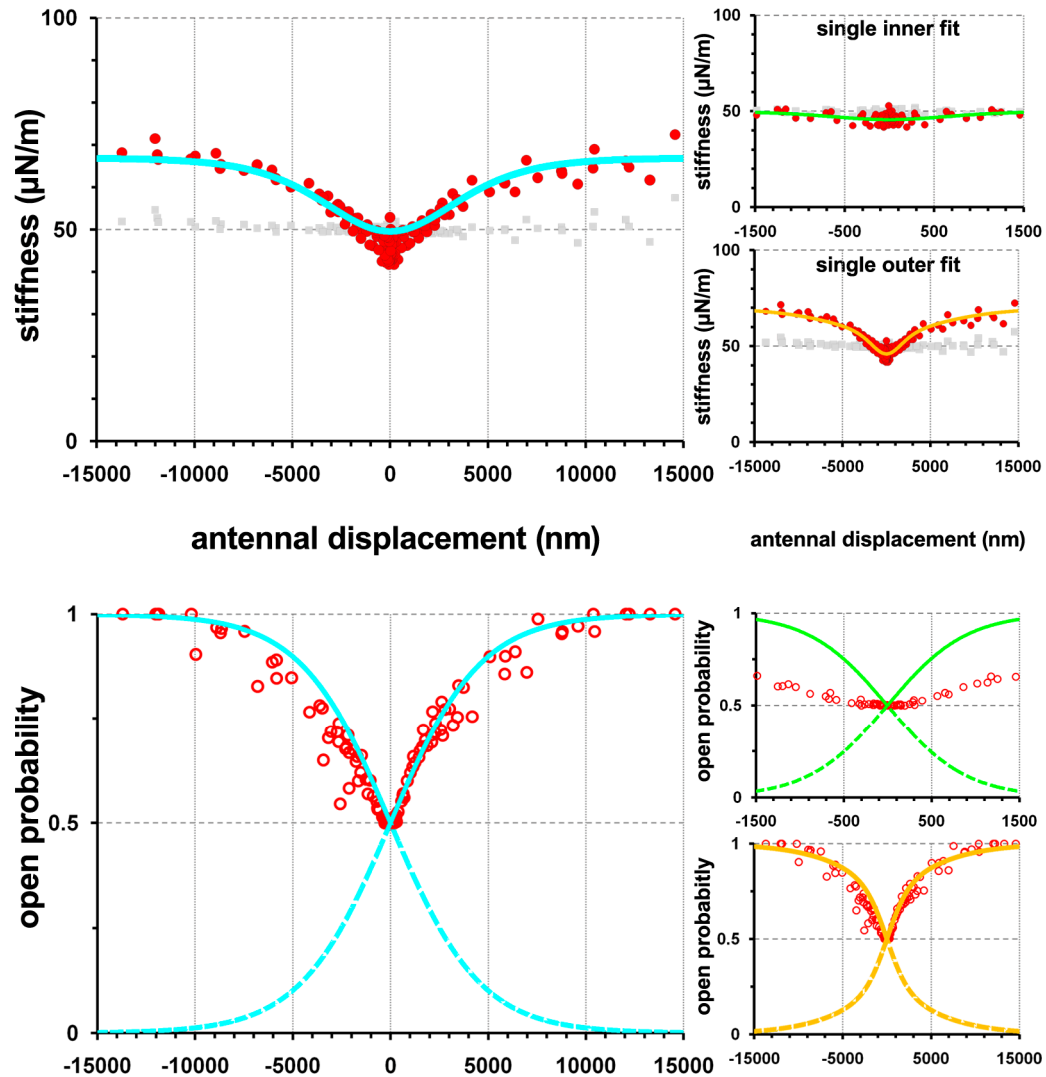
Figure 77 gating compliance fits and deduced open probabilities of flies with ablated sound-receptors

The calculated dynamic stiffness of flies with ablated sound-receptors was fitted with a 1-channel equation system over the whole range of antennal displacement (cyan). Separately only small displacements ([-1500,1500] nm; green) where fitted with a 1-channel gating compliance equation. The complete displacement range was also fitted with a 2-channel equation (yellow) (upper, small panels). The open probability was deduced from the 1-channel fit parameter z and superimposed with the normalized CAP response. To facilitated comparisons, I shifted K_{steady} and K_{peak} along the y-axis until the average K_{steady} reached 50 µN/m and plotted the data [N=5] [N=5].

3.4.7 The loss of NompC and the ablation of sound-receptors results in a decrease of the receiver's asymptotic stiffness

Comparisons of the fit parameter values of different genotypes (see table below) show that K_{steady} is constant and that, in nompC balanced flies, *nompC* mutants, and flies with ablated sound-receptors, K_{inf} is reduced. Fitting the gating compliance in flies with ablated sound-receptors yields a combined gating spring stiffness K_{GS}, of 17 µN/m for the insensitive channels, which apparently resides in gravity/wind receptor cells. Given a $K_{GScombined}$ of 32 µN/m in *Df(2L)cl^{h2}/CyO* controls, the combined gating spring stiffness K_{GS} of the sensitive channels is 32 µN/m -17 µN/m =15 µN/m. Accordingly, the receiver's asymptotic stiffness, K_{inf} should drop by ca. 15 µN/m if the sensitive channels and/or their gating springs are lost. In *nompC* mutants, the gating compliance introduced by sensitive channel gating is absent, and, compared to *Df(2L)cl^{h2}/CyO* controls, a reduction in K_{inf} of 15 µN/m is observed. Hence, in *nompC* mutants, the sensitive channel and/or their gating springs are lost.

Tab. 5 list of the parameter values obtained for different genotypes

parameter	Wild-type	$\dfrac{Df(2L)clh2}{CyO}$	$\dfrac{nompC^x}{CyO}$	*nompC* mutants	*nompC* rescue	sound-receptors ablated
K_{inf}	81 ± 1 µN/m	94 ± 1 µN/m	72 ± 2 µN/m	63 ± 2 µN/m	76 ± 2 µN/m	59 ± 2 µN/m
K_{steady}	53 ± 4 µN/m	62 ± 6 µN/m	47 ± 6 µN/m	46 ± 7 µN/m	54 ± 4 µN/m	42 ± 5 µN/m
$K_{GS\_combined}$	28 µN/m	32 µN/m	25 µN/m	17 µN/m	22 µN/m	17 µN/m
N_s	756 ± 114	774 ± 160	688 ± 281	---	281 ± 180	---
z_s	23 ± 2 fN	25 ± 2 fN	20 ± 3 fN	---	27 ± 7 fN	---
N_i	83867 ± 9649	80604 ± 22170	95309 ± 12897	57944 ± 22480	94839 ± 7659	62010 ± 9629
z_i	2.8 ± 0.2 fN	2.7 ± 0.2 fN	2.2 ± 0.2 fN	2.3 ± 0.3 fN	2.2 ± 0.1 fN	2.3 ± 0.3 fN

3.5. What might be the second channel?

Judged from the gating compliance, NompC is an essential mechanical constituent of the fly's sound transducers, but not of the insensitive transducers that mediate the transduction of gravity and wind. To test the TRP-dependence of these latter transducers, I analyzed the functional relevance of the TRP channels Nanchung, Inactive, TRP, Painless, and TRPML.

3.5.1 *nan/iav* regulate transduction

Nanchung and Inactive had been suspected to be the fly's mechanotransduction channels for hearing. The loss of either one abolishes sound-induced CAP responses [116], but hyper-amplification of sound-induced receiver vibrations in *nan* and *iav* mutants suggests that rather than serving transduction these channels modulate the amplificatory gain [133]. To directly test the roles of the channels in transduction, I analyzed JO function in *nan* and *iav* mutant flies.

3.5.1.1 The power of the sound receiver increases ca. 70-fold in *nan/iav* mutants

The fluctuations of the sound receivers of *nan* and *iav* mutants have been described [133]. I repeated the measurements to obtain a complete dataset for each individual animal, including the receiver's free fluctuations, it's sound-induced displacement response, its response to force steps, and the CAP response. In accord with previous observations [133], the average fluctuation power of *nan/iav* mutant sound receivers was 74573 ± 32245 nm², which is ca. 70 times more than in wild-types (1171 ± 573 nm²). I also found previously described spontaneous receiver oscillations [133].
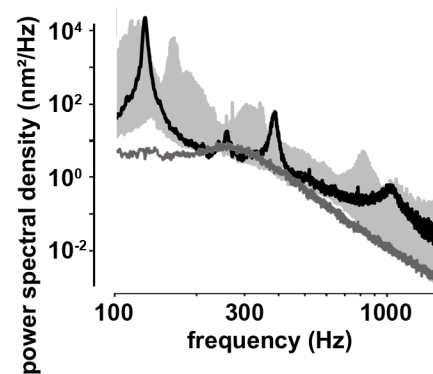

Figure 78 power spectra of nan/iav mutants

The dark grey line represents a typical wild-type free fluctuation. [N=8]

3.5.1.2   The nonlinear hyper-amplification in *nan/iav* mutants
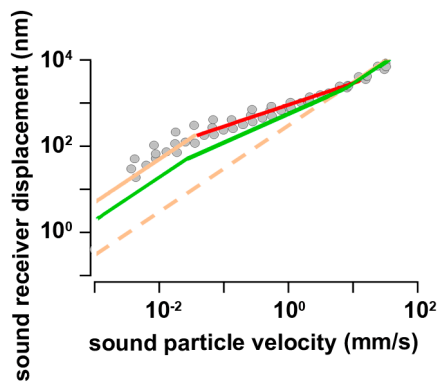

Figure 79 particle velocity induced sound receiver displacement of *nan/iav* mutants

nan/iav mutants show a hyper-amplification (wild-type=green) [N=6]

Sound receiver of *nan* and *iav* mutants oscillate spontaneously with high displacement amplitudes [133]. This leads to a hyper-amplification of sound-induced antennal displacements. I confirmed these findings by measuring an average sensitivity gain of ca. 50 ± 25 (w/t: ca. 8-fold). Like previous studies, I was not able to record any inducible CAP responses. Even at very large stimulus intensities, the flies are deaf.

3.5.1.3   The asymptotic stiffness of *nan/iav* mutants remained unaltered but the number of mechanotransduction channels is increased
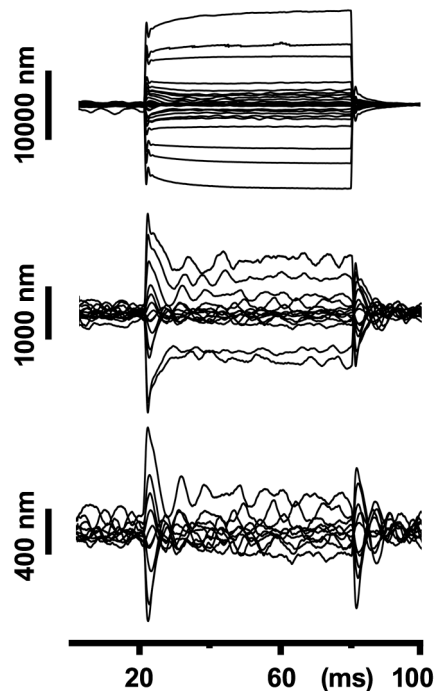
Figure 80 displacement response of different amplitudes (*iav* mutant)

small displacements are dominated by sustained oscillation of the receiver.

If Nan/Iav are mechanotransduction channels, their loss would result in a decrease of K_{inf}. K_{steady} was 54 ± 8 µN/m and K_{inf} 87 ± 4 µN/m. Thus, rather than being reduced, K_{inf} was increased with respect to the wild-type and controls (ca. 80 µN/m). The single channel gating force was decreased for the sensitive channel (z_s; 15 ± 4 fN) but remained unaltered for the insensitive channel (z_i; 2.4 ± 0.1 fN). The numbers deduced for both channel types seemed roughly doubled: the number of sensitive channels increased to 3025 ± 866 and that of the insensitive channel to 168510 ± 20610 (wild-type see Tab. 5). Hence, the regulatory function of *nan/iav* might involve

alterations in the abundance of transduction channels. The increased channel numbers are consistent with the increase of K_{inf}.
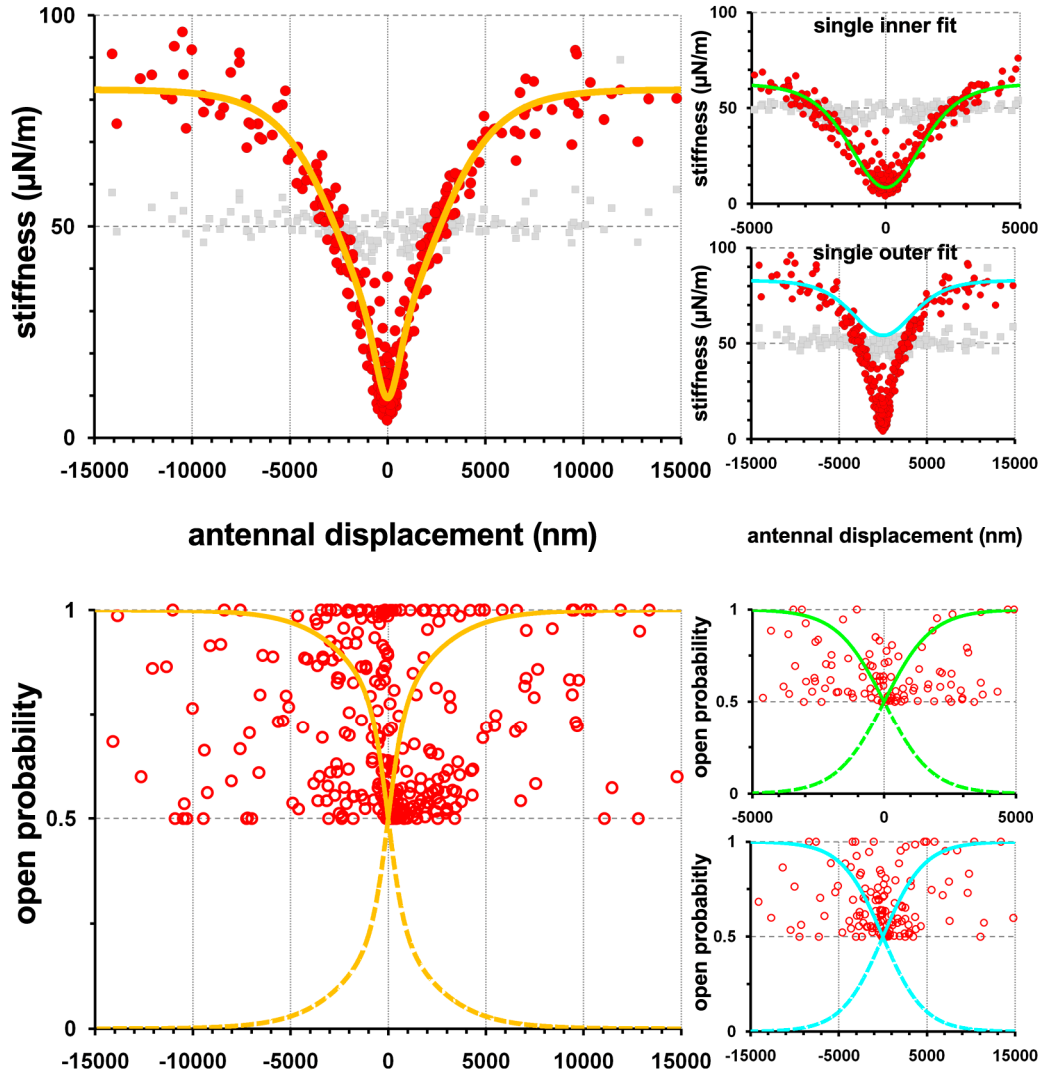

Figure 81 gating compliance fits and deduced open probabilities of *nan* and *iav* mutants

The calculated dynamic stiffness of flies with ablated sound-receptors was fitted with a 1-channel equation system over the whole range of antennal displacement (cyan). Separately only small displacements ([-1500,1500] nm; green) where fitted with a 1-channel gating compliance equation. The complete displacement range was also fitted with a 2-channel equation (yellow) (upper, small panels). No CAP response was apparent visible. To facilitated comparisons, I shifted K_{steady} and K_{peak} along the y-axis until the average K_{steady} reached 50 µN/m and plotted the data [N=5].

3.5.2 TRP is important for the energy content of the system

TRP is the eponym of the transient receptor potential family. It was first described to be the transduction channel required for the visual system. TRP has not been implicated in hearing before. I used homozygous *trp[1]* mutants to test whether JO function requires TRP.

3.5.2.1 The power of *trp* mutant sound receivers is lowered
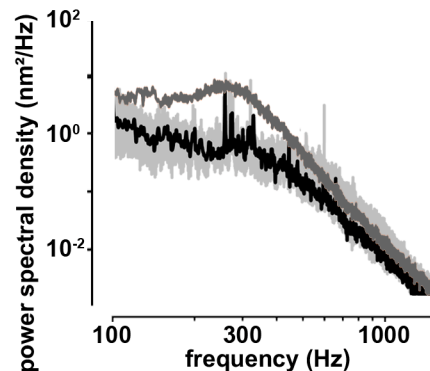
Figure 82 powerspectra of *trp[1]* mutants

The dark grey line represents a typical wild-type free fluctuation. [N=5]

The free fluctuation power of *trp* mutant sound receivers (296 ± 116 nm²) was significantly decreased when compared to wild-type flies and controls (Tab. 6). The power was still greater, however, than in *nompC* mutants (111 ± 1 nm²) or sound-receptor ablated flies (112 ± 53 nm²). The iBF was increased to 394 ± 66 Hz (see Tab. 6). The loss in power and the increase of the iBF are indicative of a reduced active amplification. To test this hypothesis, I recorded the antennal displacement responses to pure-tones of different intensities.

3.5.2.2 Sound-induced antennal displacements and CAP responses
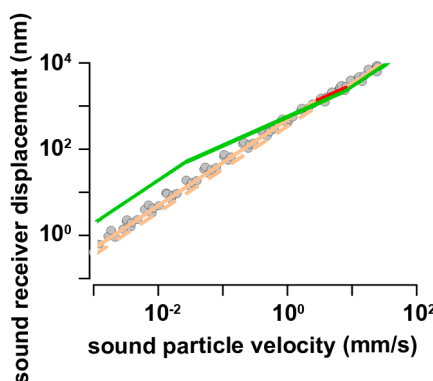
Figure 83 particle velocity induced sound receiver displacement of *trp* mutants

Trp mutants almost completely loose the active amplification. (green: wt) [N=3]

The sensitivity gain due to active amplification was significantly reduced in *trp* mutants (1.7 ± 0.3 re. ca. 8 in the wild-type and controls). Also the amplitude of the sound-induced CAP response was lowered to 11 ± 8 μV. Due to the loss of amplification, the particle velocity sensitivity of the sound receiver was decreased (0.13 ± 0.05 mm/s; wt/controls: 0.03 ± 0.01 mm/s), but the antennal displacement sensitivity of the CAP response was slightly decreased (threshold

72 ± 25 nm; wt/controls: 49.7 ± 7.6 nm). The dynamic range of the CAP responses remained unaltered with respect to antennal displacement and decreased with respect to sound particle velocity. The slightly changed displacement sensitivity could mean that TRP is a component of the transduction machinery. This was tested by analyzing correlates of transduction in the receiver's mechanics.
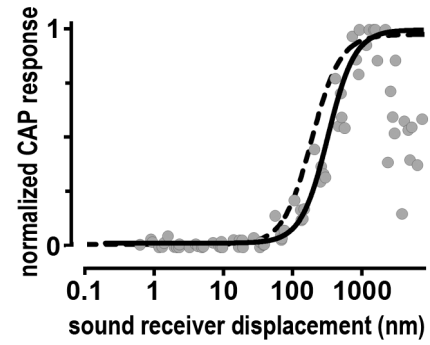

Figure 84 CAP response to sound receiver displacement (*trp* mutant)

A slightly shift of the CAP response is apparent. (dashed line: typical control response) [N=3]

3.5.2.3 gating compliance measurements of *trp* mutants

The average K_{steady} of the antennal receiver of *trp* mutants was 44 ± 1 µN/m, and its average K_{inf} was 74 ± 1 µN/m. Both figures are close to the respective values obtained for wild-type flies and controls (Tab. 5). Judged from the receiver's mechanics, both channel types are present in the mutants. The 2-channel type gating spring fit yielded 1289 ± 280 sensitive channels with a single channel gating force of 18 ± 2 fN and 58722 ± 1243 insensitive channels with a single channel gating force of 3 ± 0.2 fN. Also these values are similar to those obtained for the wild-type and controls (Tab. 5). Hence, although TRP seems to regulate amplification, it seems dispensable for transducer gating in the fly's ear.
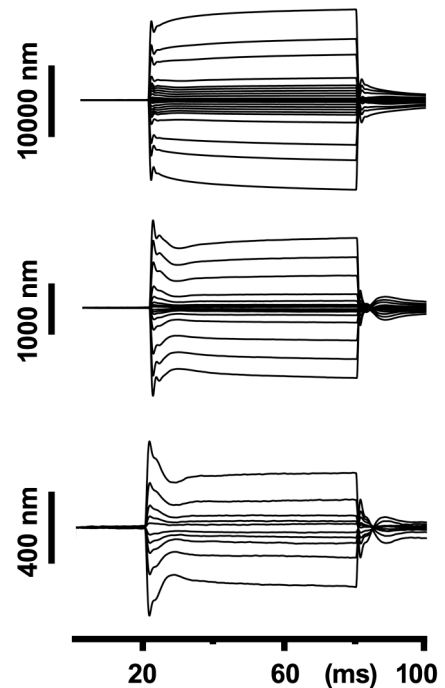

Figure 85 displacement response of different amplitudes (*trp* mutant)

Different amplitudes of sound receiver displacement. The displacement response seemed largely unaltered compared with wild-types and controls.
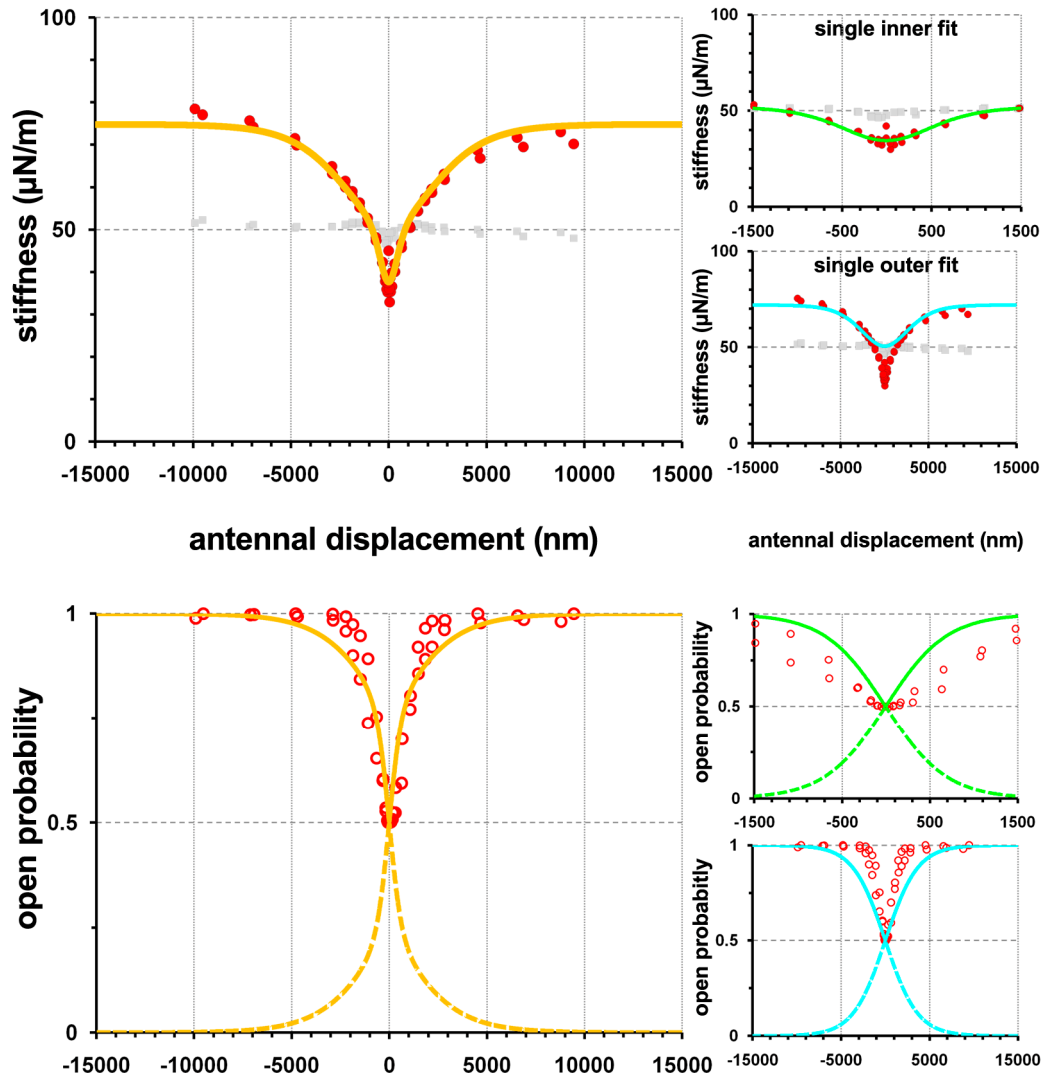
Figure 86 gating compliance fits and deduced open probabilities of *trp* mutants

The calculated dynamic stiffness of *trp* mutants was fitted with a 2-channel equation system over the whole range of antennal displacement (yellow). Separately only medium displacements ([-1500,1500] nm; green) and large displacements ([-15000,-1500] and [1500,15000] nm; cyan) were fitted with a 1-channel equation. The parameter z was used to describe the predicted open probability of the mechanotransduction channels. Based on the small and large displacement fits separate P_os were calculated. The CAP response was describable by the P_o derived from the fit of the sound receiver's mechanics. Compared with wild-types and controls the asymptotic stiffness did not drop significantly. Indicating a supporting role for TRP and not an involvement in the coupling of the sound receiving structures to the mechanotransduction channel(s). [N=3]

3.5.3 Painless (TRPA) might contribute to the mechanotransduction channel complex

Painless (Pain) is implicated in nociception and the detection of moderate temperature differences [110,111,126,128]. Recent work has shown that it is also required for gravytaxis behaviour [130]. Judged from promotor-fusion constructs, Painless is expressed in ca. 100 JO-neurons. I tested the impact of different *painless* mutants on JO function. It should be noted that the available mutants (*pain1-4*) are not nulls; *pain2* and 4 have a semi dominant mutant effect while *pain1* is a weaker allele [130]. I tested the phenotypes of flies carrying the mutations *pain1*, *2*, and *4*.

3.5.3.1 *painless* mutants show a reduced free fluctuation power

The fluctuation power of the receivers of *pain*2 and 4 mutants was significantly decreased to 221 ± 128 nm² (*pain2*) and 171 ± 119 nm² (*pain4*) compared to wild-type flies and controls (Tab. 6). Along with this reduction in power, the iBF was increased to 424 ± 58 Hz (both strains pooled). The weaker allele *pain1* showed less severe defects: the power was 398 ± 133 nm² and the iBF was 396 ± 65 Hz.
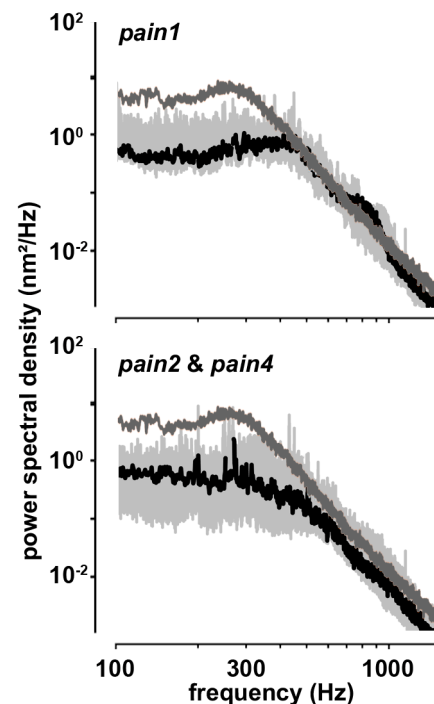
Figure 87 power spectra of *pain1* & *pain4* mutants

The power of the *painless* alleles 2 & 4 is significantly reduced and the iBF increased. The allele 1 has a less severe phenotype but is still significantly reduced. [N=10] dark grey: wild-type

3.5.3.2 The compressive nonlinearity is lost in *pain2/pain4* and reduced in *pain1* mutants
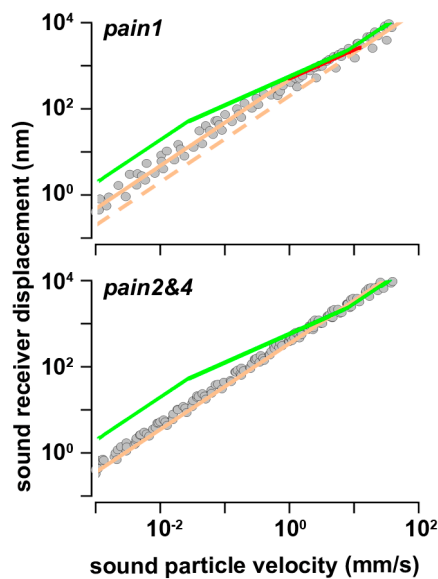
The compressive nonlinearity was virtually lost in *pain2* and *pain4* mutants (sensitivity gain: 1.4 ± 0.5). The weaker allele *pain1* reduced the sensitivity gain to 3 ± 1.6. As a consequence, the sound particle velocity sensitivity of *pain1*, *2* and *4* mutants was decreased (*pain1*: 0.17 ± 0.1 mm/s; *pain2&4*: 0.18 ± 0.07 mm/s; compare Tab. 6). The antennal displacement sensitivity of CAPs in *pain1* mutants (38 ± 10 nm) remained unchanged but was decreased in *pain2* and *pain4* mutants (60 ± 14 nm). The maximum sound-induced CAP responses were decreased in all *pain* mutants (*pain1*: 18 ± 15 µV; *pain2&4*: 10 ± 7 µV). The free fluctuation and sound-induced antennal displacement measurements indicated that *pain* is required for the nonlinear amplification and sensitive hearing. To test whether Painless contributes to transduction, I analyzed correlates of transduction in the receiver's mechanics of *pain2* and *4* mutants.
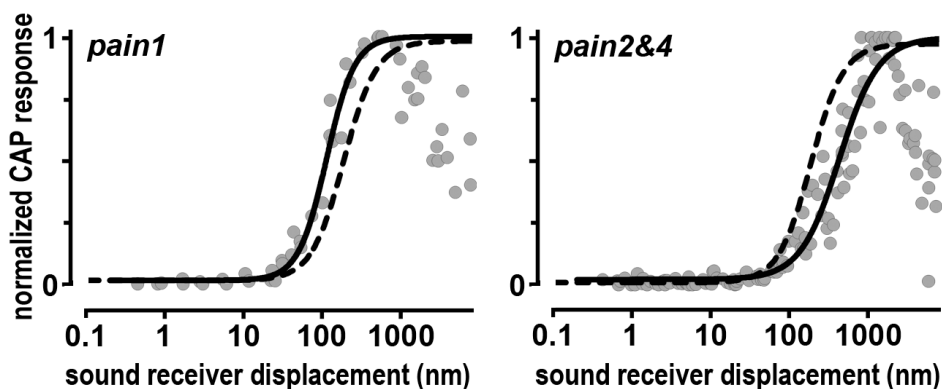

Figure 89 particle velocity induced sound receiver displacement of *pain1, 2 &4* mutants
Aa remnant compressive nonlinearity was apparent in *pain1* mutants and lost in *pain* 2 & 4 mutants. (green: wt) [N=4-6]

Figure 88 CAP response of *pain1, 2 & 4*
Dashed line typical control response [N=6]

3.5.3.3 *pain* mutant sound receivers show a decrease of asymptotic stiffness and a reduced of single channel gating force

The average K_{steady} of the antennal receivers of *pain2* and *4* mutants was 49 ± 9 µN/m, which is close to the wild-type. K_{inf} was 73 ± 2 µN/m, which is slightly less than seen in the wild-type. A gating spring model with 2 channel types was used to fit the data. It yielded 1156 ± 581 sensitive channels with a single channel gating force of 15 ± 4 fN and 103923 ± 37836 insensitive channels with a single channel gating force of 1.9 ± 0.3 fN. While both channel numbers resemble those of the wild-type, the gating forces are reduced. Together with a slightly decreased K_{inf}, this suggests that Painless is not a mechanotransduction channel proper but modulates channel gating: the single channel gating force (z) depends on the gating swing (d) and the stiffness of a single gating spring (κ), $z = \gamma \kappa d$ (γ is the scaling factor from the sound receiver down to the neuronal level). Hence, *pain2* and *4* might decrease the gating swing or spring stiffness. The slight decrease of K_{inf} indicates a change of κ [25] rather than d, because alterations in d do not affect K_{inf} [25]. A softer gating spring will inevitably reduce channel sensitivity, consistent with the reduced displacement sensitivity of the CAP response.
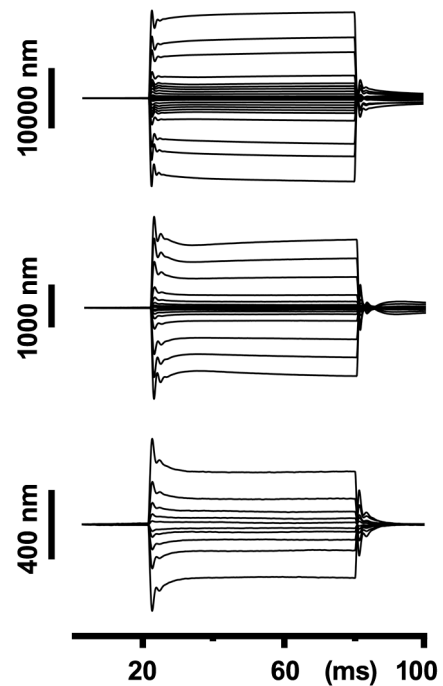

Figure 90 displacement response of different amplitudes (*painless2* mutant)

Different amplitudes of sound receiver displacement. The displacement response seemed largely unaltered compared with wild-types and controls.
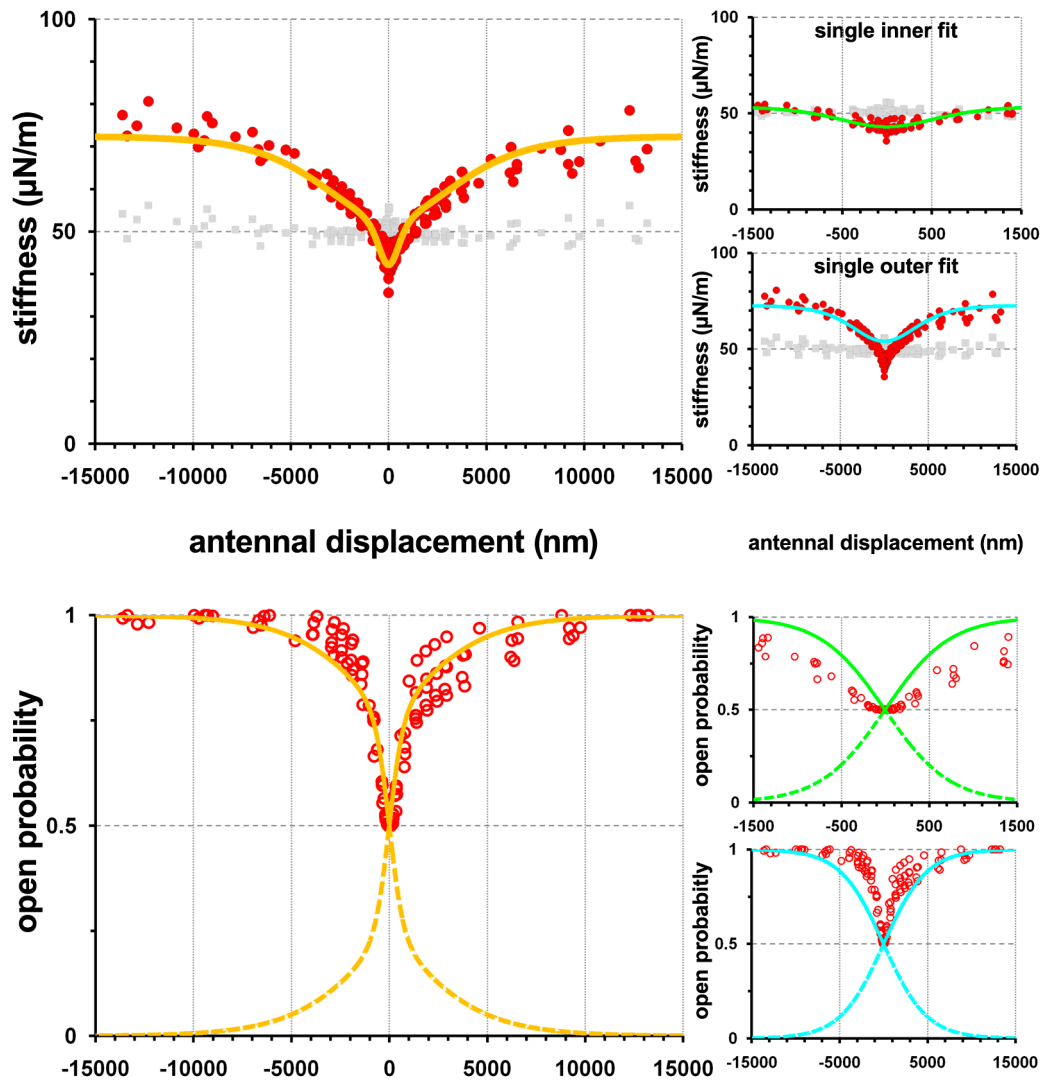
Figure 91 gating compliance and open probabilities of *pain* mutants

pain2&4 gating compliances were fitted with a 2-channel gating spring model over the whole range of antennal displacement (yellow). Separately only small displacements ([-1500,1500] nm; green) and large displacements ([-15000,-1500] and [1500,15000] nm; cyan) were fitted with a 1-channel equation. The asymptotic stiffness only dropped slightly. This indicates that Painless connects the channel(s) to the sound receiving structures. The shape of the insensitive channel's gating compliance seems unaltered only the sensitive channel is affected. The parameter *z* was used to describe the predicted open probability of the mechanotransduction channels. Based on the small and large displacement fits separate P_os were calculated. The CAP response superimposed with P_o derived from the fit of the sound receiver's mechanics. [N=6]

3.5.4 TPML is expressed in ligament cells

Mutations in mammalian TRPMLs cause hearing impairment [158,220]. Only one representative (TRPML) is known in *Drosophila*. Mammalian TRPMLs are implicated in vesicle transport and are important for hair cell maturation; they are expressed in hair cells as well as in supporting cells [157]. To localize TRPML expression in *Drosophila* we used a P-element mutant that carried a GAL4D and an UAS-YFP. This mutant (Bloomington: 19409) should show YFP expression in those cells that normally express TRPML. TRPML seems expressed in JO ligament cells (Figure 92).
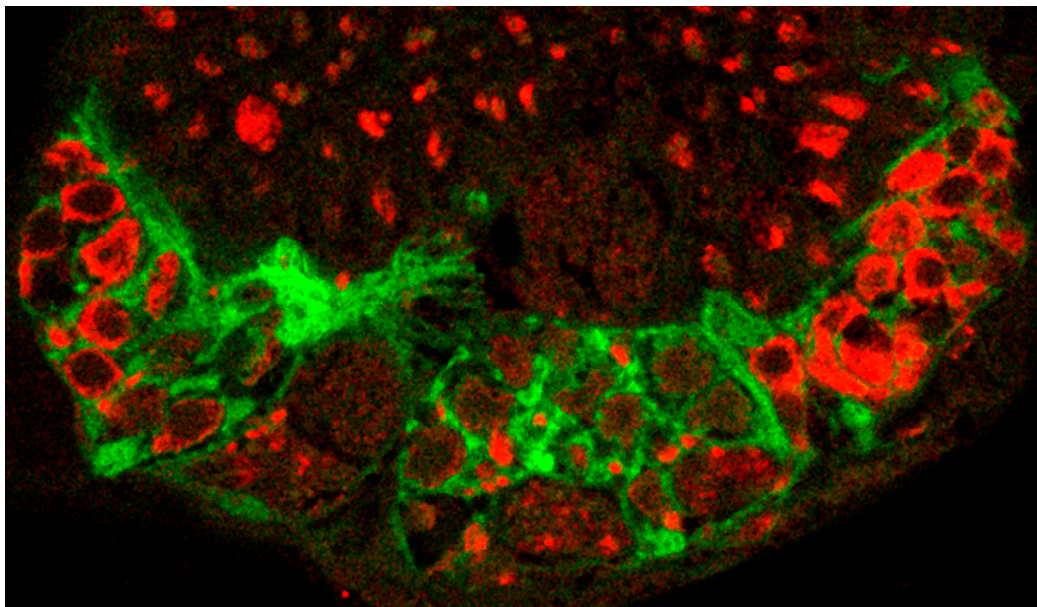
Figure 92 22c10 antibody staining (red; RFP-Anti-22c10) of JO-neurons and YFP labelling of presumably TRPML expressing cells (green)
Horizontal slice through the 2nd antennal segment. The antibody 22c10 labels neurons (red) the YFP-signal (green) presumably labels those cells that express TRPML. There is now overlap between the red and green channel. The presumably TRPML positive cells might be the ligament cells. (Slices and antibody staining performed by Seol-hee Joo)

This finding suggests that TRPML might have a supporting rather than direct function in JO mechanotransduction. If the labelling is correct, TRPML is not expressed in the sensory neurons and thus cannot contribute to the mechanotransduction machinery proper. For the following experiments, I used mutants that derived from an imprecise excision of the P-element. This excision resulted in the deletion of ca. 1000 BB around the start region of the TRPML (see Tab. 3).

3.5.4.1 Free fluctuation power decreased in *trpml[1]* mutants
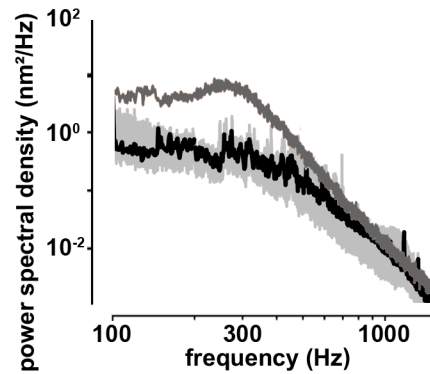
The power of TRPML mutant sound receivers was significantly decreased to 194 ± 64 nm² (wt/controls: 1171 ± 573 nm²), and their iBF was increased to 464 ± 8 Hz (wt/controls: 250 ± 49 Hz). Accordingly, proper amplification requires TRPML.

Figure 93 powerspectra of *trpml[1]* mutants
The dark grey line represents a typical wild-type free fluctuation. [N=5]
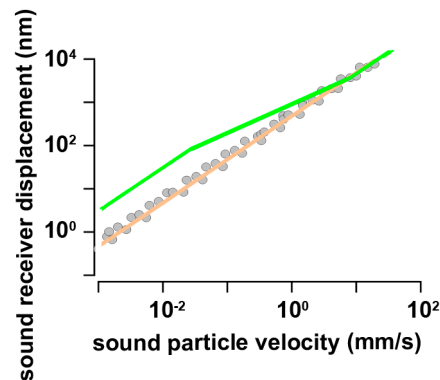
3.5.4.2 Compressive nonlinearity lost in *trpml[1]* mutants

The compressive nonlinearity is lost in *trpml[1]* mutants, and the particle velocity sensitivity of sound-induced CAP responses is decreased to 0.09 ± 0.06 mm/s (wt/controls: 0.03 ± 0.01 mm/s). The antennal displacement sensitivity of the CAP response was unaltered (*trpml[1]*: 43 ± 17 nm; wt/controls: 50 ± 8 nm). The maximum amplitude of the CAP response was reduced to 6 ± 2 µV. These findings indicate that TRPML is important for the active amplification but does not affect the sensitivity of JO to antennal displacements.

Figure 94 compressive nonlinearity lost in *trpml[1]* mutants
green: typical wild-type/control response [N=3]

3.5.4.3 The asymptotic stiffness of *trpml[1]* mutants does not drop

As in wild-type flies, the average K_{steady} of the antennal receiver of *trpml[1]* mutants was ca. 50 µN/m (50 ± 10 µN/m), and also K_{inf} was not unaltered (75 ± 2 µN/m). The numbers of sensitive (932 ± 298) and insensitive (98868 ± 23874) channel likewise remained unchanged, but whereas the single channel gating force of the insensitive channels remained constant (2.4 ± 0.4 fN), that of the sensitive channel was decreased (10.4 ± 0.2 fN). Because K_{inf} stays constant, TRPML might modulate the gating swing of the sensitive channels rather than their gating spring stiffness. The TRPML-dependence of the sensitive channels is consistent with alterations in amplification because the sound-receptors seem to harbour the sensitive channels and amplification seems to arise from these receptor cells. The complete loss of amplification suggests that in addition to altering channel gating, TRPML might also modulate transducer adaptation.
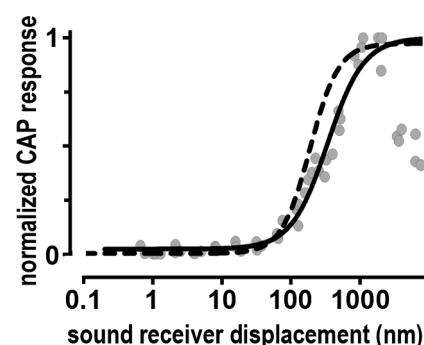
Figure 96 CAP response of JO-neurons in *trpml[1]* mutants
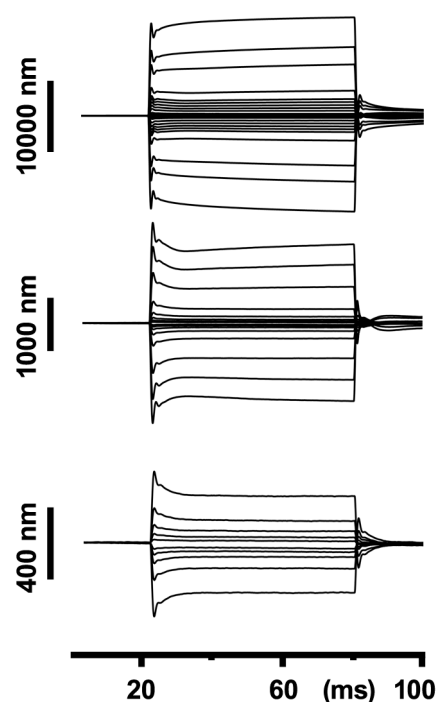CAP response relative to the antennal displacement. [N=3]

Figure 95 displacement response of different amplitudes (*trpml[1]* mutant)
Different amplitudes of sound receiver displacement. The displacement response seemed largely unaltered compared with wild-types and controls
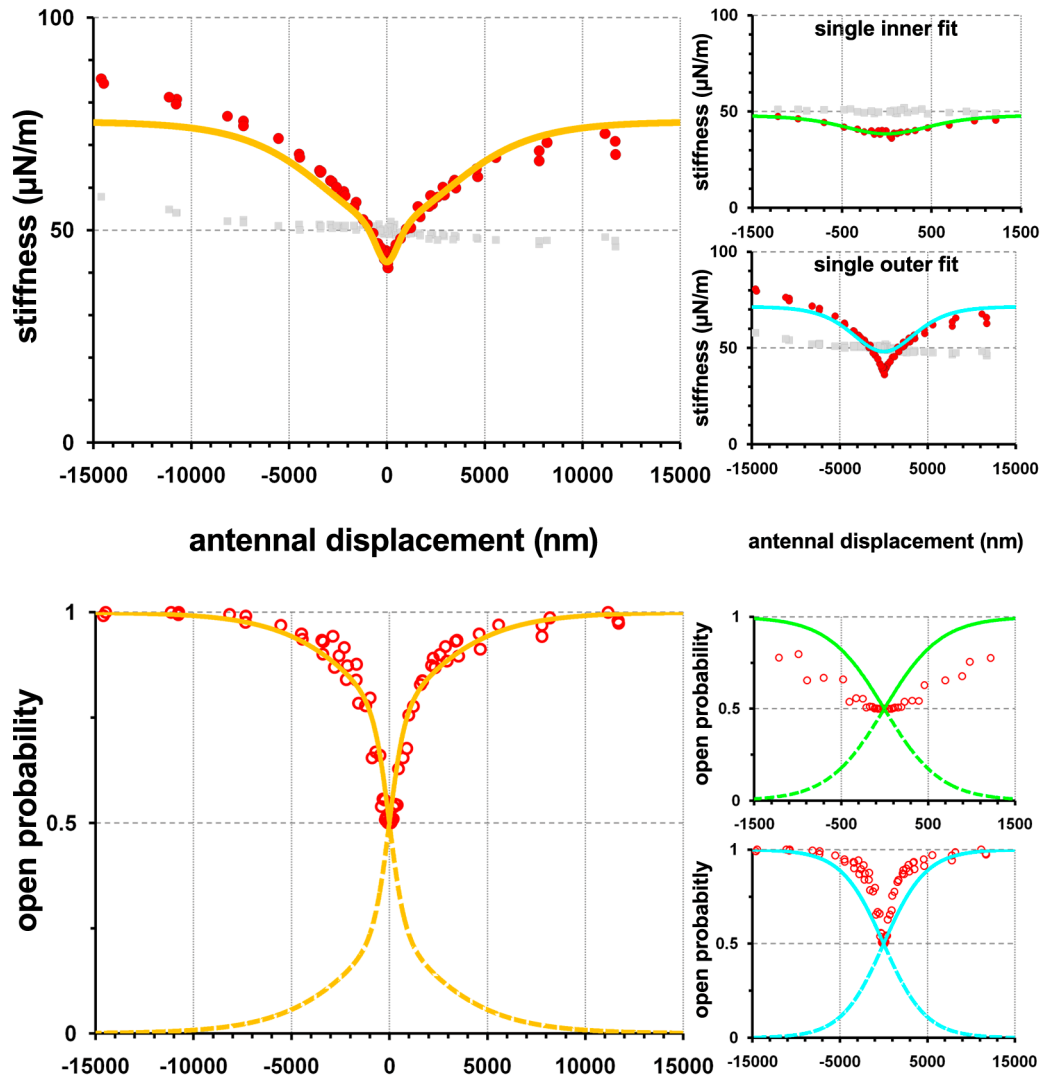
Figure 97 gating compliance fits and deduced open probabilities of *trpml[1]* mutants

The dynamic stiffness of *trpml[1]* mutants was fitted with a 2-channel equation system over the whole range of antennal displacement (yellow). Separately only medium displacements ([-1500,1500] nm; green) and large displacements ([-15000,-1500] and [1500,15000] nm; cyan) were fitted with a 1-channel equation. The parameter *z* was used to describe the predicted open probability of the mechanotransduction channels. Based on the small and large displacement fits separate P_os were calculated. The CAP response was describable by the P_o derived from the fit of the sound receiver's mechanics. Compared with wild-types and controls the asymptotic stiffness is unchanged. This indicates that *trpml* is not involved in connecting the mechontransduction channel(s) to the sound receiving structures. The shape of the insensitive channel's gating compliance seems unaltered only the sensitive channel is affected. [N=3]

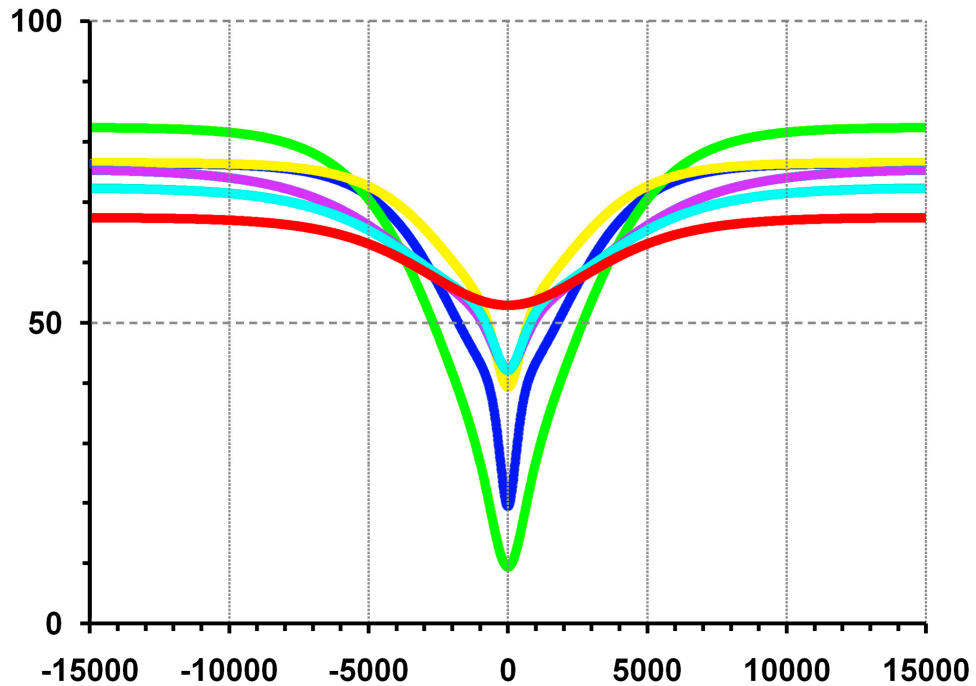## 3.6. Summary of all measured gating compliance fits

Figure 99 gating spring model fits of measured mutants and the wild-type
Blue: wild-type; red: *nompC*-mutants; yellow: *trp* mutants; green: *nan/iav* mutants; violet: *trpml* mutants; cyan: *painless* mutants
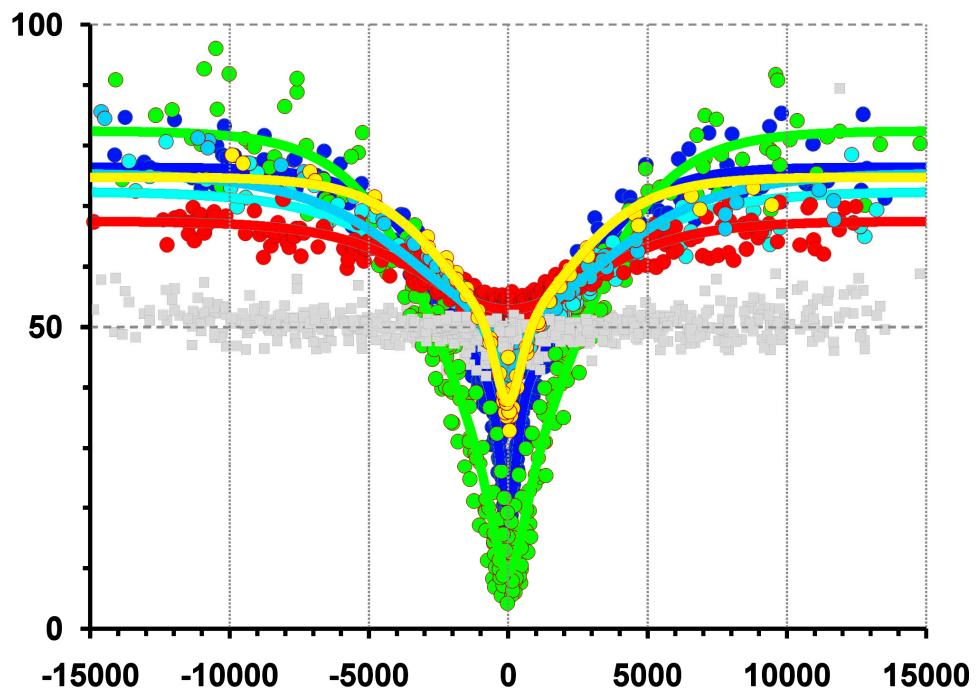

Figure 98 gating spring model fits of measured mutants and the wild-type
grey: wild-type; red: *nompC*-mutants; yellow: *trp* mutants; green: *nan/iav* mutants; violet: *trpml* mutants; cyan: *painless* mutants

4. Discussion

I have analyzed the TRP-dependence of mechanosensory transduction and amplification in the *Drosophila* ear. Several TRP channels are identified that contribute to transduction and amplification. In the following, I will present a model of TRP-function in the *Drosophila* ear that is based on the results obtained.

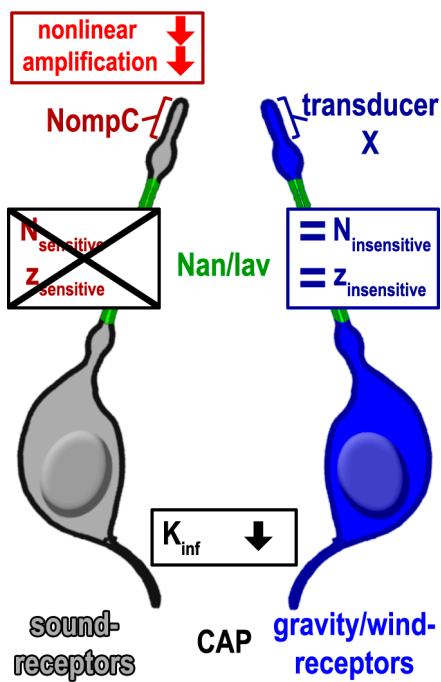## 4.1. NompC is essential for the sound-receptor function

Figure 100 Effect of the loss of NompC on sound-receptors
The ablation of sound-receptor cells and the loss of NompC results in the loss of the nonlinear amplification, reduced the asymptotic stiffness, and lowers the CAP response.

JO sound-receptor cells are required for the nonlinear amplification of sound-induced antennal vibrations (3.2.2.1, Figure 100). Likewise the loss of NompC resulted in the loss of nonlinear amplification, indicating that NompC is required for sound-receptor function (3.2.2.1). The loss of sound-receptors abolishes sensitive antennal displacement CAP responses, so does the loss of NompC (3.1.2.1). In addition, the remnant CAP response amplitudes are significantly reduced in flies with ablated sound-receptors and *nompC* mutants (3.1.1). The calcium response of sound-receptor JO-neurons is lost in *nompC* mutants (3.3.5). Ablation of sound-receptors results in the loss of the gating compliance signature of the sensitive channel type, as did the loss of NompC (3.4.4, 3.4.6). The remnant gating compliance signature in flies with ablated sound-receptors and *nompC* mutants thus resembles the insensitive channel, presumably responsible for gravity/wind-receptor function ($K_{GS\_insensitive}$ = 17 µN/m). Taken this into consideration it was possible to calculate the combined gating spring stiffness of the sensitive channel type ($K_{GS\_sensitive}$ = 15 µN/m). In addition, I showed that one copy of *nompC* is not sufficient to maintain a gating compliance that resembles the wild-type

(3.4.3,3.4.5). This was true for the balanced flies (*nompC^x/CyO*) and for the ectopically expressed heterozygous *nompC-L* rescue flies. My findings together with studies conducted in *C. elegans* [92] strongly suggest that NompC is the mechanotransduction channel required for hearing in *Drosophila* [201]. These findings also mean that NompC has no function in gravity/wind-receptor cells. The next steps will be do manipulate the sequence of the *nompC-L* rescue construct and change for example the number of ANK-repeats or alter the presumable pore region etc.. Assuming NompC is the mechanotransduction channel changes of its mechanics will be betrayed by changes of the sound receiver's mechanics. With NompC as a good mechanotransduction candidate, maybe the insensitive channel is also a member of the TRP superfamily.

4.2. Nan and Iav are required for CAP generation in sound- and gravity/wind-receptor cells

The loss of Nan or Iav results in a loss of inducible CAP responses (3.5.1.2), a hyper-amplification (3.5.1.2), and an increase of mechanotransduction channel numbers (3.5.1.3). As a result, of the increase of both channel numbers the gating compliance gets broader and K_{inf} increases. The increase of the sensitive and insensitive channel numbers could indicate that the neurons are trying to compensate for their inability to produce mechanical-induced CAPs by over expressing their mechanical sensors, the mechanotransduction channels. Hence, although Nan and Iav are important for the function of both the sound- and gravity/wind-receptors they are not part of the mechanotransduction machinery in either receptor cell population.
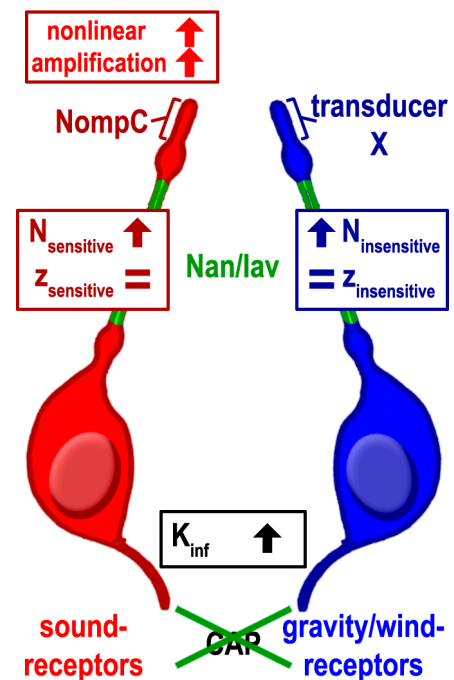

Figure 101 Effect of the loss of Nan/Iav on JO-neuron function
The loss of Nan/Iav results in an increase of the sensitive and insensitive channel numbers, the CAP response is gone and the nonlinear amplification increased drastically.

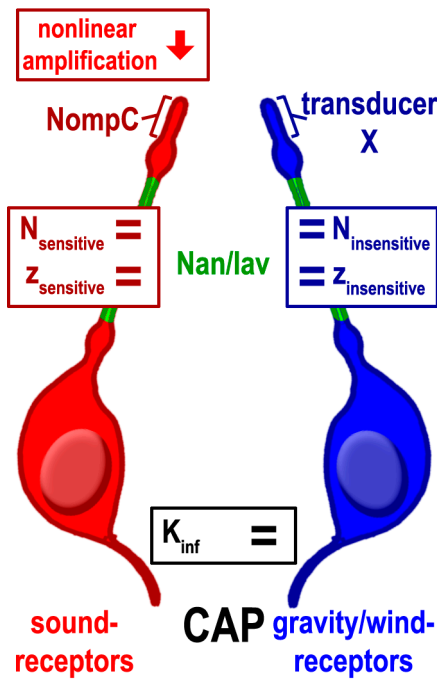## 4.3. TRP is not required for mechanotransduction

Figure 102 Effect of the loss of TRP on JO-neuron function
loss of TRP results in a loss of amplification and reduced maximal CAP responses. It did not change number of channels, their single channel gating force or the asymptotic stiffness

The loss of TRP did not result in a change of the nonlinear gating compliance, the linear stiffness, or the asymptotic stiffness of the antennal sound receiver (3.5.2.3). The nonlinear amplification, however, was reduced and the sound particle velocity sensitivity of JO-neurons decreased (3.5.2.2). To understand this we have to look at the gating spring model I used. It neglects the presence of adaptation motors. Those motors, however, could be important for the nonlinear amplification because they keep the mechanotransduction channels in an optimal working range and thus allow for transducer based amplification [40]. One might speculate that the insensitive channel is not coupled adaptation motors. That only sound-receptors are required for the nonlinear amplification supports this hypothesis.
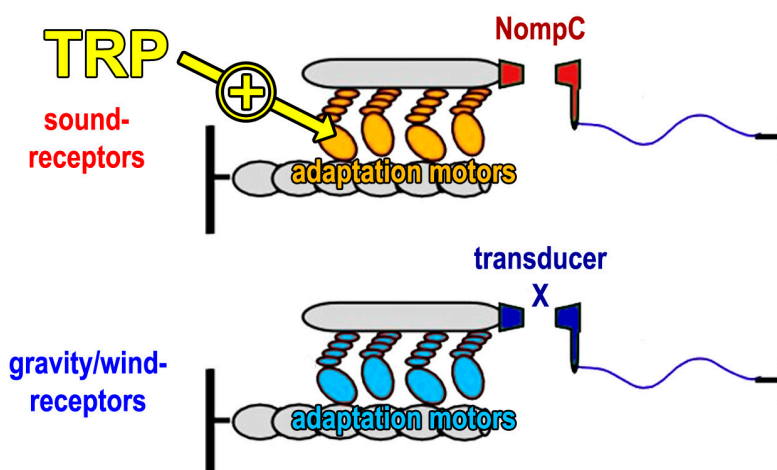

Figure 103 TRP may be required for adaptation motors of the sensitive channels
The loss of TRP results in the loss of nonlinear amplification. Although, the transducers of trp mutants remained unchanged, TRP might have an effect on the adaptation motors of the sensitive channel

4.4. Painless modulates all single channel gating forces

The loss of Painless causes the loss of the nonlinear amplification (3.5.3.2), a reduction of antennal displacement sensitive CAPs (3.5.3.2), and a slight decrease of the asymptotic stiffness of the sound receivers (3.5.3.3). These findings indicate that Painless modulates the gating of both, the sensitive and insensitive channels. Due to the decrease of the asymptotic stiffness, a change of the single channel gating springs is most likely the modus operandi of Painless. The other possibility would be a change of the gating swing, but this is unlikely because it would not explain the decreased asymptotic stiffness. How this modulation occurs has to be determined in following experiments. For example measurements of the adaptation process could yield further information.
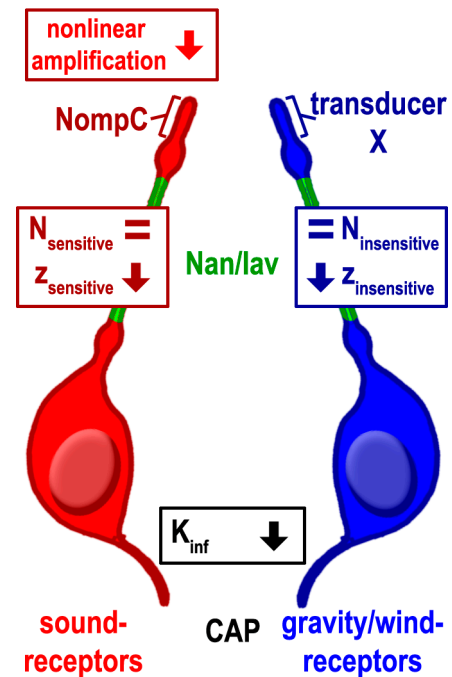
Figure 104 The effect of the loss of Painless on JO function
painless mutants showed a reduced nonlinear amplification and a reduction of the single channel gating force for both channel types. Also the asymptotic stiffness is decreased.
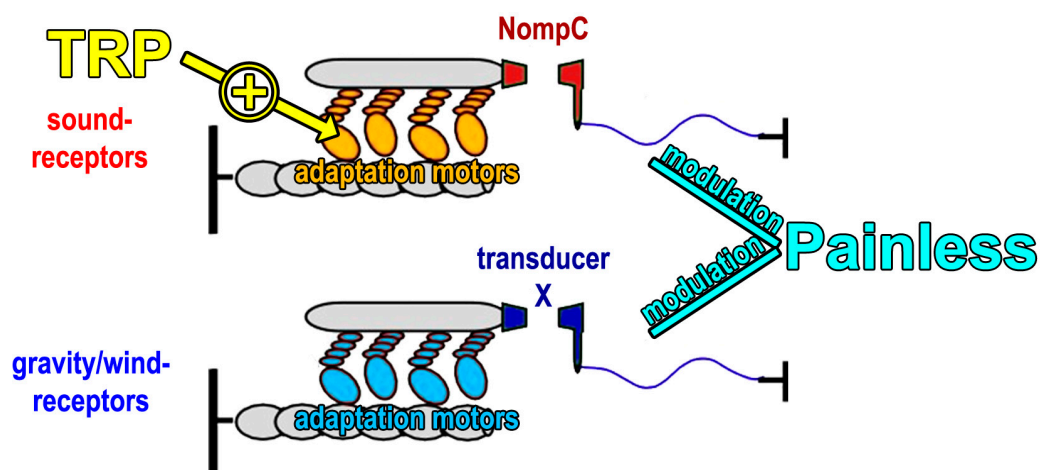

Figure 105 Painless modulates gating springs of transduction channels
The loss of Painless results in the loss of nonlinear amplification. Also the single channel gating forces and the asymptotic stiffness of the sound receiver are reduced. Hence, Painless could modulate the gating springs of both transduction channels.

4.5. TRPML modulates the single channel gating force of the sensitive channel
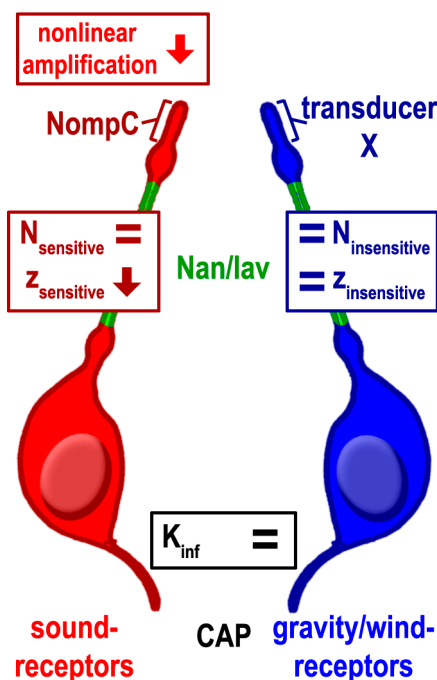

Figure 106 Effect of the loss of TRPML on JO function
The loss of TRPML causes the loss of nonlinear amplification

Similar to the effect seen in *painless* mutants, the loss of TRPML causes the loss of nonlinear amplification (3.5.4.2), a reduction of maximum CAP amplitude response (3.5.4.2), and a reduction of the single channel gating force of the sensitive channel (3.5.4.3). The asymptotic stiffness of the antennal sound receiver, however, remained unchanged, as did the numbers for the sensitive and insensitive channels. Preliminary imaging data indicates that TRPML is expressed in ligament cells, thus a direct interaction of TRPML with the mechanotransduction machinery is unlikely. While Painless most likely modulates the singe gating springs of both channel types, TRPML seems to modulate the gating swing of the sensitive channel.
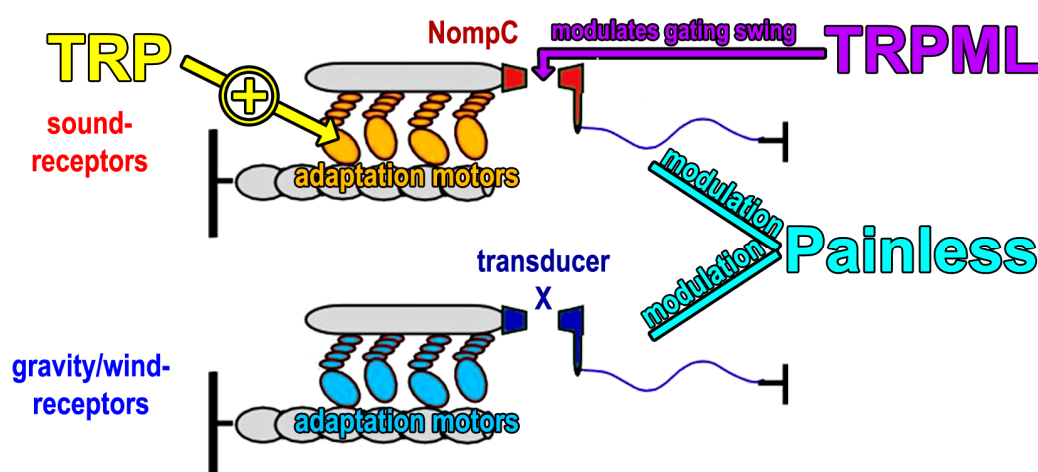

Figure 107 TRPML seems to modulate the gating swing of the sensitive channel
The loss of TRPML results in the loss of nonlinear amplification. Although TRPML is presumably in ligament cells, the most likely explanation for the observed phenotype is a modulation of the gating swing of the sensitive channel.

4.6. Methods to dissect hearing in *Drosophila*

The methods and techniques I used, improved, and developed during my PhD-thesis are well suited to analyse the function of proteins required for JO-function. Individual methods, however, give only some indications with a variety of possible interpretations but all methods combined narrow down those possibilities. Antibody staining to localize proteins would further narrow down the possible explanations for observed phenotypes. This will filter out those genes that are worthwhile for further examination.

The calcium imaging technique I adapted and improved is adequate to dissect the function of subsets of JO-neurons and test for mutant effects on all JO-neurons or different neuronal subpopulations. Further improvement of the calcium imaging technique will include high spatial- and temporal resolution that will allow to actually measure the presumable calcium wave down the dendrite into the soma. Together with force step stimulations to probe the gating of mechanotransduction channels, simultaneous CAP recording and monitoring the antennal displacements this will allow a deeper view into the inner workings of Johnston's organ than was possible before.

Although a lot of work is still to be done, the combination of probing the gating compliance of mechanotransduction channels with simultaneous measurement of intracellular calcium levels and CAP responses, will likely yield promising results and will facilitate our understanding of the hearing process in Drosophila and thus, maybe, also in vertebrates and mammals.

I want to close with a quotation from a famous, German movie: "Wat is'n Dampfmaschin? Da stella ma uns mal janz dumm und saachen n Dampfmaschin, dat is'n große, runde, schwarze Raum." (Feuerzangenbowle).

Translation: "What is a steam engine? Well, let's pretend we are dumb and say a steam engine is a big, round, black room."

I think the Johnston's organ is not unlike the famous "dampfmaschin". It is a black, unknown space and with the presented techniques, we will be able to peek at its inner workings.

5. Abbreviations

a1:	1st antennal segment; scape
a2:	2nd antennal segment; pedicel
a3:	3rd antennal segment; funicle
ar:	Arista
ANK:	ankyrin
CAP:	compound action potential
ch organs:	chordotonal sensory organs
d:	gating swing
Deg/ENaC:	degenerin/epithelial Na^{2+} channel
Df(2L)cl^{h2}:	Deficiency uncovering *nompC* mutation
eCFP:	cyan fluorescent protein
es organs:	external structure sensory organs
eYFP:	yellow fluorescent protein
FFT:	Fast Fourier Transform
FLP:	Flippase
FRET:	Förster Resonance Energy Transfer
FRT:	Flippase Recognition Target
γ:	scaling factor from the sound receiver to neurons
G/W-receptors:	gravity/wind
iav:	*inactive*
iBF:	individual best frequency
JO:	Johnston's organ
JO1:	a.k.a. NP0761 GAL4 driver for all JO-neurons
JO15:	GAL4 driver for sound-receptors
JO31:	a.k.a. NP6250 GAL4 driver for gravity/wind-receptors
κ:	single channel gating spring
K_{GS}:	combined gating spring stiffness
$K_{GS-combined}$:	combined gating spring stiffness of the sensitive and insensitive channel type

$K_{GS-sensitive}$:	combined gating spring stiffness of the sensitive channel type
$K_{GS-insensitive}$:	combined gating spring stiffness of the insensitive channel type
K_{inf}:	asymptotic, infinite stiffness
K_{steady}:	parallel, steady state stiffness
K_{peak}:	dynamic, peak stiffness (opening/closing of channels)
MEC:	mechanosensory defective
MET:	mechano-electrical-transduction channel
MRC:	mechanoreceptor current
MRP:	mechanoreceptor potential
Msc:	mechanosensitive channel
N:	number of channels
nan:	*nanchung*
nompC:	no mechanoreceptor potential C
pain:	*painless* (TRPA1 homologue in *Drosophila*)
P_o:	open probability
PSD:	power spectral density
RIP:	ribosome inactivating protein
S-receptors:	sound-receptors
TRP:	transient receptor potential
TRPA:	transient receptor potential "ankyrin"
TRPC:	transient receptor potential "canocical"
TRPM:	transient receptor potential "melastatin"
TRPML:	transient receptor potential "mucolipin"
TRPN:	transient receptor potential "nompC"
TRPP:	transient receptor potential "polycystin"
TRPV:	transient receptor potential "vanilloid"
wt/controls:	wild-type and control flies
z :	single channel gating force

6. Literature

[1]   Fritzsch B, Beisel KW (2001) Evolution and development of the vertebrate ear. *Brain Res Bull* 55:711–721.

[2]   Grinnell AD (1969) Comparative physiology of hearing. *Annu Rev Physiol* 31:545–580.

[3]   Nicolson T (2005) Fishing for key players in mechanotransduction. *Trends Neurosci* 28:140–144.

[4]   Pollack G (2000) Who, what, where? recognition and localization of acoustic signals by insects. *Curr Opin Neurobiol* 10:763–767.

[5]   Robert D (2001) Innovative biomechanics for directional hearing in small flies. *Biol Bull* 200:190–194.

[6]   Stumpner A, von Helversen D (2001) Evolution and function of auditory systems in insects. *Naturwissenschaften* 88:159–170.

[7]   Spieth H (1952) Mating behavior within the genus drosophila. *Bulletin of the American Museum of Natural History* 99:401–474.

[8]   Shorey HH (1962) Nature of the sound produced by drosophila melanogaster during courtship. *Science* 137:677–678.

[9]   Narda RD (1966) Analysis of the stimuli involved in courtship and mating in d. malerkotliana (sophophora, drosophila). *Animal Behaviour* 14:378 – 383.

[10]   Waldron I (1964) Courtship sound production in two sympatric sibling drosophila species. *Science* 144:191–193.

[11]   Hoy RR, Hoikkala A, Kaneshiro K (1988) Hawaiian courtship songs: evolutionary innovation in communication signals of drosophila. *Science* 240:217–219.

[12]   Hall JC (1994) The mating of a fly. *Science* 264:1702–1714.

[13]   von Schilcher F (1976) The role of auditory stimuli in the courtship of drosophila melanogaster. *Animal Behaviour* 24:18 – 26.

[14]   Ewing A, Bennet-Clark H (1968) The courtship songs of drosophila. *Behaviour* 31:288–301.

[15]   Ewing AW, Miyan JA (1986) Sexual selection, sexual isolation and the evolution of song in the drosophila repleta group of species. *Animal Behaviour* 34:421 – 429.

[16]   Göpfert MC, Robert D (2002) The mechanical basis of drosophila audition. *J Exp Biol* 205:1199–1208.

[17]   Johnston (1855) Auditory apparatus of the culex mosquitoes. *Q.J.Microsc* 3:97–102.

[18]   Boekhoff-Falk G (2005) Hearing in drosophila: development of johnston's organ and emerging parallels to vertebrate ear development. *Dev Dyn* 232:550–558.

[19]   Yack JE (2004) The structure and function of auditory chordotonal organs in insects. *Microsc Res Tech* 63:315–337.

[20]   Sivan-Loukianova E, Eberl DF (2005) Synaptic ultrastructure of drosophila johnston's organ axon terminals as revealed by an enhancer trap. *J Comp Neurol* 491:46–55.

[21]   Göpfert MC, Robert D (2001) Biomechanics. turning the key on drosophila audition. *Nature* 411:908.

[22]   Todi SV, Sharma Y, Eberl DF (2004) Anatomical and molecular design of the drosophila antenna as a flagellar auditory organ. *Microsc Res Tech* 63:388–399.

[23]   Caldwell JC, Eberl DF (2002) Towards a molecular understanding of drosophila hearing. *J Neurobiol* 53:172–189.

[24]   Albert JT, Nadrowski B, Göpfert MC (2007) Mechanical signatures of transducer gating in the drosophila ear. *Curr Biol* 17:1000–1006.

[25]   Albert JT, Nadrowski B, Göpfert MC (2007) Drosophila mechanotransduction–linking proteins and functions. *Fly (Austin)* 1:238–241.

[26]   Nadrowski B, Göpfert MC (2009) Modeling auditory transducer dynamics. *Curr Opin Otolaryngol Head Neck Surg* 17:400–406.

[27]   Bermingham NA, et al. (1999) Math1: an essential gene for the generation of inner ear hair cells. *Science* 284:1837–1841.

[28]   Chen P, Johnson JE, Zoghbi HY, Segil N (2002) The role of math1 in inner ear development: Uncoupling the establishment of the sensory primordium from hair cell fate determination. *Development* 129:2495–2505.

[29]   Woods C (2004) Math1 regulates development of the sensory epithelium in the mammalian cochlea. *Nature neuroscience* 7:1310–1318.

[30]   Ben-Arie N, et al. (2000) Functional conservation of atonal and math1 in the cns and pns. *Development* 127:1039–1048.

[31]   Wang VY, Hassan BA, Bellen HJ, Zoghbi HY (2002) Drosophila atonal fully rescues the phenotype of math1 null mice: new functions evolve in new cellular contexts. *Curr Biol* 12:1611–1616.

[32]   Erwin DH, Davidson EH (2002) The last common bilaterian ancestor. *Development* 129:3021–3032.

[33]   Balleza D (2010) Toward understanding protocell mechanosensation. *Orig Life Evol Biosph*.

[34]   Fritzsch B, Beisel KW (2004) Keeping sensory cells and evolving neurons to connect them to the brain: molecular conservation and novelties in vertebrate ear development. *Brain Behav Evol* 64:182–197.

[35]   Fritzsch B, Beisel KW, Pauley S, Soukup G (2007) Molecular evolution of the vertebrate mechanosensory cell and ear. *Int J Dev Biol* 51:663–678.

[36]   Lewis J (1991) Rules for the production of sensory cells. *Ciba Found Symp* 160:25–39; discussion 40–53.

[37]   Liedtke W (2008) Molecular mechanisms of trpv4-mediated neural signaling. *Ann N Y Acad Sci* 1144:42–52.

[38]   Howard J, Hudspeth AJ (1988) Compliance of the hair bundle associated with gating of mechanoelectrical transduction channels in the bullfrog's saccular hair cell. *Neuron* 1:189–199.

[39]   Martin P, Mehta AD, Hudspeth AJ (2000) Negative hair-bundle stiffness betrays a mechanism for mechanical amplification by the hair cell. *Proc Natl Acad Sci U S A* 97:12026–12031.

[40]   Nadrowski B, Albert JT, Göpfert MC (2008) Transducer-based force generation explains active process in drosophila hearing. *Curr Biol* 18:1365–1372.

[41]   Dallos P (1992) The active cochlea. *J Neurosci* 12:4575–4585.

[42]   Gale JE, Ashmore JF (1997) An intrinsic frequency limit to the cochlear amplifier. *Nature* 389:63–66.

[43]   Fettiplace R, Ricci AJ, Hackney CM (2001) Clues to the cochlear amplifier from the turtle ear. *Trends Neurosci* 24:169–175.

[44]   Robles L, Ruggero MA (2001) Mechanics of the mammalian cochlea. *Physiol Rev* 81:1305–1352.

[45]   Ashmore J, Gale J (2004) The cochlear amplifier. *Curr Biol* 14:R403–R404.

[46]   Ashmore J, et al. (2010) The remarkable cochlear amplifier. *Hear Res* 266:1–17.

[47]   Gold T (1948) Hearing. ii. the physical basis of the action of the cochlea. *Proceedings of the Royal Society of London. Series B, Biological Sciences* 135:pp. 492–498.

[48]   Gold T, Pumphrey RJ (1948) Hearing. i. the cochlea as a frequency analyzer. *Proceedings of the Royal Society of London. Series B, Biological Sciences* 135:pp. 462–491.

[49]   Granit R (1961) [the nobel prize in physiology and medicine 1961 (george von bekesy)]. *Nord Med* 66:1565–1567.

[50]   Békésy G (1952) Direct observation of the vibrations of the cochlear partition under a microscope. *Acta Otolaryngol* 42:197–201.

[51]   Naftalin L (1980) Frequency analysis in the cochlea and the traveling wave of von békésy. *Physiol Chem Phys* 12:521–526.

[52]   Davis H (1983) An active process in cochlear mechanics. *Hear Res* 9:79–90.

[53]   Ruggero MA, Rich NC, Recio A, Narayan SS, Robles L (1997) Basilar-membrane responses to tones at the base of the chinchilla cochlea. *J Acoust Soc Am* 101:2151–2163.

[54]   Göpfert MC, Humphris ADL, Albert JT, Robert D, Hendrich O (2005) Power gain exhibited by motile mechanosensory neurons in drosophila ears. *Proc Natl Acad Sci U S A* 102:325–330.

[55]   Nadrowski B, Effertz T, Senthilan PR, Göpfert MC (2010) Antennal hearing in insects - new findings, new questions. *Hear Res*.

[56]   Kamikouchi A, Albert JT, Göpfert MC (2010) Mechanical feedback amplification in drosophila hearing is independent of synaptic transmission. *Eur J Neurosci* 31:697–703.

[57]   Hudspeth AJ (2008) Making an effort to listen: mechanical amplification in the ear. *Neuron* 59:530–545.

[58]   Dallos P, Corey ME (1991) The role of outer hair cell motility in cochlear tuning. *Curr Opin Neurobiol* 1:215–220.

[59]   Eguíluz VM, Ospeck M, Choe Y, Hudspeth AJ, Magnasco MO (2000) Essential nonlinearities in hearing. *Phys Rev Lett* 84:5232–5235.

[60]   Hochmair ES, Hochmair-Desoyer IJ, Burian K (1979) Investigations towards an artificial cochlea. *Int J Artif Organs* 2:255–261.

[61]   Mann ZF, Kelley MW (2011) Development of tonotopy in the auditory periphery. *Hear Res*.

[62]   Romand R (1987) Tonotopic evolution during development. *Hear Res* 28:117–123.

[63]   Evans EF (1975) The sharpening of cochlear frequency selectivity in the normal and abnormal cochlea. *Audiology* 14:419–442.

[64]   Kittel M, Wagner E, Klump GM (2002) An estimate of the auditory-filter bandwidth in the mongolian gerbil. *Hear Res* 164:69–76.

[65]   Livshits MS (1995) [inner ear cochlear processes]. *Biofizika* 40:651–655.

[66]   Martin P, Hudspeth AJ, Jülicher F (2001) Comparison of a hair bundle's spontaneous oscillations with its response to mechanical stimulation reveals the underlying active process. *Proc Natl Acad Sci U S A* 98:14380–14385.

[67]   Nadrowski B, Martin P, Jülicher F (2004) Active hair-bundle motility harnesses noise to operate near an optimum of mechanosensitivity. *Proc Natl Acad Sci U S A* 101:12195–12200.

[68]   Géléoc GSG, Holt JR (2003) Auditory amplification: outer hair cells pres the issue. *Trends Neurosci* 26:115–117.

[69]   Fridberger A, et al. (2004) Organ of corti potentials and the motion of the basilar membrane. *J Neurosci* 24:10057–10063.

[70]   Fettiplace R (2006) Active hair bundle movements in auditory hair cells. *J Physiol* 576:29–36.

[71]   Jia S, He DZZ (2005) Motility-associated hair-bundle motion in mammalian outer hair cells. *Nat Neurosci* 8:1028–1034.

[72]   Choe Y, Magnasco MO, Hudspeth AJ (1998) A model for amplification of hair-bundle motion by cyclical binding of ca2+ to mechanoelectrical-transduction channels. *Proc Natl Acad Sci U S A* 95:15321–15326.

[73]   Dallos P (2008) Cochlear amplification, outer hair cells and prestin. *Curr Opin Neurobiol* 18:370–376.

[74]   Martin P, Hudspeth AJ (1999) Active hair-bundle movements can amplify a hair cell's response to oscillatory mechanical stimuli. *Proc Natl Acad Sci U S A* 96:14306–14311.

[75]   Ricci A (2003) Active hair bundle movements and the cochlear amplifier. *J Am Acad Audiol* 14:325–338.

[76]   Kernan MJ (2007) Mechanotransduction and auditory transduction in drosophila. *Pflugers Arch* 454:703–720.

[77]   Lukashkin AN, Russell IJ (2003) A second, low-frequency mode of vibration in the intact mammalian cochlea. *J Acoust Soc Am* 113:1544–1550.

[78]   Markin VS, Hudspeth AJ (1995) Modeling the active process of the cochlea: phase relations, amplification, and spontaneous oscillation. *Biophys J* 69:138–147.

[79]   Martin P, Hudspeth AJ (2001) Compressive nonlinearity in the hair bundle's active response to mechanical stimulation. *Proc Natl Acad Sci U S A* 98:14386–14391.

[80]   Nam JH, Fettiplace R (2008) Theoretical conditions for high-frequency hair bundle oscillations in auditory hair cells. *Biophys J* 95:4948–4962.

[81]   Camalet S, Duke T, Jülicher F, Prost J (2000) Auditory sensitivity provided by self-tuned critical oscillations of hair cells. *Proc Natl Acad Sci U S A* 97:3183–3188.

[82]   Kössl M, Möckel D, Weber M, Seyfarth EA (2008) Otoacoustic emissions from insect ears: evidence of active hearing? *J Comp Physiol A Neuroethol Sens Neural Behav Physiol* 194:597–609.

[83]   Hudspeth AJ, Jülicher F, Martin P (2010) A critique of the critical cochlea: Hopf–a bifurcation–is better than none. *J Neurophysiol* 104:1219–1229.

[84]   Johnson TA (2010) Cochlear sources and otoacoustic emissions. *J Am Acad Audiol* 21:176–186.

[85]   Oostenbrink P, Verhaagen-Warnaar N (2004) Otoacoustic emissions. *Am J Electroneurodiagnostic Technol* 44:189–198.

[86]   Corey DP, Hudspeth AJ (1983) Kinetics of the receptor current in bullfrog saccular hair cells. *J Neurosci* 3:962–976.

[87]   Howard J, Hudspeth AJ (1987) Mechanical relaxation of the hair bundle mediates adaptation in mechanoelectrical transduction by the bullfrog's saccular hair cell. *Proc Natl Acad Sci U S A* 84:3064–3068.

[88]   Hudspeth AJ, Choe Y, Mehta AD, Martin P (2000) Putting ion channels to work: mechanoelectrical transduction, adaptation, and amplification by hair cells. *Proc Natl Acad Sci U S A* 97:11765–11772.

[89]   Gillespie PG, Müller U (2009) Mechanotransduction by hair cells: models, molecules, and mechanisms. *Cell* 139:33–44.

[90]   Sukharev SI, Blount P, Martinac B, Guy HR, Kung C (1996) Mscl: a mechanosensitive channel in escherichia coli. *Soc Gen Physiol Ser* 51:133–141.

[91]   O'Hagan R, Chalfie M, Goodman MB (2005) The mec-4 deg/enac channel of caenorhabditis elegans touch receptor neurons transduces mechanical signals. *Nat Neurosci* 8:43–50.

[92]   Kang L, Gao J, Schafer WR, Xie Z, Xu XZS (2010) C. elegans trp family protein trp-4 is a pore-forming subunit of a native mechanotransduction channel. *Neuron* 67:381–391.

[93]   Perozo E (2006) Gating prokaryotic mechanosensitive channels. *Nat Rev Mol Cell Biol* 7:109–119.

[94]   Kloda A, Martinac B (2001) Mechanosensitive channels in archaea. *Cell Biochem Biophys* 34:349–381.

[95]   Haswell ES, Peyronnet R, Barbier-Brygoo H, Meyerowitz EM, Frachisse JM (2008) Two mscs homologs provide mechanosensitive channel activities in the arabidopsis root. *Curr Biol* 18:730–734.

[96]   Peyronnet R, Haswell ES, Barbier-Brygoo H, Frachisse JM (2008) Atmsl9 and atmsl10: Sensors of plasma membrane tension in arabidopsis roots. *Plant Signal Behav* 3:726–729.

[97]   Goodman MB, et al. (2002) Mec-2 regulates c. elegans deg/enac channels needed for mechanosensation. *Nature* 415:1039–1042.

[98]   Goodman MB, Schwarz EM (2003) Transducing touch in caenorhabditis elegans. *Annu Rev Physiol* 65:429–452.

[99]   Brown AL, Liao Z, Goodman MB (2008) Mec-2 and mec-6 in the caenorhabditis elegans sensory mechanotransduction complex: auxiliary subunits that enable channel activity. *J Gen Physiol* 131:605–616.

[100]   Price MP, et al. (2001) The drasic cation channel contributes to the detection of cutaneous touch and acid stimuli in mice. *Neuron* 32:1071–1083.

[101]   Drew LJ, et al. (2004) Acid-sensing ion channels asic2 and asic3 do not contribute to mechanically activated currents in mammalian sensory neurones. *J Physiol* 556:691–710.

[102]   Damann N, Voets T, Nilius B (2008) Trps in our senses. *Curr Biol* 18:R880–R889.

[103]   Montell C (2001) Physiology, phylogeny, and functions of the trp superfamily of cation channels. *Sci STKE* 2001:re1.

[104]   Montell C (2005) The trp superfamily of cation channels. *Sci STKE* 2005:re3.

[105]   Montell C, et al. (2002) A unified nomenclature for the superfamily of trp cation channels. *Mol Cell* 9:229–231.

[106]   Pedersen SF, Owsianik G, Nilius B (2005) Trp channels: an overview. *Cell Calcium* 38:233–252.

[107]   Voets T, Talavera K, Owsianik G, Nilius B (2005) Sensing with trp channels. *Nat Chem Biol* 1:85–92.

[108]   Ernstrom GG, Chalfie M (2002) Genetics of sensory mechanotransduction. *Annu Rev Genet* 36:411–453.

[109]   Rosenzweig M, et al. (2005) The drosophila ortholog of vertebrate trpa1 regulates thermotaxis. *Genes Dev* 19:419–424.

[110]   Tracey WD, Wilson RI, Laurent G, Benzer S (2003) painless, a drosophila gene essential for nociception. *Cell* 113:261–273.

[111]   Xu SY, et al. (2006) Thermal nociception in adult drosophila: behavioral characterization and the role of the painless gene. *Genes Brain Behav* 5:602–613.

[112]   Liu L, et al. (2007) Drosophila hygrosensation requires the trp channels water witch and nanchung. *Nature* 450:294–298.

[113]   Matsuura H, Sokabe T, Kohno K, Tominaga M, Kadowaki T (2009) Evolutionary conservation and changes in insect trp channels. *BMC Evol Biol* 9:228.

[114]   Sidi S, Friedrich RW, Nicolson T (2003) Nompc trp channel required for vertebrate sensory hair cell mechanotransduction. *Science* 301:96–99.

[115]   Shin JB, et al. (2005) Xenopus trpn1 (nompc) localizes to microtubule-based cilia in epithelial cells, including inner-ear hair cells. *Proc Natl Acad Sci U S A* 102:12572–12577.

[116]   Gong Z, et al. (2004) Two interdependent trpv channel subunits, inactive and nanchung, mediate hearing in drosophila. *J Neurosci* 24:9059–9066.

[117]   Kobori T, Smith GD, Sandford R, Edwardson JM (2009) The transient receptor potential channels trpp2 and trpc1 form a heterotetramer with a 2:2 stoichiometry and an alternating subunit arrangement. *J Biol Chem* 284:35507–35513.

[118]   Montell C (2005) Drosophila trp channels. *Pflugers Arch* 451:19–28.

[119]   Birnbaumer L (2009) The trpc class of ion channels: a critical review of their roles in slow, sustained increases in intracellular ca(2+) concentrations. *Annu Rev Pharmacol Toxicol* 49:395–426.

[120]   Kim J, et al. (2003) A trpv family ion channel required for hearing in drosophila. *Nature* 424:81–84.

[121]   Mutai H, Heller S (2003) Vertebrate and invertebrate trpv-like mechanoreceptors. *Cell Calcium* 33:471–478.

[122]   Georgiev P, et al. (2010) Trpm channels mediate zinc homeostasis and cellular growth during drosophila larval development. *Cell Metab* 12:386–397.

[123]   Hofmann T, et al. (2010) Drosophila trpm channel is essential for the control of extracellular magnesium levels. *PLoS One* 5:e10519.

[124]   Wood JN, et al. (2004) Ion channel activities implicated in pathological pain. *Novartis Found Symp* 261:32–40; discussion 40–54.

[125]   Al-Anzi B, Tracey WD, Benzer S (2006) Response of drosophila to wasabi is mediated by painless, the fly homolog of mammalian trpa1/anktm1. *Curr Biol* 16:1034–1040.

[126]   Montell C (2003) Thermosensation: hot findings make trpns very cool. *Curr Biol* 13:R476–R478.

[127]   Sokabe T, Tsujiuchi S, Kadowaki T, Tominaga M (2008) Drosophila painless is a ca2+-requiring channel activated by noxious heat. *J Neurosci* 28:9929–9938.

[128]   Zars T (2003) Hot and cold in drosophila larvae. *Trends Neurosci* 26:575–577.

[129]   O'Neil RG, Heller S (2005) The mechanosensitive nature of trpv channels. *Pflugers Arch* 451:193–203.

[130]   Sun Y, et al. (2009) Trpa channels distinguish gravity sensing from hearing in johnston's organ. *Proc Natl Acad Sci U S A* 106:13606–13611.

[131]   Walker RG, Willingham AT, Zuker CS (2000) A drosophila mechanosensory transduction channel. *Science* 287:2229–2234.

[132]   Cheng LE, Song W, Looger LL, Jan LY, Jan YN (2010) The role of the trp channel nompc in drosophila larval and adult locomotion. *Neuron* 67:373–380.

[133]   Göpfert MC, Albert JT, Nadrowski B, Kamikouchi A (2006) Specification of auditory sensitivity by drosophila trp channels. *Nat Neurosci* 9:999–1000.

[134]   Howard J, Bechstedt S (2004) Hypothesis: a helix of ankyrin repeats of the nompc-trp ion channel is the gating spring of mechanoreceptors. *Curr Biol* 14:R224–R226.

[135]   Lee J, Moon S, Cha Y, Chung YD (2010) Drosophila trpn(=nompc) channel localizes to the distal end of mechanosensory cilia. *PLoS One* 5:e11012.

[136]   Liang X, Madrid J, Saleh HS, Howard J (2011) Nompc, a member of the trp channel family, localizes to the tubular body and distal cilium of drosophila campaniform and chordotonal receptor cells. *Cytoskeleton (Hoboken)* 68:1–7.

[137]   Göpfert MC, Robert D (2003) Motion generation by drosophila mechanosensory neurons. *Proc Natl Acad Sci U S A* 100:5514–5519.

[138]   Gao Z, Ruden DM, Lu X (2003) Pkd2 cation channel is required for directional sperm movement and male fertility. *Curr Biol* 13:2175–2178.

[139]   Gao Z, Joseph E, Ruden DM, Lu X (2004) Drosophila pkd2 is haploid-insufficient for mediating optimal smooth muscle contractility. *J Biol Chem* 279:14225–14231.

[140]   Venglarik CJ, Gao Z, Lu X (2004) Evolutionary conservation of drosophila polycystin-2 as a calcium-activated cation channel. *J Am Soc Nephrol* 15:1168–1177.

[141]   Kumar PG, Shoeb M (2011) The role of trp ion channels in testicular function. *Adv Exp Med Biol* 704:881–908.

[142]   Nelson PL, Beck A, Cheng H (2010) Transient receptor proteins illuminated: Current views on trps and disease. *Vet J.*

[143]   Zhang SL, et al. (2006) Genome-wide rnai screen of ca(2+) influx identifies genes that regulate ca(2+) release-activated ca(2+) channel activity. *Proc Natl Acad Sci U S A* 103:9357–9362.

[144]   Kernan M, Cowan D, Zuker C (1994) Genetic dissection of mechanosensory transduction: mechanoreception-defective mutations of drosophila. *Neuron* 12:1195–1206.

[145]   Bang AG, Hartenstein V, Posakony JW (1991) Hairless is required for the development of adult sensory organ precursor cells in drosophila. *Development* 111:89–104.

[146]   Bechstedt S, Howard J (2008) Hearing mechanics: a fly in your ear. *Curr Biol* 18:R869–R870.

[147]   Lee G, et al. (2006) Nanospring behaviour of ankyrin repeats. *Nature* 440:246–249.

[148]   Sotomayor M, Corey DP, Schulten K (2005) In search of the hair-cell gating spring elastic properties of ankyrin and cadherin repeats. *Structure* 13:669–682.

[149]   Kamikouchi A, et al. (2009) The neural basis of drosophila gravity-sensing and hearing. *Nature* 458:165–171.

[150]   Yorozu S, et al. (2009) Distinct sensory representations of wind and near-field sound in the drosophila brain. *Nature* 458:201–205.

[151]   Eberl DF, Hardy RW, Kernan MJ (2000) Genetically similar transduction mechanisms for touch and hearing in drosophila. *J Neurosci* 20:5981–5988.

[152]   Nadrowski B, Göpfert MC (2009) Level-dependent auditory tuning: Transducer-based active processes in hearing and best-frequency shifts. *Commun Integr Biol* 2:7–10.

[153]   Hardie RC, Minke B (1992) The trp gene is essential for a light-activated ca2+ channel in drosophila photoreceptors. *Neuron* 8:643–651.

[154]   Montell C, Rubin GM (1989) Molecular characterization of the drosophila trp locus: a putative integral membrane protein required for phototransduction. *Neuron* 2:1313–1323.

[155]   Montell C, Jones K, Hafen E, Rubin G (1985) Rescue of the drosophila phototransduction mutation trp by germline transformation. *Science* 230:1040–1043.

[156]   Cosens DJ, Manning A (1969) Abnormal electroretinogram from a drosophila mutant. *Nature* 224:285–287.

[157]   Palma FD, et al. (2002) Mutations in mcoln3 associated with deafness and pigmentation defects in varitint-waddler (va) mice. *Proc Natl Acad Sci U S A* 99:14994–14999.

[158]   Atiba-Davies M, Noben-Trauth K (2007) Trpml3 and hearing loss in the varitint-waddler mouse. *Biochim Biophys Acta* 1772:1028–1031.

[159]   Corey DP (2006) What is the hair cell transduction channel? *J Physiol* 576:23–28.

[160]   Kidwell MG, Kidwell JF, Sved JA (1977) Hybrid dysgenesis in drosophila melanogaster: A syndrome of aberrant traits including mutation, sterility and male recombination. *Genetics* 86:813–833.

[161]   Rubin GM, Kidwell MG, Bingham PM (1982) The molecular basis of p-m hybrid dysgenesis: the nature of induced mutations. *Cell* 29:987–994.

[162]   Bingham PM, Kidwell MG, Rubin GM (1982) The molecular basis of p-m hybrid dysgenesis: the role of the p element, a p-strain-specific transposon family. *Cell* 29:995–1004.

[163]   Ryder E, Russell S (2003) Transposable elements as tools for genomics and genetics in drosophila. *Brief Funct Genomic Proteomic* 2:57–71.

[164]   O'Hare K, Rubin GM (1983) Structures of p transposable elements and their sites of insertion and excision in the drosophila melanogaster genome. *Cell* 34:25–35.

[165]   Karess RE, Rubin GM (1984) Analysis of p transposable element functions in drosophila. *Cell* 38:135–146.

[166]   Amarasinghe AK, MacDiarmid R, Adams MD, Rio DC (2001) An in vitro-selected rna-binding site for the kh domain protein psi acts as a splicing inhibitor element. *RNA* 7:1239–1253.

[167]   Robertson HM, et al. (1988) A stable genomic source of p element transposase in drosophila melanogaster. *Genetics* 118:461–470.

[168]   Cooley L, Kelley R, Spradling A (1988) Insertional mutagenesis of the drosophila genome with single p elements. *Science* 239:1121–1128.

[169]   Spradling AC, Rubin GM (1982) Transposition of cloned p elements into drosophila germ line chromosomes. *Science* 218:341–347.

[170]   Rubin GM, Spradling AC (1982) Genetic transformation of drosophila with transposable element vectors. *Science* 218:348–353.

[171]   Bier E, et al. (1989) Searching for pattern and mutation in the drosophila genome with a p-lacz vector. *Genes Dev* 3:1273–1287.

[172]   Wilson C, et al. (1989) P-element-mediated enhancer detection: an efficient method for isolating and characterizing developmentally regulated genes in drosophila. *Genes Dev* 3:1301–1313.

[173]   Janning (1997) Flyview, a drosophila image database, and other drosophila databases. *Semin Cell Dev Biol* 8:469–475.

[174]   Brand AH, Perrimon N (1993) Targeted gene expression as a means of altering cell fates and generating dominant phenotypes. *Development* 118:401–415.

[175]   Lukacsovich T, et al. (2001) Dual-tagging gene trap of novel genes in drosophila melanogaster. *Genetics* 157:727–742.

[176]   Morin X, Daneman R, Zavortink M, Chia W (2001) A protein trap strategy to detect gfp-tagged proteins expressed from their endogenous loci in drosophila. *Proc Natl Acad Sci U S A* 98:15050–15055.

[177]   Voelker RA, et al. (1984) Frequent imprecise excision among reversions of a p element-caused lethal mutation in drosophila. *Genetics* 107:279–294.

[178]   Salz HK, Cline TW, Schedl P (1987) Functional changes associated with structural alterations induced by mobilization of a p element inserted in the sex-lethal gene of drosophila. *Genetics* 117:221–231.

[179]   Keeler KJ, Gloor GB (1997) Efficient gap repair in drosophila melanogaster requires a maximum of 31 nucleotides of homologous sequence at the searching ends. *Mol Cell Biol* 17:627–634.

[180]   Rong YS, Golic KG (2000) Gene targeting by homologous recombination in drosophila. *Science* 288:2013–2018.

[181]   Rong YS, et al. (2002) Targeted mutagenesis by homologous recombination in d. melanogaster. *Genes Dev* 16:1568–1581.

[182]   Engels WR (1997) Invasions of p elements. *Genetics* 145:11–15.

[183]   Hummel T, Klämbt C (2008) P-element mutagenesis. *Methods Mol Biol* 420:97–117.

[184]   Fischer JA, Giniger E, Maniatis T, Ptashne M (1988) Gal4 activates transcription in drosophila. *Nature* 332:853–856.

[185]   Phelps CB, Brand AH (1998) Ectopic gene expression in drosophila using gal4 system. *Methods* 14:367–379.

[186]   Hong M, et al. (2008) Structural basis for dimerization in dna recognition by gal4. *Structure* 16:1019–1026.

[187]   Keegan L, Gill G, Ptashne M (1986) Separation of dna binding from the transcription-activating function of a eukaryotic regulatory protein. *Science* 231:699–704.

[188]   Gill G, Ptashne M (1988) Negative effect of the transcriptional activator gal4. *Nature* 334:721–724.

[189]   Giniger E, Ptashne M (1987) Transcription in yeast activated by a putative amphipathic alpha helix linked to a dna binding unit. *Nature* 330:670–672.

[190]   Kakidani H, Ptashne M (1988) Gal4 activates gene expression in mammalian cells. *Cell* 52:161–167.

[191]   Bram RJ, Kornberg RD (1985) Specific protein binding to far upstream activating sequences in polymerase ii promoters. *Proc Natl Acad Sci U S A* 82:43–47.

[192]   Kerr R, et al. (2000) Optical imaging of calcium transients in neurons and pharyngeal muscle of c. elegans. *Neuron* 26:583–594.

[193]   Miyawaki A, Griesbeck O, Heim R, Tsien RY (1999) Dynamic and quantitative ca2+ measurements using improved cameleons. *Proc Natl Acad Sci U S A* 96:2135–2140.

[194]   Suzuki H, et al. (2003) In vivo imaging of c. elegans mechanosensory neurons demonstrates a specific role for the mec-4 channel in the process of gentle touch sensation. *Neuron* 39:1005–1017.

[195]   Fiala A, Spall T (2003) In vivo calcium imaging of brain activity in drosophila by transgenic cameleon expression. *Science's STKE : signal transduction knowledge environment* 2003:PL6.

[196]   Fiala A, et al. (2002) Genetically expressed cameleon in drosophila melanogaster is used to visualize olfactory information in projection neurons. *Curr Biol* 12:1877–1884.

[197]   Kamikouchi A, Wiek R, Effertz T, Göpfert MC, Fiala A (2010) Transcuticular optical imaging of stimulus-evoked neural activities in the drosophila peripheral nervous system. *Nat Protoc* 5:1229–1235.

[198]   Truong K, et al. (2001) Fret-based in vivo ca2+ imaging by a new calmodulin-gfp fusion molecule. *Nat Struct Biol* 8:1069–1073.

[199]   Rudolf R, Mongillo M, Rizzuto R, Pozzan T (2003) Looking forward to seeing calcium. *Nat Rev Mol Cell Biol* 4:579–586.

[200]   Yang X, Xu P, Xu T (2005) A new pair for inter- and intra-molecular fret measurement. *Biochem Biophys Res Commun* 330:914–920.

[201]   Effertz T, Wiek R, Göpfert MC (2011) Nompc trp channel is essential for drosophila sound receptor function. *Curr Biol* 21:592–597.

[202]   Katzin BJ, Collins EJ, Robertus JD (1991) Structure of ricin a-chain at 2.5 a. *Proteins* 10:251–259.

[203]   Sandvig K, Olsnes S (1982) Entry of the toxic proteins abrin, modeccin, ricin, and diphtheria toxin into cells. ii. effect of ph, metabolic inhibitors, and ionophores and evidence for toxin penetration from endocytotic vesicles. *J Biol Chem* 257:7504–7513.

[204]   Olsnes S, Sandvig K, Madshus IH, Sundan A (1985) Entry mechanisms of protein toxins and picornaviruses. *Biochem Soc Symp* 50:171–191.

[205]   Rutenber E, et al. (1991) Crystallographic refinement of ricin to 2.5 a. *Proteins* 10:240–250.

[206]   Olsnes S, Refsnes K, Pihl A (1974) Mechanism of action of the toxic lectins abrin and ricin. *Nature* 249:627–631.

[207]   Lugnier AA, Creppy EE, Dirheimer G (1980) [ricin, the toxic protein of the castor-oil plant (ricinus communis l). structure and properties (author's transl)]. *Pathol Biol (Paris)* 28:127–139.

[208]   Olsnes S, Refsnes K (1978) On the mechanism of toxin resistance in cell variants resistant to abrin and ricin. *Eur J Biochem* 88:7–15.

[209]   Olsnes S (2004) The history of ricin, abrin and related toxins. *Toxicon* 44:361–370.

[210]   Endo Y, Mitsui K, Motizuki M, Tsurugi K (1987) The mechanism of action of ricin and related toxic lectins on eukaryotic ribosomes. the site and the characteristics of the modification in 28 s ribosomal rna caused by the toxins. *J Biol Chem* 262:5908–5912.

[211]   Endo Y, Tsurugi K (1986) Mechanism of action of ricin and related toxic lectins on eukaryotic ribosomes. *Nucleic Acids Symp Ser* pp 187–190.

[212]   Endo Y, Tsurugi K (1987) Rna n-glycosidase activity of ricin a-chain. mechanism of action of the toxic lectin ricin on eukaryotic ribosomes. *J Biol Chem* 262:8128–8130.

[213]   Sikriwal D, Ghosh P, Batra JK (2008) Ribosome inactivating protein saporin induces apoptosis through mitochondrial cascade, independent of translation inhibition. *Int J Biochem Cell Biol* 40:2880–2888.

[214]   Smith HK, et al. (1996) Inducible ternary control of transgene expression and cell ablation in <i>drosophila</i>. *Development Genes and Evolution* 206:14–24 10.1007/s004270050026.

[215]   Kamikouchi A, Shimada T, Ito K (2006) Comprehensive classification of the auditory sensory projections in the brain of the fruit fly drosophila melanogaster. *J Comp Neurol* 499:317–356.

[216]   Newsome TP, Asling B, Dickson BJ (2000) Analysis of drosophila photoreceptor axon guidance in eye-specific mosaics. *Development* 127:851–860.

[217]   Golic KG (1991) Site-specific recombination between homologous chromosomes in drosophila. *Science* 252:958–961.

[218]   Xu T, Rubin GM (1993) Analysis of genetic mosaics in developing and adult drosophila tissues. *Development* 117:1223–1237.

[219]   Zhu XD, Sadowski PD (1995) Cleavage-dependent ligation by the flp recombinase. characterization of a mutant flp protein with an alteration in a catalytic amino acid. *J Biol Chem* 270:23044–23054.

[220]   van Aken AFJ, et al. (2008) Trpml3 mutations cause impaired mechano-electrical transduction and depolarization by an inward-rectifier cation current in auditory hair cells of varitint-waddler mice. *J Physiol* 586:5403–5418.

[221]   Brewster R, Bodmer R (1996) Cell lineage analysis of the drosophila peripheral nervous system. *Dev Genet* 18:50–63.

[222]   Eberl DF (1999) Feeling the vibes: chordotonal mechanisms in insect hearing. *Curr Opin Neurobiol* 9:389–393.

[223]   Keil TA (1997) Functional morphology of insect mechanoreceptors. *Microsc Res Tech* 39:506–531.

[224]   Vervoort M, Merritt DJ, Ghysen A, Dambly-Chaudière C (1997) Genetic basis of the formation and identity of type i and type ii neurons in drosophila embryos. *Development* 124:2819–2828.

[225]   Hartenstein V, Posakony J (1989) Development of adult sensilla on the wing and notum of drosophila melanogaster. *Development* 107:389–405.

[226]   Hartenstein V (1988) Development of drosophila larval sensory organs: spatiotemporal pattern of sensory neurones, peripheral axonal pathways and sensilla differentiation. *Development* 102:869–886.

[227]   Lai EC, Orgogozo V (2004) A hidden program in drosophila peripheral neurogenesis revealed: fundamental principles underlying sensory organ diversity. *Dev Biol* 269:1–17.

[228]   Brewster R, Bodmer R (1995) Origin and specification of type ii sensory neurons in drosophila. *Development* 121:2923–2936.

[229]   Cachero S, et al. (2011) The gene regulatory cascade linking proneural specification with differentiation in drosophila sensory neurons. *PLoS Biol* 9:e1000568.

[230]   Kernan M, Zuker C (1995) Genetic approaches to mechanosensory transduction. *Curr Opin Neurobiol* 5:443–448.

[231]   Thurm U (1964) Mechanoreceptors in the cuticlle of the honey bee: fine structure and stimulus mechanism. *Science* 145:1063–1065.

[232]   Grünert U G (1987) K+ and ca++ in the receptor lymph of arthropod cuticular mechanoreceptors. *Journal of comparative physiology. A, Sensory, neural, and behavioral physiology* 161:329–333.

[233]   Thurm U (1965) An insect mechanoreceptor. i. fine structure and adequate stimulus. *Cold Spring Harb Symp Quant Biol* 30:75–82.

[234]   Thurm U (1965) An insect mechanoreceptor. ii. receptor potentials. *Cold Spring Harb Symp Quant Biol* 30:83–94.

[235]   Bromley AK, Dunn JA, Anderson M (1980) Ultrastructure of the antennal sensilla of aphids. ii. trichoid, chordotonal and campaniform sensilla. *Cell Tissue Res* 205:493–511.

[236]   Yager DD (1999) Structure, development, and evolution of insect auditory systems. *Microsc Res Tech* 47:380–400.

[237]   Eberl DF, Boekhoff-Falk G (2007) Development of johnston's organ in drosophila. *Int J Dev Biol* 51:679–687.

[238]   Hibino H, Nin F, Tsuzuki C, Kurachi Y (2010) How is the highly positive endocochlear potential formed? the specific architecture of the stria vascularis and the roles of the ion-transport apparatus. *Pflugers Arch* 459:521–533.

[239]   Mistrik P, Ashmore J (2009) The role of potassium recirculation in cochlear amplification. *Curr Opin Otolaryngol Head Neck Surg* 17:394–399.

[240]   Wangemann P (1997) [potassium ion secretion and generation of the endocochlear potential in the stria vascularis]. *HNO* 45:205–209.

[241]   Wangemann P (2006) Supporting sensory transduction: cochlear fluid homeostasis and the endocochlear potential. *J Physiol* 576:11–21.

A. Appendix A Fly husbandry

A.1. Fly husbandry

Fly stocks were kept at 18-19° C for storage purposes in cylindrical vials with a diameter of 26mm and a height of 63mm, filled to ¼ with fly food, and containing 30-60 flies. Each individual fly stock was kept in three separate vials to ensure stock safety and availability of virgins. The vials were stored in boxes á 108 vials. Fly stocks needed for crossings where kept at room temperature or at 25° C to facilitate reproduction and shorten the generation cycle. Fly stocks containing conditional mutations where kept at 32° C during experiments to ensure conditional expression of genes.

A.2. Fly food

Table 1 Fly Food ingredients for 1 Litre

Ingredient	Amount
Corn meal	80 g
Malzin	80 g
Treacle	22 g
Yeast	18 g
Agar	12.5 g
Soy bean flour	10 g
Nipagin	6.3 ml
Propionacid	1.5 g

To obtain 1 litre of fly food 12.5 g of agar were soaked overnight in 500ml water. The next day, 80g corn meal, 22g treacle, 18g yeast, and 10g soy bean flour were dissolved in 400ml water and boiled at 100°C in a Varioklav® Steam pot DT4458060. Afterwards the temperature was lowered to 55°C and 80g malzin dissolved in 100ml water was added. Once the temperature of 55°C was reached, 6.3 ml propionic acid (antibiotic), and 1.5g Nipagin (fungicide) dissolved in 5 ml EtOH, were added. With a pump (Isomatic® MCP) the warm, liquid food was pumped out of the Varioklav® Steam pot and into the vials. On the following day later after the fly food in the vials was cooled down to room temperature, the vials were closed with mite impermeable foam plugs (K-TK, Retzstadt, Germany). To keep the food fresh, it was stored in a refrigerator for no longer then four weeks.

B. Appendix B Fly Crosses

B.1. *nompC* related crosses/mutants

nompC² mutants

$$\male/\hermaphrodite\frac{w^+}{w^+};\frac{nompC^2,\ cn\ bw}{Cy\ cn};\frac{+}{+} \times \hermaphrodite/\male\frac{w^+}{w^+};\frac{nompC^2,\ cn\ bw}{Cy\ cn};\frac{+}{+}$$

$$\Downarrow$$

$$\text{Mutants: } \male/\female\ \frac{w^+}{w^+};\frac{nompC^2,\ cn\ bw}{nompC^2,\ cn\ bw};\frac{+}{+}$$

$$\text{Controls: } \male/\female\ \frac{w^+}{w^+};\frac{nompC^2,\ cn\ bw}{Cy\ cn};\frac{+}{+}$$

or

$$\male/\hermaphrodite\frac{w^+}{w^+};\frac{nompC^2,\ cn\ bw}{Cy\ cn};\frac{+}{+} \times \hermaphrodite/\male\frac{w^+}{w^+};\frac{Df(2L)cl^{h2}}{Cy\ cn};\frac{+}{+}$$

$$\Downarrow$$

$$\text{Mutants: } \male/\female\ \frac{w^+}{w^+};\frac{nompC^2,\ cn\ bw}{Df(2L)cl^{h2}};\frac{+}{+}$$

$$\text{Controls: } \male/\female\ \frac{w^+}{w^+};\frac{nompC^2,\ cn\ bw}{Cy\ cn};\frac{+}{+} \text{ or } \male/\female\ \frac{w^+}{w^+};\frac{Df(2L)cl^{h2}}{Cy\ cn};\frac{+}{+}$$

nompC³ mutants

$$\male/\hermaphrodite\frac{w^+}{w^+};\frac{nompC^3,\ cn\ bw}{Cy\ cn};\frac{+}{+} \times \hermaphrodite/\male\frac{w^+}{w^+};\frac{nompC^3,\ cn\ bw}{Cy\ cn};\frac{+}{+}$$

$$\Downarrow$$

$$\text{Mutants: } \male/\female\ \frac{w^+}{-};\frac{nompC^3,\ cn\ bw}{nompC^3,\ cn\ bw};\frac{+}{+}$$

$$\text{Controls: } \male/\female\ \frac{w^+}{-};\frac{nompC^3,\ cn\ bw}{Cy\ cn};\frac{+}{+}$$

or

$$\male/\hermaphrodite\frac{w^+}{w^+};\frac{nompC^3,\ cn\ bw}{Cy\ cn};\frac{+}{+} \times \hermaphrodite/\male\frac{w^+}{w^+};\frac{Df(2L)cl^{h2}}{Cy\ cn};\frac{+}{+}$$

$$\Downarrow$$

$$\text{Mutants: } \male/\female\ \frac{w^+}{w^+};\frac{nompC^3,\ cn\ bw}{Df(2L)cl^{h2}};\frac{+}{+}$$

$$\text{Controls: } \male/\female\ \frac{w^+}{w^+};\frac{nompC^3,\ cn\ bw}{Cy\ cn};\frac{+}{+} \text{ or } \male/\female\ \frac{w^+}{w^+};\frac{Df(2L)cl^{h2}}{Cy\ cn};\frac{+}{+}$$

nompC⁴ mutants

$$\male/\female\frac{w^+}{w^+};\frac{nompC^4,\ cn\ bw}{Cy\ cn};\frac{+}{+}\ \times\ \female/\male\frac{w^+}{w^+};\frac{nompC^4,\ cn\ bw}{Cy\ cn};\frac{+}{+}$$

$$\Downarrow$$

Mutants: $\male/\female\ \dfrac{w^+}{w^+};\dfrac{nompC^4,\ cn\ bw}{nompC^4,\ cn\ bw};\dfrac{+}{+}$

Controls: $\male/\female\ \dfrac{w^+}{w^+};\dfrac{nompC^4,\ cn\ bw}{Cy\ cn};\dfrac{+}{+}$

or

$$\male/\female\frac{w^+}{w^+};\frac{nompC^4,\ cn\ bw}{Cy\ cn};\frac{+}{+}\ \times\ \female/\male\frac{w^+}{w^+};\frac{Df(2L)cl^{h2}}{Cy\ cn};\frac{+}{+}$$

$$\Downarrow$$

Mutants: $\male/\female\ \dfrac{w^+}{w^+};\dfrac{nompC^4,\ cn\ bw}{Df(2L)cl^{h2}};\dfrac{+}{+}$

Controls: $\male/\female\ \dfrac{w^+}{w^+};\dfrac{nompC^4,\ cn\ bw}{Cy\ cn};\dfrac{+}{+}$ or $\male/\female\ \dfrac{w^+}{w^+};\dfrac{Df(2L)cl^{h2}}{Cy\ cn};\dfrac{+}{+}$

nompC³ background *UAS-nompC-L* rescue

$$\male/\female\frac{w^+}{w^+};\frac{nompC^3,\ UAS-nompC-L}{Cy};\frac{+}{+}\ \times\ \female/\male\frac{w^+}{w^+};\frac{nompC^3,\ cn\ bw}{Cy\ cn};\frac{JO1}{JO1}$$

$$\Downarrow$$

$$\male/\female\ \frac{w^+}{w^+};\frac{nompC^3,\ UAS-nompC-L}{nompC^3,\ cn\ bw};\frac{JO1}{+}$$

Ablation of sound-receptors with *UAS-Ricin Toxin A*

$$\female\frac{JO2}{FM7c};\frac{+}{+};\frac{UFWTRA19}{TM3\ Ser}\ \times\ \male\frac{w^+}{-};\frac{eyFLP}{Cy};\frac{JO15}{TM6b\ Sb\ Tb}$$

$$\Downarrow$$

Mutants: $\male\ \dfrac{JO2}{-};\dfrac{eyFLP}{+};\dfrac{JO1}{UFWTRA19}$

Controls: $\male/\female\ \dfrac{JO2}{-};\dfrac{eyFLP}{+};\dfrac{JO1}{TM3\ Ser}$ or $\male/\female\ \dfrac{JO2}{-};\dfrac{eyFLP}{+};\dfrac{TM6b\ Sb\ Tb}{TM3\ Ser}$

or

$$\male/\female\frac{+}{+};\frac{+}{+};\frac{UFWTRA19}{TM3\ Ser}\ \times\ \female/\male\frac{w^+}{w^+};\frac{eyFLP}{Cy};\frac{JO15}{TM6b\ Sb\ Tb}$$

$$\Downarrow$$

Mutants: $\male\ \dfrac{+}{w^+};\dfrac{eyFLP}{+};\dfrac{JO1}{UFWTRA19}$

Controls: $\male/\female\ \dfrac{+}{w^+};\dfrac{eyFLP}{+};\dfrac{JO1}{TM3\ Ser}$ or $\male/\female\ \dfrac{+}{w^+};\dfrac{eyFLP}{+};\dfrac{TM6b\ Sb\ Tb}{TM3\ Ser}$

Ablation of gravity/wind receptors with *UAS-ricin toxin A chain*

$$\female \frac{+}{+};\frac{+}{+};\frac{UFWTRA19}{TM3\ Ser} \times \male \frac{w^+}{w^+};\frac{JO31}{Cy};\frac{eyFLP}{TM6b\ Sb\ Tb}$$

$$\Downarrow$$

$$\text{Mutants: } \male\ \frac{+}{w^+};\frac{JO31}{+};\frac{eyFLP}{UFWTRA19}$$

$$\text{Controls: } \male/\female\ \frac{+}{+};\frac{JO31}{+};\frac{eyFLP}{TM3\ Se} \text{ or } \male/\female\ \frac{+}{+};\frac{JO31}{+};\frac{UFWTRA19}{TM3\ Ser}$$

B.2. *nanchung* and *inactive* related crosses/mutants

***inactive* mutant flies**

$$\text{Mutants: } \male/\female\ \frac{iav^1}{iav^1};\frac{+}{+};\frac{+}{+}$$

***nanchung* mutant flies**

nan^{dy5} $\qquad$ $\text{Mutants: } \male/\female\ \frac{w^+}{w^+};\frac{+}{+};\frac{nan^{dy5}}{nan^{dy5}}$

$$\text{Controls: } \male/\female\ \frac{w^+}{w^+};\frac{+}{+};\frac{nan^{dy5}}{TM6b\ Sb\ Tb}$$

nan^{36a} $\qquad$ $\text{Mutants: } \male/\female\ \frac{w^+}{w^+};\frac{+}{+};\frac{nan^{36a}}{nan^{36a}}$

B.3. *painless* related crosses/mutants

pain^1

$$\text{Mutants: } \male/\female\ \frac{w^*}{w^*};\frac{P\{w[+mC]=EP\}pain[EP2451]}{P\{w[+mC]=EP\}pain[EP2451]};\frac{+}{+}$$

$$\text{Controls: } \male/\female\ \frac{w^*}{w^*};\frac{P\{w[+mC]=EP\}pain[EP2451]}{CyO};\frac{+}{+}$$

pain^2

$$\text{Mutants: } \male/\female\ \frac{w^*}{w^*};\frac{P\{w[+mC]=EP\}pain[EP2621]}{P\{w[+mC]=EP\}pain[EP2621]};\frac{+}{+}$$

$$\text{Controls: } \male/\female\ \frac{w^*}{w^*};\frac{P\{w[+mC]=EP\}pain[EP2621]}{CyO};\frac{+}{+}$$

pain³

Mutants: ♂/♀ $\frac{w^*}{w^*}$; $\frac{P\{w[+mC]=EP\}pain[EP2251]}{P\{w[+mC]=EP\}pain[EP2251]}$; $\frac{+}{+}$

Controls: ♂/♀ $\frac{w^*}{w^*}$; $\frac{P\{w[+mC]=EP\}pain[EP2251]}{CyO}$; $\frac{+}{+}$

B.4. *trp* related crosses/mutants

Mutants: ♂/♀ $\frac{w^{1118}}{w^{1118}}$; $\frac{+}{+}$; $\frac{trp^1}{trp^1}$

Controls: ♂/♀ $\frac{w^{1118}}{w^{1118}}$; $\frac{+}{+}$; $\frac{trp^1}{TM6b\ Tb}$

B.5. *trpml* related crosses/mutants

Mutants: ♂/♀ $\frac{w^{1118}}{w^{1118}}$; $\frac{+}{+}$; $\frac{trpml^1}{trpml^1}$

Controls: ♂/♀ $\frac{w^{1118}}{w^{1118}}$; $\frac{+}{+}$; $\frac{trpml^1}{TM6b\ Tb}$

B.6. Calcium imaging

Intact organ *Cam2.1* => JO-all

$$♂/⚥\frac{w^+}{w^+};\frac{Cam2.1}{Cam2.1};\frac{MKRS}{TM6b\ Sb\ Tb} \ \textbf{x}\ ⚥/♂\frac{w^-}{w^-};\frac{Sp}{Cy};\frac{JO1}{JO1}$$

$$⇓$$

$$♂/♀\ \frac{w^+}{w^-};\frac{Cam2.1}{Cy(Sp)};\frac{JO1}{MKRS(TM6b)}$$

Intact organ *Cam2.1* => JO sound-receptors

$$♂/⚥\frac{w^+}{w^+};\frac{Cam2.1}{Cam2.1};\frac{MKRS}{TM6b} \ \textbf{x}\ ⚥/♂\frac{w^-}{w^-};\frac{Sp}{Cy};\frac{JO15}{JO15}$$

$$⇓$$

$$♂/♀\ \frac{w^+}{w^-};\frac{Cam2.1}{Cy(Sp)};\frac{JO15}{MKRS(TM6b)}$$

Intact organ *Cam2.1* => JO-gravity/wind receptors

$$\sigma/\rlap{\female}\frac{w^+}{w^+};\frac{Sp}{Cy};\frac{Cam2.1}{Cam2.1} \times \rlap{\female}/\sigma\frac{w^-}{w^-};\frac{JO31}{JO31};\frac{MKRS}{TM6b}$$

$$\Downarrow$$

$$\sigma/\female \; \frac{w^+}{w^-};\frac{JO31}{Cy(Sp)};\frac{Cam2.1}{MKRS(TM6b)}$$

***nompC³ nulls* for calcium imaging (*Cam2.1* => JO-all)**

$$\sigma/\rlap{\female}\frac{w^+}{w^+};\frac{nompC^3,\ cn\,bw}{Cy\ cn};\frac{JO1}{TM6b} \times \rlap{\female}/\sigma\frac{w^+}{w^+};\frac{nompC^3,\ cn\,bw}{Cy\ cn};\frac{Cam2.1}{TM6b}$$

$$\Downarrow$$

$$\sigma/\female \; \frac{w^+}{w^+};\frac{nompC^3,\ cn\,bw}{nompC^3,\ cn\,bw};\frac{JO1}{TM6b}$$

***nompC³ nulls* for calcium imaging (*Cam2.1* => JO sound-receptors)**

$$\sigma/\rlap{\female}\frac{w^+}{w^+};\frac{nompC^3,\ cn\,bw}{Cy\ cn};\frac{JO15}{TM6b} \times \rlap{\female}/\sigma\frac{w^+}{w^+};\frac{nompC^3,\ cn\,bw}{Cy\ cn};\frac{Cam2.1}{TM6b}$$

$$\Downarrow$$

$$\sigma/\female \; \frac{w^+}{w^+};\frac{nompC^3,\ cn\,bw}{nompC^3,\ cn\,bw};\frac{JO15}{TM6b}$$

C. Appendix C

Tab. 6 Table of sound receiver properties important for nompC measurements

	Genotype	Best frequency (Hz)	STD	Power	STD	N
wild-type	*Oregon R*	197	35	1411	633	9
	Canton-S	249	8	2316	883	5
	cn bw	285	17	957	317	6
	w^1118	179	2	1735	486	8
controls	*NP1046;; JO15/UFWTRA19 or ; eyFLP; JO15/TM6b*	310	58	1119	306	9
	NP6250; eyFLP/TM6b or UFWTRA19/TM6b	191	59	1016	200	11
	Df(2L)clh2/Cy cn	292	27	907	163	7
	nompC2 cn bw/Cy cn	271	20	556	183	5
	nompC3 cn bw/Cy cn	282	17	525	115	9
Sound-receptor ablated	*NP1046; eyFLP; JO15/UFWTRA19*	443	80	112	53	22
Gravity/wind-receptors ablated	*NP6250; eyFLP/UFWTRA19*	259	18	960	214	7
nompC mutants	*nompC2 cn bw and nompC2 cn bw/Df(2L)clh2*	523	12	111	35	9
	nompC3 cn bw and nompC3cn bw/Df(2L)clh2	541	14	113	39	25
	nompC4 cn bw and nompC4cn bw/Df(2L)clh2	532	19	110	53	5
nompC rescue	*nompC3, UAS-nompC-L; JO1/+*	280	64	1033	462	8

Tab. 7 wild-type, control, and mutant sensitivity gain

	Genotype	Sensitivity gain	STD
Wild-type	*Oregon*	10	2.4
	Canton-S	7.9	1.3
controls	*cn bw*	54.7	0.6
	w^{1118}	11	1.5
	NP1046;; JO15/UFWTRA19 or ; eyFLP; JO15/TM6b	5.4	1.6
	NP6250; eyFLP/TM6b or UFWTRA19/TM6b	6.7	0.6
	Df(2L)clh2/Cy cn	8	1.4
	nompC2 cn bw/Cy cn	3.4	0.3
	nompC3 cn bw/Cy cn	3.8	0.3
Sound-receptors ablated	*NP1046; eyFLP; JO15/UFWTRA19*	1.2	0.2
Gravity/wind-receptors ablated	*NP6250; eyFLP/UFWTRA19*	6.1	1.5
nompC mutants	*nompC2 cn bw* and *nompC2 cn bw/Df(2L)clh2*	1.1	0.1
	nompC3 cn bw and *nompC3cn bw/Df(2L)clh2*	1.1	0.1
	nompC4 cn bw and *nompC4cn bw/Df(2L)clh2*	1.1	0.1
nompC rescue	*nompC3, UAS-nompC-L; JO1/+*	4.7	1.2

D. Appendix D

D.1. Mechanoreception in Drosophila melanogaster

The Drosophila PNS harbours ciliated (type I) and nonciliated (type II) mechanosensory organs [76,221-224].

Type I sensory organs consist of sensory units containing one or more bipolar neurons that are surrounded by specialized supporting cells connecting them to the cuticle [22] (Figure 108).

Type II based sensory organs consist of one non-ciliated multidendritic (md) or bipolar neuron and are devoid of accessory cells (with one exception) [224] (Figure 108).

Developmentally, type I sensory organs are derived from a single sensory organ precursor cell (SOP) [225-227]. This cell undergoes four asymmetric mitotic divisions, leading to five distinct cells, which differentiate into supporting cells

Figure 108 Type I & type II mechanosensory organs in Drosophila melanogaster
A: type I sensory organs, chordotonal (cs) & external sensory organs (es). Colours indicate corresponding cell types in both organs (altered after [71]). B: type II sensory organ, multidendritic, arborised md-neuron

respectively sensory neuron(s) or enter apoptosis (Figure 109). The SOP cell divides into the pIIa & pIIb cell. The pIIa cell devides once more and differentiates together with its daughter cell into sensory organ specific supporting cells. The pIIb cell gives rise to a daughter cell (pIIIb) and differentiates in to a sensory organ specific supporting cell or an md neuron (type II cell lineage). The pIIIb cell divides once more and differentiates together with its daughter cell into a sensory organ specific supporting cell and the sensory neuron. In sensory organs that harbour more than one sensory neuron per unit, the neuronal precursor cell divides once or twice (e.g. in chordotonal organs). The cell linage of type II sensory neurons associated with type I sensory organs is comparable to the type I cell lineage, with the difference that only one daughter cell of the pIIb precursor

cell survives and gives rise to the md neuron, the rest enters apoptosis. Unassociated type II sensory cells derive from secondary SOPs [228].

Figure 109 Developmental cell lineage of type I sensory organs
The sensory organ precursor cell (SOP) gives rise to two daughter cells (pIIa & pIIb). The pIIa cell divides and differentiates into different cell types, depending on the sensory organ. The pIIb cell gives rise to the pIIIb cell and a sensory organ specific final cell. The pIIIb cell undergoes a final cell divison and gives rise to the neuron(s) and sheat/scolopale cells depending on the sensory organ.

D.1.1 Type I sensory organs

The type I sensory organs can be divided into two subtypes: external sensory (*es*) organs and chordotonal (*ch*) organs [223,229].

D.1.2 external sensory (es) organs

es organs possess external cuticular structures that can be deflected or deformed by mechanical stimuli. Mechanosensitive bristles on the fly's exoskeleton are *es* organs for example [223] (Figure 110). The external structure of the bristle is its shaft. The shaft protrudes through the cuticle and its base connects to the dendrite of the sensory neuron. The dendrite is divided into an outer and inner segment. Presumably the mechanosensitive channel resides in the outer segment. The inner or proximal segment of the dendrite is filled by an irregular array of microtubules, the tubular body [144,230,231]. While the rest of the neuron faces the normal hemolymph space its dendrite faces the receptor lymph space, which is formed by the socket cell. Similar to the endolymph in a mammalian cochlea, the

Figure 110 type I sensory organ, subtype *es* organ
Colour code as in Figure 3, indicating the cell lineage. A deflection of the shaft towards the cuticle will result in a stretch of the sensory process of the neuron. The mechanical forces will directly open transduction channels in the sensory neuron and beyond stimulus threshold elicit a response. The neuronal sensory process faces a separated receptorlymph-space, which is formed by the socket cell and shows a high potassium concentration.

receptor lymph shows a high potassium concentration [232]. The receptor rlymph also enters the hollow shaft, which allows for the recording of transepithelial current/voltage changes during stimulation [131]. Stimulation is thought to occur when a movement of the external structure leads to a compression of the ciliary membrane between the dendritic cap and the tubular body [131,233,234].

D.1.3   chordotonal (ch) organs

ch organs are intersegmental stretch receptors serially arranged along the insect body. The organs detect the relative movement of adjacent body parts [222,235,236]. *ch* organs are composed of multicellular units called chordotonal sensilla or scolopidia. A scolopidium consists of 1-3 sensory neurons that are surrounded by three different supporting cells. Those supporting cells are: The scolopale cell (thecogen cell) that forms a cavity around the outer ciliary dendrite of the sensory neurons (scolopale space); the ligament cell (trichogen cell) that connects the scolopidium to the proximal cuticle; the cap cell (tormogen cell) that connects the scolopidium to the distal cuticle [237]. Similar to hair bundles of hair cells in the organ of Corti, the dendritic cilium of *ch* neurons faces a potassium rich environment in the scolopale space. The potassium concentration in the scolopale space is approximately five times higher (121 ± 15 mM scolopale space; 25 ± 7 mM hemolymph) than in the hemolymph space [232], most likely leading to a static potential. This endolymphatic potential might facilitate sensory neuronal function, not unlike the endocochlear potential in the mammalian organ of Corti [238-241]. The endochlear potential (also known as microphonic potential) is known to be

Figure 111 Type I sensory organ, subtype chordotonal organ (*ch*), scolopidia

Colour code as in Figure 3, indicating the cell lineage. The basic subunit of all chordotonal organs is the scolopidia, consisting of the sensory neuron(s) and its supporting cells. Chordotonal organs are found between every segment of an insect body and serve as stretchreceptors. The mechanical forces are relayed to the sensory neuron by the cap-cell (distal) and the ligament cell (proximal).

116

important for the active process in mammalian ears. It is maintained by the stria vascularis cells. The similarities between the endolymphatic potential and the endocochlear potential suggest a comparable function in the fly.

D.2. Type II sensory organs

Type II or nonciliated sensory organs are composed of so-called multidentiric (md) neurons. Compared to type I sensory organs they lack supporting cells. Their dendritic pattern varies and is subdivided into bipolar-, arborisation-, and tracheal-md-neurons. They are muscular stretch receptors and are also implicated in nociception, proprioception, and thermo sensation. Little is known of the transduction processes underlying those functions [228]. Developmentally the cell lineage is similar to that of type I sensory organs, with both the pIIa and pIIIb cell entering apoptosis and the second daughter cell of pIIb becoming a md neuron (compare Figure 109).

E. Appendix E

E.1. LDV Setup for sound stimulation

- Air table: Linus Photonics series 63 table, Art.-No. 436356401 (dimensions 900 × 1200 × 100 mm)

- Laser Doppler Vibrometer (LDV): Polytec, PSV-400 equipped with an OFV-700 close-up unit (70 mm focal length)

- A/D converter: Cambridge Electronic Devises, micro 1401 MKII

- HiFi amplifier: dB Technologies MA1060

- Loudspeaker: Visaton W130S

- Micro manipulators:
  - 5 x MM33 with magnetic stand, Kanetec MB-K (animal holder; electrophysiology reference electrode; microphone; anterior and posterior electrostatic actuator electrodes)
  - HS6, Märzhäuser (electrophysiology recording electrode)

- Attenuator: Custom-build resistor based attenuator, attenuation range from 0 - 100 dB in 1 dB steps

- Extracellular amplifier: 4-channel amplifier MA102

- Hum Bug Quest Scientific

- Microphone: Emkay NR 3158 miniature pressure-gradient microphone with an integrating amplifier, Knowles Electronics Inc., Itasca, Illinois, USA

- Dissection microscope: Stereo microscope PZMIII-BS, World Precision Instruments

- Lightsource: Fiberopticlamp, Novaflex Bifurcated Light Guide Nova-186, World Precision Instruments
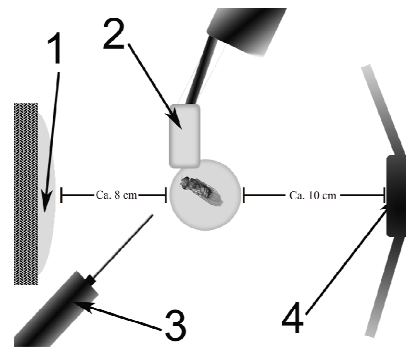
Figure 112 experimental setup for sound intensity measurements
The LDV (1), measures the movement of the fly's antenna ins response to sound stimuli emitted by a loudspeaker (4). A particle velocity sensitive microphone (2) measures the stimulus intensity at the position of the antenna. An etched tungsten electrode (3) is inserted between the scape and head of the fly to record the compound action potential changes of the antennal nerve.

E.2. Calcium Setup

- Air table Scientific Products

- Laser Doppler Vibrometer (LDV): Polytec, OFV-534 compact sensor head

- Custom build animal holder

- A/D converter: Cambridge Electronic Devises, micro 1401 MKII

- Extracellular amplifier: 4-channel amplifier MA102

- Hum Bug Quest Scientific

- Visitron VisiFRET system

  - Zeiss Examiner.D1

  - Photometrics Cascade II 512 CCD camera

  - VisiChrome High Speed Polychromatic Illumination System

  - DualView Beamsplitter DV^2

- Motor driven 3-axis Micromanipulator

F. Figure legends

Figure legends

Acknowledgement

Curriculum vitae

Personal Information

Name: Thomas Effertz

Date of Birth: 18th April 1980

Place of Birth: Cologne, Germany

Nationality: german

Education

2007-present   PhD-Student, University of Goettingen

Thesis: Candidate mechanosensitive transduction channels in *Drosophila melanogaster*

Committee: Prof. Dr. Martin C Göpfert (Supervisor), Prof. Dr. André Fiala, Prof. Dr. Andreas Stumpner

Affiliations: Göttingen Graduate School for Neurosciences and Molecular Biosciences (GGNB), program of "Sensory and Motor Neuroscience"

February 2007   Diploma Grade in Biology,   University of Cologne

Thesis: Response of mechanosensitive neurons in the *Drosophila*-ear

Advisor: PD Dr. Martin Göpfert

Affiliation: Volkswagen Foundation research group, University of Cologne

2000-2006   Study of Biology, University of Cologne

Recent Publications

Effertz T, Wiek R, Göpfert MC. (2011) NompC TRP channel is essential for *Drosophila* sound-receptor function. *Current Biology doi: 10.1016/j.cub.2011.02.048*

Kamikouchi A, Wiek R, Effertz T, Göpfert MC, Fiala A. Transcuticular optical imaging of stimulus-evoked neural activities in the Drosophila peripheral nervous system. *Nature Protocols 2010; 5(7):1229-1235*

Kamikouchi A, Inagaki HK, Effertz T, et al. The neural basis of Drosophila gravity-sensing and hearing. *Nature. 2009 Mar 12;458(7235):165-71.*